Reliability Improvement and Power Loss Reduction in Distribution System

(Case Study: Hormat Substation II)

Getahun Shanko Kefeni

A Thesis Submitted to

The Department of Electrical Power and Control Engineering

School of Electrical Engineering and Computing

Presented in Partial Fulfillment of the Requirement for the Degree of Master's in

Electrical Power and Control Engineering (Power System Engineering)

Office of Graduate Studies

Adama Science and Technology University

July, 2023

Adama, Ethiopia

Reliability Improvement and Power Loss Reduction in Distribution System

(Case Study: Hormat Substation II)

Getahun Shanko Kefeni

Advisor: Dr. Prathibha Ekanthaiah Kotraiah

A Thesis Submitted to
The Department of Electrical Power and Control Engineering
School of Electrical Engineering and Computing
Presented in Partial Fulfillment of the Requirement for the Degree of Master's in
Electrical Power and Control Engineering (Power System Engineering)

Office of Graduate Studies
Adama Science and Technology University

July, 2023

Adama, Ethiopia

DECLARATION

I declare that this Master Thesis entitled “Reliability Improvement and Power Loss Reduction in Distribution System (Case Study: Hormat Substation II)” is my own work and has not been submitted to any university for a similar purpose. Proper citations duly recognize the references used in this thesis.

Getahun Shanko Kefeni	_____	_____
Name of student	Signature	Date

RECOMMENDATION OF ADVISOR/ SUPERVISOR

I, the advisor of this thesis, hereby certify that I have read the revised version of the thesis entitled "Reliability Improvement and Power Loss Reduction in Distribution System (Case Study: Hormat Substation II)" prepared under my guidance by Getahun Shanko Kefeni submitted in partial fulfillment of the requirements for the degree of Masters of Science in Power System Engineering.

Therefore, I recommend the submission of the revised version of the thesis to the department following the applicable procedures.

Dr. Prathibha Ekanthaiah Kotraiah	_____	_____
Major Advisor	Signature	Date

APPROVAL SHEET

I, the advisor of the thesis entitled "Reliability Improvement and Power Loss Reduction in Distribution System (Case Study: Hormat Substation II)" and developed by Getahun Shanko Kefeni, hereby certify that the recommendation and suggestions made by the board of examiners are appropriately incorporated into the final version of the thesis.

Dr. Prathibha Ekanthaiah Kotraiah ____ _____ _____

Major Advisor Signature Date

We, the undersigned, members of the Board of Examiners of the thesis open defense by Getahun Shanko Kefeni have read and evaluated the thesis entitled ''Reliability Improvement and Power Loss Reduction in Distribution System (Case Study: Hormat Substation II) " and examined the candidate during open defense. This is, therefore, to certify that the thesis is accepted for partial fulfillment of the requirement of the degree of Master of Science in Power System Engineering.

_____ _____ _____

Chairperson Signature Date

_____ _____ _____

Internal Examiner Signature Date

_____ _____ _____

External Examiner Signature Date

Finally, approval and acceptance of the thesis is contingent upon the submission of its final copy to the Office of Postgraduate Studies (OPGS) through the Department Graduate Council (DGC) and School Graduate Committee (SGC).

_____ _____ _____

Department Head Signature Date

_____ _____ _____

School Dean Signature Date

_____ _____ _____

Office of Postgraduate Studies, Dean Signature Date

ACKNOWLEDGEMENT

First and foremost, I would like to thank God, for nothing is possible without his will. Secondly, I would like to express my sincere gratitude to my advisor Dr. Prathibha Ekanthaiah Kotraiah for her guidance, and encouragement throughout the thesis. I also express my special thanks to Mr. Mesfin Jarso PhD student at Adama Science and Technology University for his continuous support as respective advisor through my work. I must also express my sincere thanks to the staff of the EEP Hormat substation, and the EEU Ambo district workers, who provided me with numerous valuable data and for their hospitable service.

I would never forget special thanks to my parents; it was never possible without your prayers and support. The tireless prayers of my mother Mrs. Keneni Mamo, and the extraordinary support of my wife Mrs. Kume Desea enabled me to reach this landmark. Without them, I wouldn't be able to complete my thesis. I also express thanks to my kids Bonuskon Getahun, and Kenenuf Getahun for living with constant behavior without disturbing their mother while I am far from them.

TABLE OF CONTENTS

LIST OF TABLES

LIST OF FIGURES

LIST OF ACRONOMYS AND ABBREVATIONS

AENS	Average Energy Not supplied
ASAI	Average Service Availability Index
ASUI	Average Service Unavailability Index
BCBV	Branch Current to Bus Voltage
BIBC	Bus Injection to Branch Current
DG	Distributed Generation
DPEF	Distribution Permanent Earth Fault
DPSC	Distribution Permanent Short Circuit
DTEF	Distribution Temporary Earth Fault
DTSC	Distribution Temporary Short Circuit
EEP	Ethiopian Electric Power
ETAP	Electrical Transient Analysis Program
EENS	Electrical Energy Not Supplied
EEU	Ethiopian Electric Utility
GUI	Graphical User Enter phase
GMR	Geometric Mean Radius
HO	Horizontal Surface
MOPSO	Multi-Objective Particle Swarm Optimization
MATLAB	Matrix Laboratory
MTBF	Mean Time between Failure
MTTF	Mean Time to Failure
MTTR	Mean Time to Repair

OPSDO	Optimal Size of Distributed Generation
RDS	Radial Distribution System
SAIDI	System Average Interruption Duration Index
SAIFI	System Average Interruption Frequency Index

ABSTRACT

The distribution system connects high-voltage transmission networks with end users. Most of the time, power plants are situated distant from the consumer's location. This results a large loss of power in both distribution and transmission systems. However, distribution system losses are typically greater than transmission line side losses. The main objective of this study is to reduce power losses and improve system reliability using Distributed Generation (DG) in the case of Hormat Substation II. Hormat distribution substation II has three feeder lines that provide energy for different customers. From these feeders, the Ambo town feeder has been chosen since it is frequently interrupted. The chosen feeder has been modeled in ETAP software, and simulation results have been done with both ETAP, and MATLAB software, and the results show that the feeder has a power loss of 759.7 KW and 403.5 kVar active and reactive respectively. Additionally, the study has been able to investigate the existing reliability indices of SAIFI, SAIDI, and EENS which has values of 355.0820 f/cust.yr, 335.9636 hr/cust.yr, and 2851.479 MWhr/yr respectively. Multi-Objective Particle Swarm Optimization algorithm have been suggested to decide the best size and position of DG. After renewable distributed Generation penetrated to the network, the real and reactive power loss reduced from 759.7 KW and 403.5 kVar to 412.9 Kw, and 203.12 KVar respectively. Additionally, the SAIFI, SAIDI, and EENS system reliability indices were improved from 355.0820 f/cust.yr, 335.9636 hr/cust.yr, and 2851.479 MWhr/yr to 44.053 f/cust.yr, 55.648 hr/cust.yr, and 460.955MWh/yr respectively. At the end, reliability indices, and line losses before, and after Distributed Generations penetrated to the network have been compared. In general, the simulation results indicate that the suggested method is efficient to maintain system reliability and minimize power losses.

***Keywords**: Distributed Generation, ETAP, MATLAB, MOPSO, Reliability Improvement.*

CHAPTER ONE

1. INTRODUCTION

1.1. Background of the Study

The main function of power system is to deliver electrical energy to the customers adequately and efficiently. In other words, the aim of any power system is to provide reliable and affordable electricity to its users. Without proper planning and maintaining reliability, this power has negative economic effects on both the utility and its customers due to cost of interruptions and power outages (Debrul, 2016).

Uninterruptible and affordable access to electric power is essential for sustained economic growth and the achievement of high standards of living. Any nation's ability to maintain and develop a modern economy and society depends on a reliable power supply. The most crucial aspect of designing and planning distribution systems that should function efficiently with little disruption of customer loads is reliability assessment.

The system's capacity to provide sufficient electrical energy for the intended amount of time under the actual operating conditions can be used to define reliability. The term "power system reliability" includes all facts of the system's ability to satisfy customers load requirement (Manadhar, 2013).

1.2. Geographical information of the research area

Hormat substation II is found in West part of Ethiopia, located in Oromia region west shoa zone nearest to Ambo town. The study area has a latitude and longitude of 8.98 North, and 37.93 East. Hormat substation II is far away from Addis Ababa at a distance of around 130 km, and the substation supplies electric power to Ambo town, Guder town, and Ambo mineral water. Hormat substation II supplies electricity for around 24,628 consumers.

1.3. Statement of the problem

For both utilities and customers, electric distribution systems reliability is important. However, Hormat substation II's outgoing feeders facing repetitive power outages. Due to a number of factors, the frequent power outages at Hormat substation II have become a serious issue. The human factor, shortage power, equipment failure, extreme weather, and tree are the most factors that lead

to distribution system failures. Because of this, all customer i.e. residential, commercial, and industrial sectors are affected with the problem. Power outages are especially difficult to tolerate for industrial sectors, because they result in significant income loss during power outage. Because of this, the reliability of the distribution system has a substantial effect on electricity prices, and satisfaction of the customer. So, in order to enhance utility performance and maintain customer satisfaction, system reliability must be increased. As a result, power distribution companies can reduce costs associated with maintaining and operating distribution systems after a power outage by increasing system reliability.

In this study area, due to population growth, and an increase in the number of people moving from rural to urban areas, the demand for electricity is rapidly increasing. However, the customer's demand for power cannot be met by the available power. As a result, the distribution system become more complicated and its current draw has increased, which brings power losses within the system. This study has been focused on distribution system integration with renewable distributed generation to enhance the current system reliability indices of SAIFI, SAIDI, and EENS are 355.082 f/cust.yr, 335.96 hr/cust.yr, and 2,851.48 MWh/yr respectively in order to minimize these system indices values. To overcome these problems, the study considered Photo Voltaic distributed generation which provides a means to beat incremental increase in energy demand, to improve distribution system reliability and decrease power loss by generating electric power at the distribution system.

1.4. Objectives

1.4.1. General Objective

The main objective of this thesis is to improve reliability, and reduce power loss of distribution substation by integrating distributed generation (DG).

1.4.2. Specific Objectives

The specific objectives of this thesis are: -

- To model and integrate DG to the distribution network by using ETAP software.
- To carry out reliability analysis of the system with optimal placement and size of DGs.
- To examine the impacts of integrating DGs in distribution network, and compare the results before and after DGs integration.

- To estimate cost of Distributed Generation (DG).

1.5. Significance of the study

The study makes a significant contribution to find the best way to lower distribution losses and improve reliability. The following contributions has been included in the research output.

In general, it is believed that this study will be beneficial to both the electric power serving utility, and its customers in;

- ✓ Identifying the primary reasons for power outages and other issues that frequently affect the power distribution system.
- ✓ Enhancing overall system reliability.
- ✓ Preventing the loss of a significant amount of money due to a power outage.
- ✓ Improve the utility and the society's economy.
- ✓ Reduce power supply interruptions.
- ✓ Increase the industrial and commercial sectors.
- ✓ Minimizing distribution losses by allocating DG to the existing network.

1.6. Scope of the study

This research would have focused on studying and analyzing reliability improvement and power loss reduction in the case of Hormat substation II by integrating distributed generation (DG) to the worst case feeder of the distribution network. Among the Hormat substation II feeders, Ambo town feeder was selected, since it has high interruptions, and frequently outage. Additionally, the study examined the substation's current power system reliability issues, and the percentage of improvements that can be realized by integrating distributed generation to the existing. System model was developed by ETAP software.

1.7. Limitation of the study

This work has been restricted to reliability improvement and power loss reduction in the case of Hormat substation II by integrating distributed generation (DG) to the worst case feeder of the distribution network. There is no hardware implementation in this work, because it is expensive, time-consuming, and difficult to find the necessary components. System model and simulation studies was conducted by ETAP, and MATLAB software.

1.8. Organization of the thesis

This thesis organized into five chapters as follows:

A brief background, geographic area of the work, problem statement, objectives, significance, research methodology, scope, and research limitation are covered in Chapter one of the research. Chapter two provides information on the theoretical context and a discussion of various previous works which are related to loss reduction and reliability improvement. Chapter three provides a detailed explanation of the methodology and approaches, starting with a site description, data collection, and analysis. Modeling and simulation of systems were done in Chapter four. Results and discussions have also been conducted in this chapter. Finally, the research's conclusion and recommendations were covered in Chapter five.

CHAPTER TWO

2. LITERATURE REVIEW AND THEORETICAL BACKGROUND

2.1. Introduction

Electrical power is the largest and most complex system, which is a vital element of any modern economy. For economic growth, and development of once country power supply must be available at a fair price. Therefore, the distribution system must be upgraded, and maintained appropriately to meet customer demands. According to a global analysis, around 80% of all customer reliability issues are caused by issues in the distribution system (Mehammed, 2020).

Scheduled and unplanned activities disturb typical working conditions and can cause outages and interruptions. The transmission and distribution system's reliability is assessed using a variety of indicators. The ability to give continuous power for customers at all points of utilization is known as distribution system reliability. In order to achieve power delivery goals and increase customer satisfaction, distribution system reliability is crucial. By reducing the number of interruptions and the length of interruptions, utility profits are generated. For an electrical distribution system, reliability can be interpreted in a variety of ways. These include the availability of the power system and the continuation of services to meet customer demand(Bimrew Sendekie Belay, 2022). There is a logical division of the system reliability into the following two fundamental aspects of the power system.

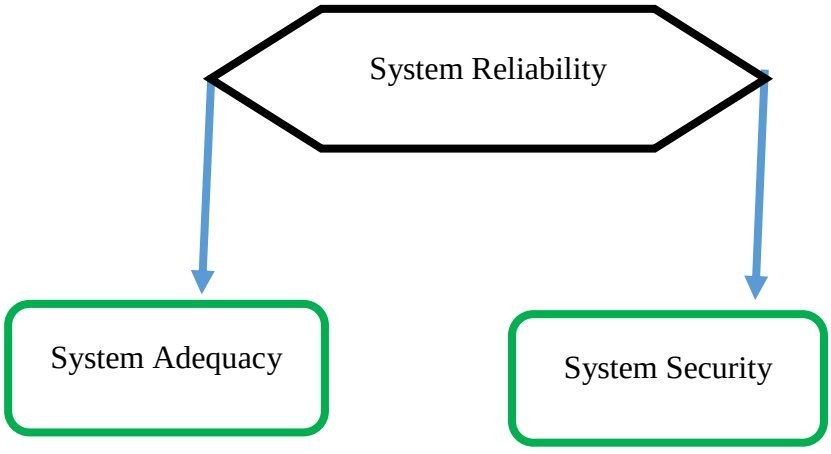

Figure 2.1 Classification of System Reliability

2.2. Electrical Power Distribution Systems

Generating stations, transmission lines, and distribution networks work together to produce and deliver electrical energy to customers in cost-effective, and reliable manner.

To avoid power outages, the distribution system must be carefully designed, and it can be divided into three main categories. They are radial, ring main, and inter-connected.

2.2.1. Radial Distribution Systems

In a radial distribution system (RDS), lateral-branch circuits and sub feeders help primary feeders transport electricity from the distribution substation to the load areas. Due to its simplicity and low cost of construction, this system is the most widely used (Talukdar, 2019). A radial system is vulnerable to numerous interruption possibilities because it is only connected to one source of supply. In comparison to feeders with an alternative supply capability, radial feeders typically have lower reliability. This is the simplest distribution circuit and has the lowest initial cost(Bewketu Getie, 2020).

2.2.2. Ring Main Distribution System

In ring main, the loop circuit starts from the substation bus bars, travels around the area being served, and then returns to the substation. Distribution transformers allow the distributors to be tapped at various locations along the feeder. The main advantage of the ring main system is the consumer terminals less affected by voltage fluctuations.

2.2.3. Inter Connected Distribution System

A system is referred to as interconnected when the feeder node is powered by different generating stations. Through distribution transformers, distributors are connected to the feeder ring points. The benefits of the interconnected system include, any area served by one substation during times of peak load can also be served by the other substation.

2.3. Over View of Distribution System Reliability

Reliability is used to describe a system's capacity to deliver a sufficient amount of electrical energy (Borges & Falcão, 2003). In order to achieve power delivery goals and increase customer satisfaction, distribution system reliability is very important. For an electrical distribution system,

reliability can be interpreted in a variety of ways. These consist of the availability and continuity of services that meet customer demand(Mindaye,2020).

Every system consists of components that determine and show how well it is working. This unique component consists of two different systems: a parallel system and a series system. The type of system will determine the probability that it will perform well and reliably (Braide, 2018).

Parallel System

With this type of system structure, the issue is that reliability increases less quickly as the number of components rises. Two or more components must simultaneously be in an outage state for the system to be disrupted.

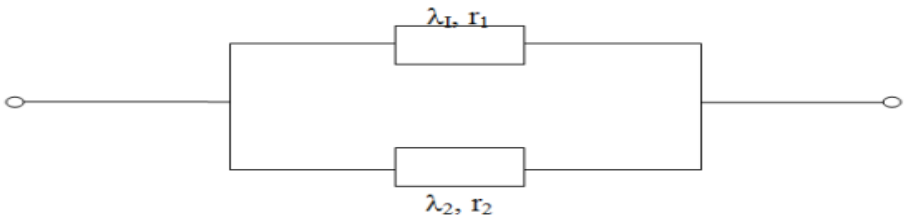

Figure 2.2 Parallel structure(Braide, 2018)

The load point failure modes in this case involve overlapping outages, which means that at least two components must be down simultaneously for a load point to be interrupted, as shown in figure 2.2.

Average failure rate of the system;

$$\lambda p = \frac{\lambda 1 \lambda 2 (r1+r2)}{1+\lambda 1 r1+ \lambda 2 r2} = \lambda 1 \lambda 2 (r1 + r2) \quad (2.1)$$

Where λ1r1, and λ2r2 usually <<1

Average outage time of the system; $rp = \frac{r1 * r2}{r1+r2}$ (2.2)

System average annual outage of time; $\mu p = \lambda p * rp$ (2.3)

Where λ1, and λ2 are the failure rates and r1 and r2 are the outage times for components 1 and 2 respectively.

Series System

This type of system structure cannot exist unless every component is in a functional state. A radial system is made up of a similar series of parts, including circuit breakers, lines, switches, transformers, and "consumers." In the parallel structure, both parts must fail for the system to stop working, whereas in the series structure, both parts must be intact for the system to function normally.

Figure 2.3 Series structure(Braide, 2018)

Here, as observed in figure 2.3, both are connected in series, and these equations are written as follows:

Average failure rate of the system; $\lambda s = \lambda 1 \lambda 2 = \sum_{i=1}^{n} \lambda i$ (2.4)

Average Outage time of the system; $rs = \frac{\lambda 1 r1 + \lambda 2 r2 + \lambda 1 \lambda 2 + r1 r2}{\lambda 1 \, \lambda 2} = \sum \frac{\lambda i ri}{\lambda i}$ (2.5)

Average Annual Outage time; $\mu s = \lambda srs$ (2.6)

Where λi, is the failure rate at node i ri is the outage time at node i.

2.4. Modeling of System Reliability

The reliability indices are commonly used to evaluate the Electric Distribution Network reliability (Jaleel & Abd, 2021), given as follows.

1. Average Failure Rate (λ)

$$\lambda = \frac{\text{Number of outage on component in agiven period}}{\text{Total time component is in operation}} \quad (2.7)$$

2. Mean Time to Failure (MTTF)

The estimated length of time (in years) that the component will remain in a failed state.

$$\text{MTTF} = \frac{1}{\lambda} = \frac{\text{Total system operating ours}}{\text{Amount of failures}} \quad (2.8)$$

3. Mean Time between Failures (MTBF)

MTBF describes the total time the components in operation. As a result, it expressed as;

$$\text{MTBF} = \frac{\text{Total system operation hours}}{\text{Number of failures}} \quad (2.9)$$

4. Mean Time to Repair (MTTR)

It is the amount of time (in hours) needed to restore an element back to working normally. Usually, it is expressed by r. $MTTR = r$

It is the typical amount of time required to locate a failure, fix that failure, and return the component to normal operation. It is defined as

$$\text{MTTR} = \frac{\text{Total Duration of outages}}{\text{Frequency of outages}} = \frac{\text{Total System down time}}{\text{Amount of failures}} \quad (2.10)$$

5. Average Repair Rate (μ):

Mathematically it is the frequency of repair and occurrence per year $\mu = \frac{8760}{\text{MTTR}}$ (2.11)

Availability (U):

The length of time a component is operational at any given time is measured by its availability. It is formulated as;

$$\text{Availability(U)} = \frac{\text{MTBF}}{\text{MTBF+MTTR}} \quad (2.12)$$

$$MTBF = MTTF + MTTR/8760 \quad (2.13)$$

2.5. Reliability Analysis Methods

There are two basic approaches used to evaluating distribution system network. These are analytical methods and the Monte Carlo simulation method (Hegvik, 2012).

2.5.1. Analytical Method of reliability Analysis

A Markov model (analytical method) is one of the techniques used in quantitative reliability analysis and operates with failure frequency (λ), and repair time(r). This approach can be used to

assess the reliability of radial systems using a straightforward mathematical formula (Meteku, 2020).

2.5.2. Numerical Method

The numerical method is another name for the Monte Carlo simulation technique. This method analyzes the system's random behavior using a simulation of a physical relationship. Contrary to analytical methods, this technique may produce reliability indices with average values as well as expected probability distributions. In a Monte Carlo simulation, system states are randomly selected, tested for acceptability, and then their contributions to reliability indices fall below per-specified tolerances (Behailu Abebe, 2015).

2.6. Reliability Indices

The given distribution system reliability has been measured using a variety of reliability indices. The reliability indices represent the sum of the reliability data, which may have been gathered from customers, feeders, or loads. These indices are determined by taking into account the entire distribution system's average duration, frequency, customers number, connected load, and power interruptions. Based on system topology and component failure data, this predicts the future performance of the system (Bewketu Getie, 2020).

Power is delivered via a distribution system from a substation to specific customer load points. The degree of service continuity can be described using three fundamental reliability indices. The average annual unavailability time (U), as well as the load point average failure rate (λ), and average outage time (r). The average failure duration at the load point is the average outage time. The average annual outage time is the sum of all outages experienced at the load point over the year.These reliability indices are expected values and reflect average values over the long term(Bewketu Getie, 2020).

2.6.1. System Reliability Indices

An overall distribution system with system reliability indices can be used to evaluate the overall system performance. In addition to the fundamental reliability indices, system-oriented and energy-oriented reliability indices are needed to fully understanding the system. These system-oriented indices: System Average Interruption Frequency Index (SAIFI), System Average Interruption Duration Index (SAIDI), Customer Average Interruption Duration Index (CAIDI), Average

System Availability Index (ASAI), Average System Unavailability Index (ASUI), and energy oriented indices namely: Energy Not Supplied(ENS), Average System Interruption Frequency Index (ASIFI), Average System Interruption Duration Index (ASIDI) (B. S. et al., 2020).

1. **System Average Interruption Frequency Index (SAIFI)**

This index measures the typical number of sustained customer interruptions encounters in a unit of time (generally 1 year). SAIFI measurement can be calculated as: -

$$\text{SAIFI} = \frac{\text{Number of customers interrupted}}{\text{Number of customers served}} \left(\frac{\text{f}}{\text{cust}}/\text{yr}\right) \tag{2.14}$$

2. System Average Interruption Duration Index (SAIDI)

This index shows the typical number of customer interruptions experiences over the time cycle (1 year). The indices are typically expressed interruption hours per year for customers. It is calculated by dividing the total number of customer interruptions over a year by the total number of customer served. SAIDI measurement is calculated as -

$$\text{SAIDI} = \frac{\text{sum of interruption durations of customers}}{\text{Total number of customer served}} \left(\frac{\text{hr}}{\text{yr}}\right) \tag{2.15}$$

3. Customer Average Interruption Duration Index (CAIDI)

The CAIDI shows the typical amount of time needed to restore the service. It is calculated by dividing the total number of customer sustained interruptions over a one-year period by the total number of customer sustained interruptions.

$$\text{CAIDI} = \frac{\text{sum of customer interrruption durations}}{\text{Total number of customer interruptions}} = \frac{\text{SAIDI}}{\text{SAIFI}} (\text{hr}) \tag{2.16}$$

4. The Average Service Availability Index (ASAI)

ASAI specifies the percentage of time that a customer has power during the predetermined period of time. ASAI is calculated as,

$$\text{ASAI} = \frac{\text{customer hours of available service}}{\text{customer hours demanded}} \tag{2.17}$$

5. Average Service Unavailability Index (ASUI)

ASUI is the percentage of time customers run without electricity over a predetermined period of time. It is stated as,

$$\text{ASUI} = (100\text{-ASAI})\ \% \text{ or ASUI} = \frac{\text{Duration of outage in hourse}}{\text{Total hours demanded}} = \frac{8760-\text{SAIDI}}{8760} = 1 - \text{ASAI} \qquad (2.18)$$

2.6.2. Energy Oriented Reliability Indices

The average load at each load point is one of the most crucial parameters needed for the evaluation of load and energy-oriented indices. The load and energy indices are expressed in the following formula:

1. Energy Not Supplied Index (ENS)

ENS details the typical energy that the customer has not received in the designated time. The failure rate, typical outage duration, and annual unavailability are the three fundamental system indices connected to system load points. This index displays the overall energy that the system is not supplying. And it's provided by,

$$\text{ENS} = \sum \text{La(i) Ui} \qquad (2.19)$$

Where, La (i) is the average load given by:

$$\text{La(i)} = \text{LP(i)} \times \text{LF(i)} = \frac{\text{Ed}}{\text{t}} \qquad (2.20)$$

Where, LP =peak load, Lf =load factor, Ed= average energy and T=time required.

2. Average Energy Not Supplied Index (AENS)

This index represents the typical energy that the system does not supply.

$$\text{AENS} = \frac{\text{Total energy not supplied}}{\text{Total number of customer served}} = \frac{\sum \text{La(i)Ui}}{\sum \text{Ni}} \qquad (2.21)$$

2.7. Reliability Improvement Techniques

In order to achieve better reliability results, it is crucial to implement the mitigation techniques after developing the reliability improvement strategy. Therefore, it is crucial to identify the root cause and apply mitigation strategies. The distribution system is directly impacted by the electrical

mitigation strategies, which also have an impact on the distribution system analysis. These techniques can be done by,

- Install various distributed generation
- Applying distribution system protection
- Decreasing system automation and equipment failure
- FACTS devices usage and etc.

2.7.1. Distributed Generation (DG)

DG is a small-scale power generation technology that connects to consumer loads via a utility's distribution network in order to deliver electricity at a location that is more convenient for customers than a central station generation. A novel method based on renewable energy sources called distributed generation (DG) has the potential to be a vital component of the future electric power system (Fernnandez Sarabia, 2011).

2.7.2. Distributed Generation Technologies

The two types of distributed generation technologies are non-renewable and renewable, which as depicted in figure 2.4. There are various distribution generation technologies in each form (Adefarati And Bansal 2017; Bewketu Getie 2020).

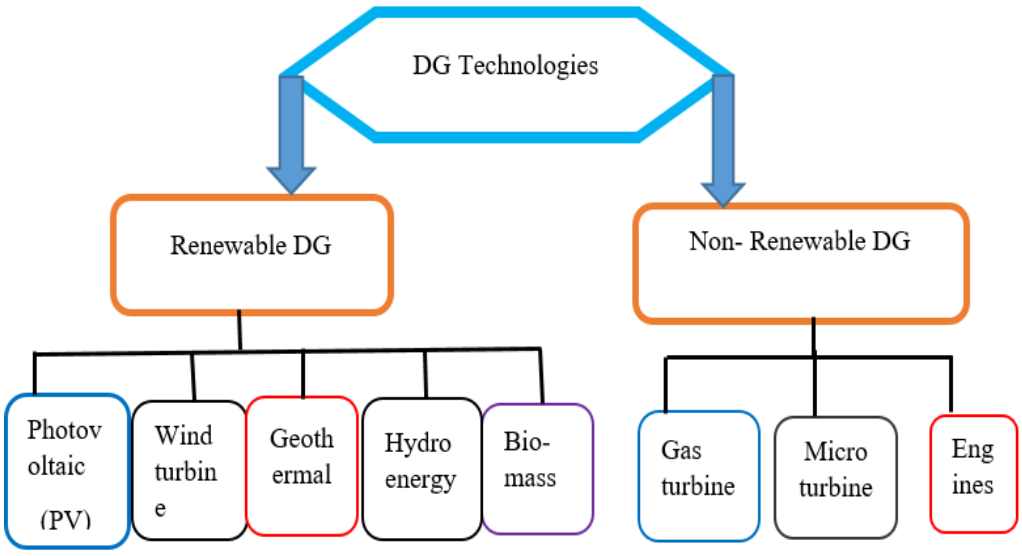

Figure 2.4: Types of DG technologies (by researcher)

A. Non-Renewable DG Technologies

Non-renewable technologies generate energy for various operations using fossil fuels such as natural gas, coal, and petroleum. Non-renewable resources cannot be replaced by natural means and are not sustainable. Due to the high rate of energy demand from non-renewable energy resources and the rate of regenerating them within the Earth, they will eventually run out of use. Reciprocating engines, gas turbines, micro-turbines, and steam turbines are some non-renewable energy sources(Adefarati & Bansal, 2016).

B. Renewable DG Technology

Fuel Cells

Fuel Cells (FC) classified under the category of unconventional generators. They are electro chemical devices that combine oxygen and hydrogen without combustion to convert chemical energy from a fuel directly into electrical energy (Hailemariam, 2018). This electrochemical reaction produces high-current, low-voltage DC power.

Photovoltaic

Photovoltaic (PV) generation is a renewable energy source technology, which converts sunlight directly into electricity. PV based DG systems can be easily integrated into a variety of locations, including, distribution networks, buildings and rooftops. The forward potential drop across the semiconductor p-n junction regulates the generated voltage potential. The surface area and density of the solar power radiation both affect how much current is generated (Hailemariam, 2018).

Wind Turbines

One of the most well-liked renewable energy sources in the world is wind power. A wind farm is typically created by combining several wind turbines that have been integrated to the distribution voltage level. Wind turbines, like PV systems, don't use fuel, emit no emissions, and generate DC power. High initial costs and unpredictable energy production are the main drawbacks of wind turbines. Additionally, they are inappropriate for CHP applications (Hailemariam, 2018).

2.7.3. Benefits of Renewable Distributed Generation on Distribution System

DG is a small-scale power generation technology that is connected to consumer loads and used to generate electricity at a location closer to the consumer than a central station. A novel method based

on renewable energy sources called distributed generation (DG) has great potential in future electrical power. As a result, incentives, flexibility, gas emission free operation, and energy resource recycling make distributed generation the most preferable energy source. Additionally, DG has benefits in terms of economic, technical, and environmental considerations(Adefarati & Bansal, 2016).

A. Impact of Renewable DG in Distribution System Reliability

In order to meet the rising demand for electricity and boost the reliability of the power system, researchers are concentrating on creating distributed generation systems that are practical, affordable, and time-saving. The power system is significantly impacted by distributed generation, which changes the flow of power and reliability factors. The effects of distributed generation on the distribution system's reliability would include increased reliability, financial gains, and reduced environmental pollution. Most of the time distributed generation is placed close to customer premises to achieve maximum reliability improvement, allowing for the most access to customer numbers (Bewketu Getie, 2020).

B. Benefits of DG on Power Loss Reduction

Reducing the system's electrical power losses is one of the main justifications for integrating renewable DG units. If renewable DG units are integrated into the distribution system, the amount of current flowing in the feeders or other areas of the network will be reduced to a specific percentage. The effect of renewable distributed generation (DG) on power losses depends on the DGs size, location, load size, and network configuration(Bewketu Getie, 2020).

C. Economic Benefits of Renewable DG

Since renewable DG is located at or close to load points, the economic benefits of renewable DG penetration can be attained by omitting any investment cost on the distribution and transmission system. Integration of renewable DGs reduces power system losses that should have been transmitted to consumers as high energy costs. The cost of generating electricity must be lower than the cost of selling it for a power plant to be optimally and economically viable (Bewketu Getie, 2020). The benefit-to-cost ratio can be used to estimate the economic benefits of using renewable DG in the distribution system (Maradin et al., 2017).

2.8. Previous Related Works

This work, (Maduforo et al., 2020) analyzed sensitivity based method for optimal placement of distributed generation in order to improving the voltage profile and power loss in the power system network. The study was used Loss sensitivity and Voltage sensitivity index, and it has been concluded that loss reduction in loss sensitivity method is more and it is better in terms of selecting the optimal location for the placement of DG. However, the study does not considered the reliability issue, and investment cost required to install the DG. Again this work does not considered types of DG, and its power factor.

In this study (Hussain et al., 2021), the researchers attempted to increase system efficiency by integrating various DG capacities into a radial distribution feeders. In this case, the outcomes have been mathematically analyzed, and the simulation was taken by ETAP software. The drawback of this work is, it does not considered cost analysis rather than integrating many DG to the network.

This study (Essallah et al., 2018) presents an appropriate method for DG sizing and placement that will reduce line losses, increase voltage profile, and improve system stability. In this work, based on sensitivity methods, the sensitive buses were chosen for optimal DG allocation, and size by using quadratic curve-fitting method. In this case, different DG units has been considered. System modelling and simulation results have been performed by MATLAB/PSAT tool box software. However, this research does not study power system reliability.

The main objective of this study(Rind ++ et al., 2019) was, to find optimal size and placement of solar PV to improve voltage profile at all the nodes, and reduce power losses in radial distribution network using particle swarm optimization algorithm. In this study, two scenarios were taken into account. The integration of a single DG was scenario one, and the integration of two DGs was scenario two. Furthermore, results obtained indicate that adding more DGs improves voltage at each node of the radial distribution network, and lowers losses. But this study does not considered reliability of the system, it only focused on power loss and voltage profile issues.

This paper (Jaleel & Abd, 2021) has performed research on "Reliability Evaluation of Distribution Network with Different Distributed Generators." In this study, by analyzing the reliability models of various DGs, reliability analysis for distribution networks with multiple - types of DG was proposed, and the multi-state model for DG output power was carried out. The simulation results

indicate that the suggested approach is practical, simple, and reliable. In this study, different scenarios were considered with installing three DG's having different sizes. But, Investment cost required to install the DG was not calculated, and also DG type was not taken into account, and also the effect of DG on power losses does not taken into account.

This paper (Hiluf, 2020) used an analytical method based on an outage data obtained from the northern region of electric power utility office, Maychew distribution system reliability was assessed. Five feeders' monthly reliability for 2011E/C was assessed. Generally, the researcher come to the conclusion as the distribution performs poorly. The drawback of this study was, it does not considered the improvement issues rather than analyzing the existing system. In addition to this, only one-year data was analyzed.

This research (Ogunsina et al., 2021) determine the best locations and size of distributed generation in distribution network with ant colony optimization method. The result obtained show that voltage profile, and total power loss of the distribution network was improved significantly with ACO-based approach. Therefore, the researcher suggested that rather than using non-renewable DG source, various types of renewable energy DG sources must be expanded. Therefore, in this case, the integrated DG is not renewable DG source; it was generic DG source.

This study (Idowu et al., 2021) analysis the impact of Distributed Generation on the reliability of distribution system. In this work, five injection substations were used as case studies. With and without DG units, the network's reliability was examined. When DG units were integrated into the network at various locations, the network's reliability increased. The system's reliability was further increased by multiple DG integration into the network close to load points. The drawback of this study is, it does not considered the impact of DGs on power losses, and DG cost was not analyzed.

The study (Hussain et al., 2021) obtained reduced line losses for a radial distribution system by allocating a distributed generator at a specific location. The results show that as DG integration increases, line losses decrease in accordance with load rating. The DG integration is also influenced by the terminal voltage, phase, and synchronization frequency. This study focused only on power loss reduction.

In this study,(Okereafor, F. C.1, Idoniboyeobu, D.C.2, and Bala, 2017) the performance of a 33/11KV substation using distributed generation (DG) units was examined in order to address

issues with power losses and low voltage profiles. In addition to this, injection substation transformers are also upgraded for adequate power flow without overloading the transformers. The analysis ensure that adequate placement of DG and optimal size is investigated and adopted. In general, this research's findings indicated a significant reduction in power losses and voltage stability. But, the study does not consider reliability issues.

This study (Sasi Kumar et al., 2018) focused on reducing power losses and improving the reliability of the Radial Distribution System after it was reconfigured with the placement of Distribution Generation. In this case, the LSF method was used to determine the best switch combinations and DG placements in order to minimize losses. The drawback of this work is, cost to implement is high, because it requires additional switches in addition to multiple DGs. In addition to this, optimal DG sizing and placement was carried out by analytical method.

In this work,(Yadav & Choube, 2021) a placement selection method for DGs was used, with the goal of minimizing power loss. Then, with the placement of 1-DG and 2-DG, the results were obtained. It was concluded that, the placement of the DG was found to have improved the voltage profile and decreased system losses. However, the study does not consider reliability of the system, and also cost analysis of the installed DG was not estimated, DG-type not discussed.

This paper (Aditya Prasad Padhy, 2020)contributes an analytical method allocation and size selection of distributed generations for radially distribution systems. Comparing the proposed technique to other methods, it is computationally faster. Improve voltage profiles at each node and a decrease an overall active power loss was the main objective of this work. In this work, Voltage stability indicator (VSI) was used to identify the loaded bus in the system. The bus with the highest load was chosen as the best location for the DG. The continuous increment of step size (CISS) technique was used to determine the size of the DG at identified location. However, the study does not considered reliability improvement, and also DG placement and sizing was done by analytical method.

This work(Maduforo et al., 2020) provides a sensitivity-based method to allocating distributed generation with the goal of improving voltage profile and reducing power losses to narrow the gap between power produced and required by consumers. In this study, 153 kW DG was assigned to bus 5 using the Loss Sensitivity Method, brings power reduction by 46% and an improve voltage

profile. At each node, the voltage sensitivity index was calculated, and bus 17 was found to have the minimum VSI. In this case, DG sizes were tested at various power factors of 1.0, 0.9, 0.85, and 0.8 in steps of 17.5 kW, ranging from 30 kW to 170 kW. In this study, reliability of the system was not studied, and DG installation cost and type was not taken into account. Additionally, optimal DG placement and sizing must be carefully done with the consideration of different types of DG.

Generally, the above listed literatures explain that reliability improvement of distribution networks with DGs has drawn attention of researchers in power systems engineering. Many researchers have analyzed distribution systems with renewable resources such as solar and wind energy in order to implement these resources in reliability studies. Reliability assessment of distribution system is required for secure and adequacy of power system distribution and minimum operating cost of utility. To evaluate it, the way of reliability evaluation of distribution system and reliability indices plays the major tasks. However, research or review articles reported so far on power reliability improvement did not give a great emphasis to the effect of DGs on power losses in the network. This thesis therefore, gave due attention to the mentioned gap above by considering the impact of DGs on power losses.

Some of the related works have considered optimization of power system distribution network through power loss and voltage stability improvement using different optimization algorithm. However, distribution network optimization (power loss minimization) with considering DGs investment cost is their own gap. In addition, some research has not considered algorithm for DGs placing and sizing rather than using analytical method while penetrating to the distribution network. In order to alleviate the gaps observed in the aforementioned reviews, this thesis work proposed backward forward sweep load flow analysis with particle swarm optimization method to find the optimal size and placement of DGs in radial distribution system for the selected feeder using MATLAB software.

All the above literature has their own gaps as indicated or discussed under each paper reviewed. This research is therefore targeted to fill these gaps by using Multi-Objective Particle Swarm Optimization algorithm. Moreover, no assessment or no any research work has been carried out to address the existing issues on the Hormat substation II so far.

CHAPTER THREE

3. DATA COLLECTION AND ANALYSIS

3.1. Introduction

A complete set of reliability indices, such as SAIFI, SAIDI, CAIDI, ASAI, ASUI, ENS, AENS, etc., describe the reliability of a distribution system. Two years recorded data of interruptions, and other factors are considered for evaluating reliability. The distribution system data that have been gathered and are required for reliability assessment are presented in this chapter.

These data are analyzed to identify the current reliability status of the selected feeder and to identify the main problems of interruption. Generally, the following methodology has been followed in conducting data collection:

Literature review: - Numerous published sources on reliability analysis and power loss minimization have been examined in a variety of books, articles, unpublished papers, and other materials.

Data collection: - In order to complete this thesis, various data have been gathered from National Meteorological Agency, EEU, EEP, and customer utility services.

In this thesis work, the data has been collected through various methods like surveys, observations, personal interviews and technical collection from the site and concerned offices. The collected data include: Interruption data, distribution transformers with their rating, line length between buses, real, and reactive power at each node, conductor type, resistance and reactance of conductor, and sunshine data of the selected area. In case of data collection, QGIS, and RET Screen software is used for conductor impedance determination, and resource available at the selected site respectively.

3.2. Collected Data from Hormat Distribution Substation II

Data from EEU has been gathered for the analysis. Data that was gathered and recorded include fault types, interruptions frequency and duration of outgoing feeders, line data, load data, population size and etc. The gathered data from the substation is data of two years (2021 and 2022). In the context of this study, Hormat distribution substation II has three outgoing feeders namely, Ambo town feeder, Guder town feeder, and Ambo mineral water feeder. Figure 3.1 below shows a single line diagram of Hormat Substation II.

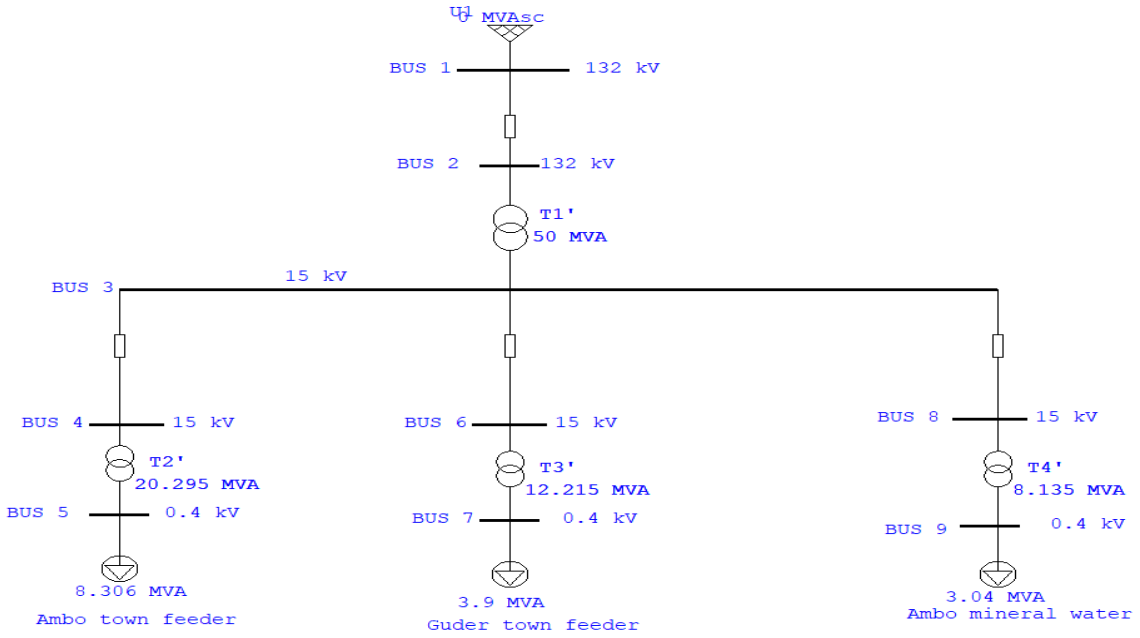

Figure 3.1: Single line diagram of Hormat substation II

All necessary information data was collected from district utility office, substation station, customer service centers, and summarized as follows;

Table 3.1 Overview of Hormat Substation II

Name of Substation	Voltage (kV)	Transformer Number	Transformer Power (MVA)	Incoming Feeder
Hormat	132KV/15KV	1	50	Gedo

In Table 3.2 below, the all low voltage transformers' system loads currently available at work site, and other important data's are listed.

Table 3. 2 Existing system data of Hormat substation II outgoing feeders

S/N	Substation Name	Feeder Name	Number of Distribution Transformers	Transformers (kVA)	Overall number of Customers	Length of feeder (Km)
1	Hormat	Ambo town	88	20,295	12,266	35.25
2	Hormat	Guder town	75	12,215	10,454	67
3	Hormat	Ambo mineral water	28	8,135	1,908	15
Total			**191**	**40,645**	**24,628**	

Table 3.3 General over view of the feeders

Feeder Name	Ambo town	Guder town	Ambo mineral water
Voltage Level (KV)	15	15	15
Peak Load (MW)	8.14	3.9	3.04

Table 3.4 Total capacities and customer's data connected to each transformer of the feeder

S/N	Transformer ID	Rating in (KVA)	Total Customer connected	Peak load (KW)	Peak load (KVAR)
1	DT-012505	200	107	60	45
2	DT-012500	630	437	337.8	253.35
3	DT-012518	315	156	111	83.25
4	DT-012509	25	17	14	10.5
5	DT-012511	200	97	49	36.75
6	DT-012512	200	94	61	45.75
7	DT-012508	200	84	53	39.75
8	DT-012515	100	69	41	30.75
9	DT-012516	100	74	45	33.75
10	DT-012517	50	53	13	9.75
11	DT-012514	25	15	12	9
12	DT-012519	50	30	9	6.25
13	DT-012520	100	60	45	33.75

14	DT-012521	100	65	33	24.75
15	DT-012522	100	68	25	18.75
16	DT-012473	315	172	123.6	92.7
17	DT-012479	630	470	363	272.25
18	DT-010481	315	164	117.3	87.9
19	DT-012480	200	104	69	51.75
20	DT-012481	100	73	31	23.25
21	DT-012483	315	180	129.9	97.4
22	DT-012484	200	114	77	57.75
23	DT-012485	50	37	15	11.25
24	DT-012486	100	45	21	15.75
25	DT-012491	315	226	153.3	114.9
26	DT-012492	315	375	287	215.25
27	DT-012493	50	32	11	8.25
28	DT-012494	315	374	286.6	214.95
29	DT-012495	315	405	311.4	233.55
30	DT-012496	630	641	487.4	365.55
31	DT-012497	100	40	17	12.75
32	DT-012498	25	16	13	9.75
33	DT-012499	100	62	35	26.25
34	DT-012506	315	250	186.2	139.65
35	DT-012501	315	361	261.8	196.35
36	DT-012502	315	297	244.4	168.3
37	DT-012503	800	397	305	228.75
38	DT-012504	315	195	142.5	106.8
39	DT-012676	100	42	17	12.75
40	DT-012808	50	38	16	12
41	DT-012809	630	406	212.6	134.45
42	DT-012810	315	211	155	116.3

43	DT-012811	800	317	241	180.75
44	DT-012812	200	124	85	63.75
45	DT-012813	100	70	27	20.25
46	DT-012814	315	148	104.7	78.5
47	DT-012815	50	25	20	15
48	DT-012816	25	12	10	7.5
49	DT-012818	200	134	93	69.75
50	DT-012819	315	159	98.4	93.8
51	DT-012820	315	133	92	69
52	DT-012822	100	37	15	11.25
53	DT-012824	200	74	45	33.75
54	DT-012825	100	47	23	17.25
55	DT-012859	315	135	79.5	59.6
56	DT-012866	200	69	41	30.75
57	DT-012867	315	102	66.9	50
58	DT-012827	200	60	33	24.75
59	DT-012828	200	144	101	75.75
60	DT-012831	25	14	11	8.25
61	DT-012832	315	245	167.7	127.7
62	DT-012833	315	188	123.2	92.15
63	DT-012834	50	22	18	13.5
64	DT-012835	200	69	41	30.75
65	DT-012840	100	85	39	29.25
66	DT-012843	630	344	162.2	96.6
67	DT-012845	200	213	157	117.75
68	DT-012868	200	243	181	135.75
69	DT-012870	200	228	169	126.75
70	DT-012873	315	174	111	83.25
71	DT-012875	25	11	9	6.75

72	DT-012876	100	72	43	32.25
73	DT-012869	200	55	29	21.75
74	DT-012890	200	50	25	18.75
75	DT-012891	100	48	9	6.75
76	DT-123444	315	109	73.2	54.9
77	DT-008296	25	10	8	6
78	DT-008297	100	25	20	15
79	DT-057323	315	94	60.6	45.45
80	DT-057336	315	96	48	36
81	DT-057337	315	86	54.3	40.7
82	DT-057412	315	78	48	36
83	DT-057413	200	60	33	24.75
84	DT-076500	100	35	13	9.75
85	DT-076501	630	331	137	77.75
86	DT-075230	200	95	61.8	46.35
87	DT-076470	100	25	20	15
88	DT-076471	200	211	155	116.25

3.2.1. Impedance Calculation of Overhead Medium Line

Type and length of conductor used is the primary data needed for this study. The stranded conductor types used in the Ambo town feeder are $AAC - 50mm^2$, and $AAC - 95mm^2$. Hence, dividing the impedance per kilometer by the length of the line, positive sequence impedances for the line sections are calculated.

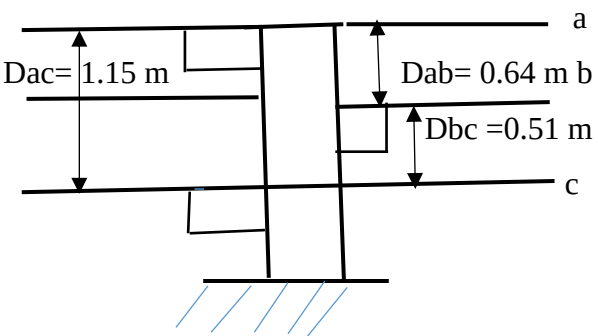

Figure 3.2 Overhead conductor arrangement (by researcher)

Table 3.5 Overhead medium voltage conductor size

Conductor type	Nominal area (mm^2)	Actual area (mm^2)	Wire diameter and Strand	Over all diameter (mm)	Actual diameter (mm)	Resistance (Ω/km)	GMR (mm)
AAC-50	50	49.48	7/3	9	7.9377	0.5785	2.88
AAC-95	95	93.27	19/2.5	12.5	10.8975	0.3085	4.129

The parameters of the overhead conductors are listed in Table 3.6 below; the conductor resistances were taken from the standard overhead conductor data sheet, and Equation 3.1 given below is used to calculate the GMRs.

GMR for stranded conductors is defined as:

GMR = k. r (3.1)

Where: k = GMR factor, and r = actual conductor radius.

Table 3.6 GMR factor (k) and strand relationship for AAC conductor

Strands	1(solid)	3	7	19	37	61
GMR factor(k)	0.7788	0.6778	0.7256	0.7577	0.7678	0.7722

By having the above given data, mutual and self-impedances are given by:

$$Zii = ri + j0.062832ln\frac{1}{\text{GMRi}}\ \Omega/km \quad (3.2)$$

$$Zij = j0.062832ln\frac{1}{\text{Dji}}\ \Omega/km \quad (3.3)$$

Where: Zii = conductor's self-impedance in ohm per kilometers.

Zij = mutual impedance between conductors i and j in ohm per kilometers

ri = conductor resistance in per kilometers, and

Dij= is the measured distance between conductors i and j.

From Table 3.6 and applying Equations 3.2 and 3.3, results the following.

1. The self-impedance for phase conductors of AAC-95mm^2 conductor type

$$Zaa = ra + 0.049348 + j0.062832\ln(\frac{1}{\text{GMRa}} + 6.837026)\ \Omega/km \quad (3.4)$$

$$Zaa = 0.3085 + 0.049348 + j0.062832\ln(\frac{1}{0.004129} + 6.837026\ )\Omega/km$$

$$Zaa = 0.357848 + j0.774514\ \Omega/km$$

$$Zaa = Zbb = Zcc$$

Applying Equation 3.3, mutual impedances can be calculated as follows,

$$Zab = 0.049348 + j0.062832\ln(\frac{1}{\text{Dab}} + 6.837026)\ \Omega/km \quad (3.5)$$

$$Zab = 0.049348 + j0.062832\ln(\frac{1}{0.64} + 6.837026)\ \Omega/km$$

$$Zab = 0.049348 + j0.457625\ \Omega/km$$

$$Zac = 0.049348 + j0.062832\ln(\frac{1}{\text{Dac}} + 6.837026)\ \Omega/km \quad (3.6)$$

$$Zac = 0.049348 + j0.062832\ln(\frac{1}{1.15} + 6.837026)\ \Omega/km$$

$$Zac = 0.049348 + j0.420802\ \Omega/km$$

$$Zbc = 0.049348 + j0.062832\ln(\frac{1}{\text{Dbc}} + 6.837026)\ \Omega/km \quad (3.7)$$

$$Zbc = 0.049348 + j0.062832\ln(\frac{1}{0.51} + 6.837026)\ \Omega/km$$

$$Zbc = 0.049348 + j0.471892\ \Omega/km$$

Using Equations 3.4–3.7, the positive sequence impedance can be calculated. The self - impedance is:

$$Zs = \frac{1}{3}(Zaa + Zbb + Zcc)\Omega/km \quad (3.8)$$

$$= (0.357748+\text{j } 0.774514)\ \Omega/km$$

Mutual impedance is:

$$Zm = \frac{1}{3}(Zab + Zbc + Zac)\Omega/km \quad (3.9)$$

$$= \frac{1}{3}((0.049348 + j0.457625) + (\ 0.049348 + j0.471892) + (0.049348 + j0.420802))\Omega/km$$

$$= 0.049348 + \text{j}0.450106\ \Omega/km$$

Positive sequence impedance (+Z) of $\text{AAC} - 95$ is obtained as:

$$Z+= \text{Zs} - \text{Zm}\ \Omega/km \quad (3.10)$$

$$Z+= (0.357748 + \text{j } 0.774514) - (0.049348\ +\ \text{j}0.450106\ )\ \Omega/km$$

$$= \ 0.3085+\text{j}0.3244\ \Omega/km$$

2. For AAC-50mm^2 conductor type

To obtain the impedance of the feeder for AAC-50 conductor type, the same process and equations are used as in AAC-95.

$$Z+= \text{Zs} - \text{Zm}\ \Omega/km \quad (3.11)$$

$$Z+= \text{Zs} - \text{Zm}\ \Omega/km$$

= (0.627848+j0.797149) – (0.049348+j0.450140) Ω/km

= 0.5785+j0.3470 Ω/km

Finally, the line impedance (resistance, and reactance) were calculated and tabulated in Table 3.7 given below.

Table 3.7: Calculated line and load data of the selected feeder

S/N	Sending end	Receiving end	Conductor type	Length (Km)	Resistance (Ω)	Reactance (Ω)	Pload (Kw)	Qload (Kvar)
1	1	2	AAC-95(mm^2)	2.7	0.8329	0.87588	0	0
2	1	3	AAC-95(mm^2)	0.15	0.0463	0.0487	337.8	253.35
3	2	4	AAC-95(mm^2)	0.65	0.2	0.21	111	83.25
4	4	5	AAC-95(mm^2)	0.05	0.0154	0.0162	0	0
5	5	6	AAC-95(mm^2)	0.1	0.031	0.0324	0	0
6	5	7	AAC-95(mm^2)	0.5	0.1543	0.1622	0	0
7	7	8	AAC-95(mm^2)	0.5	0.1543	0.1622	0	0
8	8	9	AAC-95(mm^2)	0.5	0.1543	0.1622	305	228.75
9	8	10	AAC-95(mm^2)	0.3	0.0926	0.0973	0	0
10	10	11	AAC-95(mm^2)	0.1	0.031	0.0324	0	0
11	11	12	AAC-95(mm^2)	0.3	0.0926	0.0973	16	12
12	12	13	AAC-95(mm^2)	0.35	0.1079	0.1135	0	0
13	13	14	AAC-95(mm^2)	0.15	0.0463	0.0487	0	0
14	14	15	AAC-95(mm^2)	0.1	0.031	0.0324	27	20.25
15	14	16	AAC-95(mm^2)	0.1	0.031	0.0324	0	0
16	16	17	AAC-95(mm^2)	0.05	0.0154	0.0162	20	15
17	16	18	AAC-95(mm^2)	0.05	0.0154	0.0162	0	0
18	18	19	AAC-95(mm^2)	0.1	0.031	0.0324	0	0
19	18	20	AAC-95(mm^2)	0.25	0.0771	0.0811	0	0
20	20	21	AAC-95(mm^2)	0.05	0.0154	0.0162	0	0
21	20	22	AAC-95(mm^2)	0.35	0.1079	0.1135	0	0

22	7	23	AAC-95(mm^2)	0.05	0.0154	0.0162	79.5	59.6
23	23	24	AAC-95(mm^2)	0.15	0.0463	0.0487	0	0
24	23	25	AAC-95(mm^2)	0.05	0.0154	0.0162	29	21.75
25	25	26	AAC-95(mm^2)	0.05	0.0154	0.0162	25	18.75
26	26	27	AAC-95(mm^2)	0.15	0.0463	0.0487	0	0
27	26	28	AAC-95(mm^2)	0.7	0.216	0.2271	73.2	54.9
28	28	29	AAC-50(mm^2)	0.3	0.1736	0.1041	0	0
29	28	30	AAC-50(mm^2)	0.45	0.26	0.156	60	45
30	30	31	AAC-50(mm^2)	0.2	0.116	0.069	14	10.5
31	30	32	AAC-50(mm^2)	0.1	0.05785	0.0347	25	18.75
32	32	33	AAC-50(mm^2)	0.25	0.1446	0.0868	142.5	106.8
33	33	34	AAC-50(mm^2)	0.05	0.0289	0.0174	17	12.75
34	34	35	AAC-50(mm^2)	0.05	0.0289	0.0174	312.6	234.45
35	35	36	AAC-50(mm^2)	0.05	0.0289	0.0174	104.7	78.5
36	35	37	AAC-50(mm^2)	0.25	0.1446	0.0868	10	7.5
37	37	38	AAC-50(mm^2)	0.2	0.116	0.069	93	69.75
38	37	39	AAC-50(mm^2)	0.15	0.0868	0.0521	98.4	93.8
39	36	40	AAC-50(mm^2)	0.15	0.0868	0.0521	92	69
40	40	41	AAC-50(mm^2)	0.1	0.05785	0.0347	9	67.5
41	40	42	AAC-50(mm^2)	0.05	0.0289	0.0174	15.5	11.625
42	42	43	AAC-50(mm^2)	0.3	0.1736	0.1041	0	0
43	43	44	AAC-50(mm^2)	0.25	0.1446	0.0868	49	36.75
44	44	45	AAC-50(mm^2)	0.2	0.116	0.069	61	45.75
45	44	46	AAC-50(mm^2)	0.35	0.2025	0.1215	53	39.75
46	46	47	AAC-50(mm^2)	0.3	0.1736	0.1041	41	30.75
47	46	48	AAC-50(mm^2)	0.1	0.05785	0.0347	45	33.75
48	47	49	AAC-50(mm^2)	0.15	0.0868	0.0521	0	0

49	46	50	AAC-50(mm^2)	0.4	0.2314	0.1388	13	9.75
50	33	51	AAC-50(mm^2)	0.2	0.116	0.069	0	0
51	51	52	AAC-50(mm^2)	0.1	0.05785	0.0347	12	9
52	51	53	AAC-50(mm^2)	0.3	0.1736	0.1041	0	0
53	53	54	AAC-50(mm^2)	0.1	0.05785	0.0347	9	6.25
54	54	55	AAC-50(mm^2)	0.2	0.116	0.069	0	0
55	54	56	AAC-50(mm^2)	0.1	0.05785	0.0347	45	33.75
56	56	57	AAC-50(mm^2)	0.15	0.0868	0.0521	33	24.75
57	57	58	AAC-50(mm^2)	0.35	0.2025	0.1215	0	0
58	25	59	AAC-50(mm^2)	0.35	0.2025	0.1215	123.6	92.7
59	59	60	AAC-50(mm^2)	0.4	0.2314	0.1388	0	0
60	60	61	AAC-50(mm^2)	0.25	0.1446	0.0868	363	272.25
61	60	62	AAC-50(mm^2)	0.05	0.0289	0.0174	0	0
62	62	63	AAC-50(mm^2)	0.4	0.2314	0.1388	117.3	87.9
63	62	64	AAC-50(mm^2)	0.2	0.116	0.069	69	51.75
64	64	65	AAC-50(mm^2)	0.05	0.0289	0.0174	0	0
65	65	66	AAC-50(mm^2)	0.05	0.0289	0.0174	0	0
66	65	67	AAC-50(mm^2)	0.05	0.0289	0.0174	17	12.75
67	67	68	AAC-50(mm^2)	0.15	0.0868	0.0521	13	9.75
68	68	69	AAC-50(mm^2)	0.2	0.116	0.069	0	0
69	68	70	AAC-50(mm^2)	0.2	0.116	0.069	35	26.25
70	70	71	AAC-50(mm^2)	0.25	0.1446	0.0868	186.2	139.65
71	70	72	AAC-50(mm^2)	0.5	0.2893	0.1735	261.8	196.35
72	67	73	AAC-50(mm^2)	0.2	0.116	0.069	244.4	168.3
73	73	74	AAC-50(mm^2)	0.25	0.1446	0.0868	31	23.25
74	74	75	AAC-50(mm^2)	0.55	0.3182	0.191	129.9	97.4
75	74	76	AAC-50(mm^2)	0.05	0.0289	0.0174	0	0

76	76	77	AAC-50(mm^2)	0.15	0.0868	0.0521	0	0
77	77	78	AAC-50(mm^2)	0.15	0.0868	0.0521	77	57.75
78	77	79	AAC-50(mm^2)	0.05	0.0289	0.0174	15	11.25
79	79	80	AAC-50(mm^2)	0.1	0.05785	0.0347	0	0
80	80	81	AAC-50(mm^2)	0.15	0.0868	0.0521	21	15.75
81	80	82	AAC-50(mm^2)	0.15	0.0868	0.0521	0	0
82	79	83	AAC-50(mm^2)	0.05	0.0289	0.0174	153.3	11.49
83	83	84	AAC-50(mm^2)	0.2	0.116	0.069	0	0
84	83	85	AAC-50(mm^2)	0.05	0.0289	0.0174	287	21.525
85	85	86	AAC-50(mm^2)	0.1	0.05785	0.0347	0	0
86	86	87	AAC-50(mm^2)	0.25	0.1446	0.0868	286.6	214.95
87	87	88	AAC-50(mm^2)	0.1	0.05785	0.0347	0	0
88	85	89	AAC-50(mm^2)	0.05	0.0289	0.0174	11	8.25
89	89	90	AAC-50(mm^2)	0.05	0.0289	0.0174	487.4	365.55
90	90	91	AAC-50(mm^2)	0.1	0.05785	0.0347	0	0
91	91	92	AAC-50(mm^2)	0.05	0.0289	0.0174	155	11.63
92	92	93	AAC-50(mm^2)	0.25	0.1446	0.0868	0	0
93	93	94	AAC-50(mm^2)	0.3	0.1736	0.1041	241	180.75
94	94	95	AAC-50(mm^2)	0.25	0.1446	0.0868	85	63.75
95	94	96	AAC-50(mm^2)	0.15	0.0868	0.0521	15	11.25
96	96	97	AAC-50(mm^2)	0.1	0.05785	0.0347	0	0
97	97	98	AAC-50(mm^2)	0.15	0.0868	0.0521	23	17.25
98	98	99	AAC-50(mm^2)	0.35	0.2025	0.1215	41	30.75
99	93	100	AAC-50(mm^2)	0.25	0.1446	0.0868	0	0
100	100	101	AAC-50(mm^2)	0.15	0.0868	0.0521	262.2	196.6
101	101	102	AAC-50(mm^2)	0.35	0.2025	0.1215	0	0
102	91	103	AAC-50(mm^2)	0.5	0.2893	0.1735	157	117.75

103	103	104	AAC-50(mm^2)	0.2	0.116	0.069	181	135.75
104	104	105	AAC-50(mm^2)	0.4	0.2314	0.1388	0	0
105	104	106	AAC-50(mm^2)	0.25	0.1446	0.0868	169	126.75
106	106	107	AAC-50(mm^2)	0.1	0.05785	0.0347	111	83.25
107	107	108	AAC-50(mm^2)	0.25	0.1446	0.0868	66.9	50
108	107	109	AAC-50(mm^2)	0.1	0.05785	0.0347	0	0
109	89	110	AAC-50(mm^2)	0.45	0.2603	0.1562	0	0
110	110	111	AAC-50(mm^2)	0.4	0.2314	0.1388	33	24.75
111	111	112	AAC-50(mm^2)	0.05	0.0289	0.0174	101	75.75
112	111	113	AAC-50(mm^2)	0.05	0.0289	0.0174	11	8.25
113	110	114	AAC-50(mm^2)	0.2	0.116	0.069	167.7	127.7
114	114	115	AAC-50(mm^2)	0.35	0.2025	0.1215	136.2	102.15
115	115	116	AAC-50(mm^2)	0.05	0.0289	0.0174	18	13.5
116	116	117	AAC-50(mm^2)	0.15	0.0868	0.0521	41	30.75
117	116	118	AAC-50(mm^2)	0.05	0.0289	0.0174	39	29.25
118	118	119	AAC-50(mm^2)	0.25	0.1446	0.0868	0	0
119	119	120	AAC-50(mm^2)	0.15	0.0868	0.0521	9	6.75
120	119	121	AAC-50(mm^2)	0.05	0.0289	0.0174	43	32.25
121	121	122	AAC-50(mm^2)	0.2	0.116	0.069	8	6
122	122	123	AAC-50(mm^2)	0.2	0.116	0.069	20	15
123	123	124	AAC-50(mm^2)	0.05	0.0289	0.0174	0	0
124	124	125	AAC-50(mm^2)	0.2	0.116	0.069	0	0
125	125	126	AAC-50(mm^2)	0.05	0.0289	0.0174	48	36
126	126	127	AAC-50(mm^2)	0.45	0.2603	0.1562	60.6	45.45
127	123	128	AAC-50(mm^2)	0.05	0.0289	0.0174	54.3	40.7
128	128	129	AAC-50(mm^2)	0.1	0.05785	0.0347	0	0
129	128	130	AAC-50(mm^2)	0.35	0.2025	0.1215	48	36

130	130	131	AAC-50(mm^2)	0.25	0.1446	0.0868	0	0
131	130	132	AAC-50(mm^2)	0.05	0.0289	0.0174	33	24.75
132	132	133	AAC-50(mm^2)	0.2	0.116	0.069	0	0
133	132	134	AAC-50(mm^2)	0.5	0.2893	0.1735	13	97.5
134	134	135	AAC-50(mm^2)	0.15	0.0868	0.0521	337	177.75
135	134	136	AAC-50(mm^2)	0.2	0.116	0.069	0	0
136	136	137	AAC-50(mm^2)	0.25	0.1146	0.0868	61.8	46.35
137							20	15

3.2.2. Factors that Causes Power Outages in the Hormat Substation II

Earth faults, and short circuits are the most common major faults in Hormat substation II. Additionally, scheduled interruptions occur for maintenance and operational reasons. The main faults that are present can be either momentary or sustained in nature. There are two types of interruptions: planned and unplanned interruptions. Construction, preventative maintenance, and repairs are the main reasons for planned interruptions (also known as operational outages). When an interruption is planned, it happens at a less disruptive time for the customers and they are informed in advance. Unplanned interruptions can occur for a variety of reasons, such as the clearing of faults, unintended the protective system operating, or an unintended human action causing a switching device to open.

Distribution Earth fault

A conducting connection between an electric conductor and a material that is grounded or has the potential to become grounded results distribution earth fault. In a ground fault, electricity travels to the ground along a path that was not intended for it, like through a person's body.

The earth fault is a plant engineering issue that results from insulating loss between an exposed conductive portion and a live conductor. It may result total damage.

Distribution Short Circuit

The most frequent description of a power outage's root cause is short circuit. It happens when an electrical current flows through a circuit in a different direction than it was intended to. This results in an excessive electric current that can damage circuits and cause fires and explosions. In actuality,

short circuits are among the main reasons for electrical fires all over the world. Additionally, it happens when the wiring's insulation fails.

3.2.3. Power Interruption Data

Interruptions frequently happen as the system responds to a fault. Ambo distribution system are faced by earth faults and short circuits. These faults can be divided into two categories: temporary faults and permanent faults. The majority of faults in distribution systems are temporary(Arram et al., 2015). As shown in Tables 3.8 below, the collected interruption data are condensed for two years of annual power outages with full frequency and duration interruption.

Table 3.8: Frequency and duration of interruptions at the selected site

Year	Name of feeder	Reason of interruptions										Total interruption (Forced+op)	
		DPEF		DPSC		DTEF		DTSC		OP			
		F	D(H)	F	D(H)	F	D(H)	F	D(H)	F	D(H)	F	D(H)
2021	Ambo water	2	17.55	36	68.13	6	1.89	24	13.58	43	68.06	111	169.31
	Ambo town	17	27.32	78	108.76	17	21.05	98	33.36	113	89.43	323	279.92
	Guder	20	41.32	95	130.48	15	13.29	79	13.69	78	74.58	287	263.36
2022	Ambo water	17	32.41	28	51.11	4	0.25	17	4.65	86	136.31	152	224.73
	Ambo town	33	71.03	119	143.84	35	31.85	76	39.17	124	108.08	387	393.97
	Guder	64	95.16	162	221.12	17	1.53	34	2.63	78	56.84	355	377.28
Av. 2021 and 2022	Ambo water	9.5	24.98	32	59.62	5	1.07	20.5	9.115	64.5	102.185	131.5	197.02
	Ambo town	25	49.175	98.5	126.3	26	26.45	87	36.265	118.5	98.755	355	336.945
	Guder	42	68.24	128.25	175.8	16	7.41	56.5	8.16	78	65.71	321	320.32

According to Table 3.8 above, the frequency and duration of interruptions for Ambo mineral water and Guder town feeders are less frequent and shorter than Ambo town feeder. In other words, Ambo town feeder is more frequent and longer duration interruptions than others.

Due to the time and its complexity, the study is restricted on one feeder. Out of the mentioned feeders above, Ambo town feeder has been chosen for my study of reliability evaluation in this thesis. Because this feeder service many government, and non-government universities, Hospitals, factories, and different commercial centers in addition to domestic customers. And also this feeder has high frequency and duration of interruptions as compared with other feeders of the substation.

Table 3.9: Ambo town feeder interruption data in 2021

Year.	Name of feeder	Main reason of interruptions										Total interruption (Forced+op)	
		DPEF		DPSC		DTEF		DTSC		OP			
2021		F	D(H)	F	D(H)	F	D(H)	F	D(H)	F	D(H)	F	D(H)
	Ambo town	17	27.32	78	108.76	17	21.05	98	33.36	113	89.43	323	279.92

According to Table 3.9, the main causes of interruptions in the distribution system are short circuit faults and operational needs. Earth faults and short circuit faults are the major types of faults that frequently happen in this distribution system.

Table 3.10 Ambo town feeder interruption data in 2022

Year.	Name of feeder	Main reason of interruptions										Total interruption (Forced+op)	
		DPEF		DPSC		DTEF		DTSC		OP			
2022		F	D(H)	F	D(H)	F	D(H)	F	D(H)	F	D(H)	F	D(H)
	Ambo town	33	71.03	119	143.84	35	31.85	76	39.17	124	108.08	387	393.97

According to Table 3.10, the duration and frequency of interruptions in the Ambo town feeder were high in 2022. The duration and frequency of interruptions were relatively lower in 2021.

From Table 3.9 and Table 3.10 the average interruption duration and frequency of the two years' period by taking the contribution of each type of faults can be calculated.

Table 3. 11 Average interruption frequency and duration of Ambo feeder in year 2021 and 2022

Year.	Name of feeder	Main reason of interruptions										Total interruption (Forced+op)	
Av. 2021& 2022		DPEF		DPSC		DTEF		DTSC		OP			
		F	D(H)	F	D(H)	F	D(H)	F	D(H)	F	D(H)	F	D(H)
	Ambo town	25	49.175	98.5	126.3	26	26.45	87	36.265	118.5	98.755	355	336.945

Based on Table 3.11, it is possible to determine percentage contribution that each type of interruptions on duration and frequency over the two years' period, and tabulated as Table 3.12, and Table 3.13 below.

Table 3.12 Percentage contribution of each type of outages in frequency and duration

	DPEF		DPSC		DTEF		DTSC		OP	
Percentage frequency & duration	F	D(H)	F	D(H)	F	D(H)	F	D(H)	F	D(H)
	7.0423	14.6	27.75	37.484	7.32	7.85	24.51	10.763	33.38	29.31

Table 3.12 Shows that the types of outages due to short circuits (both permanent and temporary), and operation is taking larger percentage when compared to earth faults.

Table 3.13 Percentage of outages in terms of frequency in two years

	DPEF	DPSC	DTEF	DTSC	OP
% frequency	7.0423	27.75	7.32	24.51	33.38

As observed from the Table 3.13, 52.25% (27.75% + 24.5%) Int. /year of the interruption frequency is due the short circuit (both temporary and permanent), 33.38% is due to operation, and 14.36% due to earth fault.

Table 3.14 Percentage of outages in terms of duration over two years

	DPEF	DPSC	DTEF	DTSC	OP
% duration	14.6	37.484	7.85	10.763	29.31

According to Table 3.14, 48.24% (hr. /year) of the interruption duration is due the short circuit, 29.3% is due to operation, and 22.45% due to earth fault.

3.3. Solar Power Resource Assessment

Before installing a solar panel at a specific location, it is advisable to investigate the viability of solar power-based DG installation on the selected area. PV cells must be able to produce energy during the hours of sunlight and solar irradiation. Therefore, daylight hour was taken into account during design and according to (Gana & Akpootu, 2013), it has to be between 4-6 Kwh/m²/day. The national meteorology Agency of Ethiopia records the Ambo site's sunshine hour, and the data obtained is tabulated in Table 3.15 given below.

Table 3.15 Monthly average sunshine data of Ambo site (National Meteorology Agency)

Year	**Month**											
	Jan	**Feb**	**Mar**	**Apr**	**May**	**Jun**	**Jul**	**Aug**	**Sep**	**Oct**	**Nov**	**Dec**
2016	11.5	8.8	7.5	6.4	6.5	4.7	3.9	3.6	5.1	8.4	9.1	8.2
2017	10.5	7.9	8.1	7.5	5.8	4.6	3.7	3.8	4.5	8.2	8.9	8.9
2018	10.8	8.2	7.6	6.9	8.2	5.2	4.2	4.2	6.5	7.8	7.9	9.9
2019	10.2	9	7.9	7.6	8.4	4.8	3.9	3.9	4.1	8.7	8.1	7.5
2020	10.6	8	7.6	6.9	6.4	5.3	3.8	4.1	4.9	8.8	9.7	9.9
2021	10.3	8.3	8.4	6.5	7.4	6.1	4.6	4.3	4.7	8.5	8.7	9.8
2022	10.5	8.8	8.6	7.2	7.3	5.8	5.1	4.7	5.2	8.9	9.5	9.7
Aver.	**10.62**	**8.43**	**7.95**	**7.26**	**7.14**	**5.21**	**4.17**	**4.1**	**5.18**	**8.47**	**8.84**	**9.13**

According to Table 3.15 above, the monthly average sunshine hour is sufficient for solar power design. The monthly solar radiation of the site is determined using a variety of methods. Among those several models, the Angstrom-Prescott estimating model is the most commonly used and preferable method (Gana & Akpootu, 2013). The original regression formula for the Angstrom-Prescott type, which considers the daily radiation averaged over a month to clear day radiation in a specific place and the average proportion of potential hours of sunshine is given in equation (3.12) below:

$$\frac{H}{Ho} = a + b(\frac{S}{So}) \tag{3.12}$$

Where, H -is the daily average global radiation on the horizontal surface in (Kwh/m² /day), HO-average monthly extraterrestrial radiation of the horizontal surface (Kwh/m² /day), S-average monthly daily sunshine hour. So - average daily length for the month, and 'a' and 'b' are the Angstrom constants. Equation 3.13 below used to compute the average daily extraterrestrial radiation of the horizontal surface (HO).

$$Ho = \left(\frac{24}{\pi}\right) Isc \left[1 + 0.033Cos\left(\frac{360n}{365}\right)\right] * [Cos\varphi \text{Cos}\delta \text{Sin}\omega s + (\frac{2\pi\omega s}{360})Sin\varphi \text{Sin}\delta \tag{3.13}$$

Where, Isc- solar constant having 1367 W/m^2, φ- is selected site latitude, δ- solar declination, ωs - average sunrise hour angle for the given month, and n- is the number of days of the year starting from January. The solar declination (δ) and average sunrise hour angle (ωs) can be calculated by equation (3.14) and (3.15) respectively (Gana & Akpootu, 2013):

$$\delta = 23.45Sin\left(360\frac{284+n}{365}\right) \tag{3.14}$$

$$\omega s = Cos^{-1}(-tan\varphi tan\delta) \tag{3.15}$$

The maximum possible sunshine duration (So) can be obtained by using the equation (3.16) given below:

$$So = \frac{12}{15}\omega s \tag{3.16}$$

The Angstrom constants has been obtained from the relationship given as in equation (3.17) and (3.18) (Gana & Akpootu, 2013):

$$a = -0.11 + 0.235Cos\varphi + 0.323(\frac{S}{S0}) \quad (3.17)$$

$$b = 1.449 - 0.553Cos\varphi - 0.694(\frac{S}{S0}) \quad (3.18)$$

By having the above relation, the solar radiation of Ambo site is calculated, and tabulated as in Table (3.16).

Let, be start the calculation for January, which has an average sunshine hour value of 10.62; from equation (3.12), $\frac{H}{Ho} = a + b(\frac{S}{So})$.

Where, $Ho = \left(\frac{24}{\pi}\right) Isc \left[1 + 0.033Cos\left(\frac{360n}{365}\right)\right] * [Cos\varphi \text{Cos}\delta \text{Sin}\omega s + (\frac{2\pi\omega s}{360}) Sin\varphi \text{Sin}\delta$. Then, first ωs, and δ value must be determined. Therefore, from equation (3.14), and (3.15) we have$\delta = 23.45Sin\left(360\frac{284+n}{365}\right)$, and $\omega s = Cos^{-1}(-tan\varphi tan\delta)$. By using these given formulas, we can calculate the δ, and ωs values as follow;

$\delta = 23.45Sin\left(360\frac{284+n}{365}\right)$ = 23.4Sin $(360\frac{284+365}{365})$ = -23.086

$\omega s = Cos^{-1}(-tan\varphi tan\delta)$= $\omega s = Cos^{-1}(-\tan(8.98)\tan(-23.086))$= 89.9

And from equation (3.16), $So = \frac{12}{15}\omega s$. $Hence, So = \frac{12}{15}(89.9)$= 12 Therefore,

$Ho = \left(\frac{24}{3.14}\right) 1367 \left[1 + 0.033Cos\left(\frac{360*365}{365}\right)\right] * [Cos(8.98)\text{Cos}(-23.086)\text{Sin}(89.9) + \left(\frac{2*3.14*89.9}{360}\right) Sin(89.9)\text{Sin}(-23.086)]$ = 9,929.75Wh/m2

From equation (3.17) and (3.18), the regression coefficients ‘’a ‘’and ‘’b’’ has been obtained as follow;

$$a = -0.11 + 0.235Cos\varphi + 0.323(\frac{S}{S0})$$

$a = -0.11 + 0.235Cos(8.98) + 0.323(\frac{S}{S0})$ = 0.125+$0.323(\frac{S}{S0})$

$$b = 1.449 - 0.553Cos\varphi - 0.694(\frac{S}{S0})$$

b = $1.449 - 0.553Cos(8.98) - 0.694\left(\frac{S}{S0}\right) = 0.896 - 0.694(\frac{S}{S0})$

From equation (3.12), we have$\frac{H}{Ho} = a + b(\frac{S}{So})$. Therefore, from this equation we can drive for H. Then, $H = Ho(a + b\left(\frac{S}{So}\right))$. No we have Ho, a, b, S, and So values, by simple substitution we can obtained H value.

$H = 9{,}929.75[(0.125 + 0.323\left(\frac{10.62}{12}\right)) + (0.896 - 0.694\left(\frac{10.62}{12}\right))\left(\frac{10.62}{12}\right)]$ = 6,547.69 Wh/m^2 = **6.55 Kwh**/m^2/day**.** By, following the same formula, and procedure, the overall solar radiation of Ambo site has obtained, and organized in Table (3.16) below.

Table 3.16: Monthly average daily solar radiation of Ambo site for seven years (2016-2022).

Av. Solar radiation in (Kwh/m^2/day)	**Month**											
	Jan	Feb	Mar	Apr	May	Jun	Jul	Aug	Sep	Oct	Nov	Dec
	6.55	6.34	6.23	6.04	6.01	5.19	4.63	4.56	5.17	6.4	6.46	6.5

The performance of the solar panel is determined by the average monthly daily solar radiation. The solar irradiation measured exists within the estimated range of 4.56-6.55 kwh/m^2/day. The solar radiation of the Ambo location shows that it has sufficient potential solar energy resources, even when compared to developed countries that utilize more renewable energy sources.

Table 3.17 Monthly average daily solar radiation of Ambo (Hagere Hiywet) site (from NASA)

RETScreen - Climate database

Map
Search
Data

Country		Ethiopia		
Province/State				
Climate data location	See map	Hāgere Hiywet		
Latitude		°N	9.0	
Longitude		°E	37.9	Source
Climate zone		3A	Warm - Humid	NASA
Elevation		m	1,983	NASA
Heating design temperature		°C	10.8	NASA
Cooling design temperature		°C	26.2	NASA
Earth temperature amplitude		°C	16.2	NASA

Month	Air temperature	Relative humidity	Precipitation	Daily solar radiation - horizontal	Atmospheric pressure	Wind speed	Earth temperature	Heating degree-days 18 °C	Cooling degree-days 10 °C
	°C	%	mm	kWh/m²/d	kPa	m/s	°C	°C-d	°C-d
January	19.8	38.0%	19.93	6.15	80.3	3.5	23.8	0	304
February	21.0	36.1%	22.85	6.47	80.3	3.2	25.5	0	309
March	21.5	43.4%	70.01	6.40	80.2	3.0	26.0	0	357
April	20.0	60.4%	77.42	6.32	80.2	3.1	23.2	0	299
May	18.2	74.4%	145.23	6.11	80.3	2.9	20.2	0	253
June	17.0	79.2%	218.66	5.50	80.4	3.0	18.3	32	209
July	16.1	80.1%	272.33	4.81	80.4	2.6	17.0	60	188
August	16.2	80.1%	212.73	4.92	80.4	2.3	17.1	57	191
September	16.5	78.1%	144.18	5.71	80.4	2.2	17.5	45	195
October	16.5	67.3%	103.13	6.14	80.4	2.7	17.4	46	202
November	17.3	50.2%	30.48	6.23	80.3	3.2	18.8	22	218
December	18.5	42.0%	18.60	6.12	80.4	3.5	21.3	0	264
Annual	**18.2**	**60.9%**	**1,335.54**	**5.90**	**80.3**	**2.9**	**20.5**	**263**	**2,987**
Source	NASA	NASA	NASA	NASA	NASA	NASA	NASA	NASA	NASA

Location | Climate data

Location

	Unit	Climate data location	Facility location
Name		Ethiopia - Hāgere Hiywet	Ethiopia - Oromia Region - Ambo
Latitude	°N	9.0	9.0
Longitude	°E	37.9	37.9
Climate zone		3A - Warm - Humid	3A - Warm - Humid
Elevation	m	1983	2110

Climate data

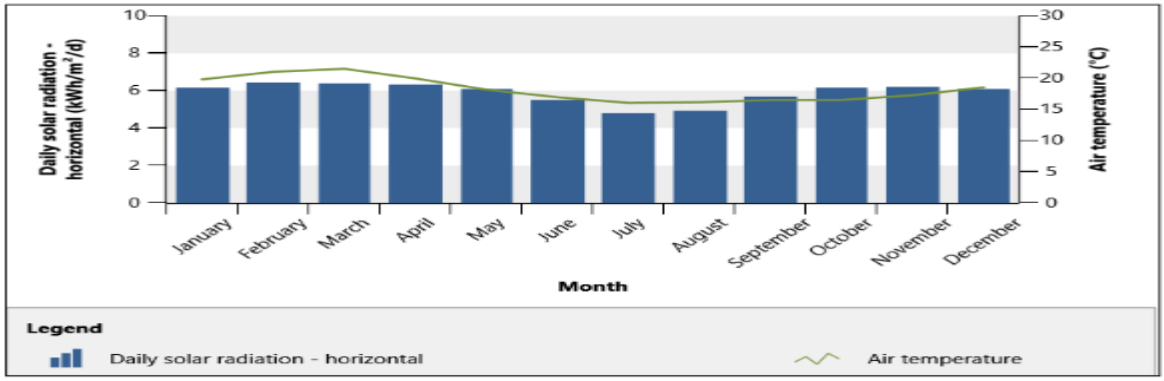

Figure 3.3 Monthly average daily solar radiation of Ambo site obtained from NASA

3.4. Calculation of Reliability Indices

For 2021–2022, reliability indices are computed. Then, using the equations (2.14) to (2.21) given in chapter two, it is possible to calculate the present substation's reliability indices. We can determine the reliability indices for 2021 and 2022, as well as the average of the two years data provided in Tables 3.9, 3.10, and 3.11. Tables 3.18, 3.19, and 3.20 shows the Ambo town feeder's reliability indices for 2020, 2022, and the average over two years.

Table 3.18: 2021 Reliability Indices

	Indices				
Year	SAIFI	SAIDI	CAIDI	ASAI	ASUI
2021	323	279.92	0.866	0.968	0.032

Table 3.19: 2022 Reliability Indices

	Indices				
Year	SAIFI	SAIDI	CAIDI	ASAI	ASUI
2022	387	393.97	1.02	0.955	0.045

According to Tables 3.18 and 3.19, the feeder's availability decreased over the two years, going from 0.968 to 0.955.

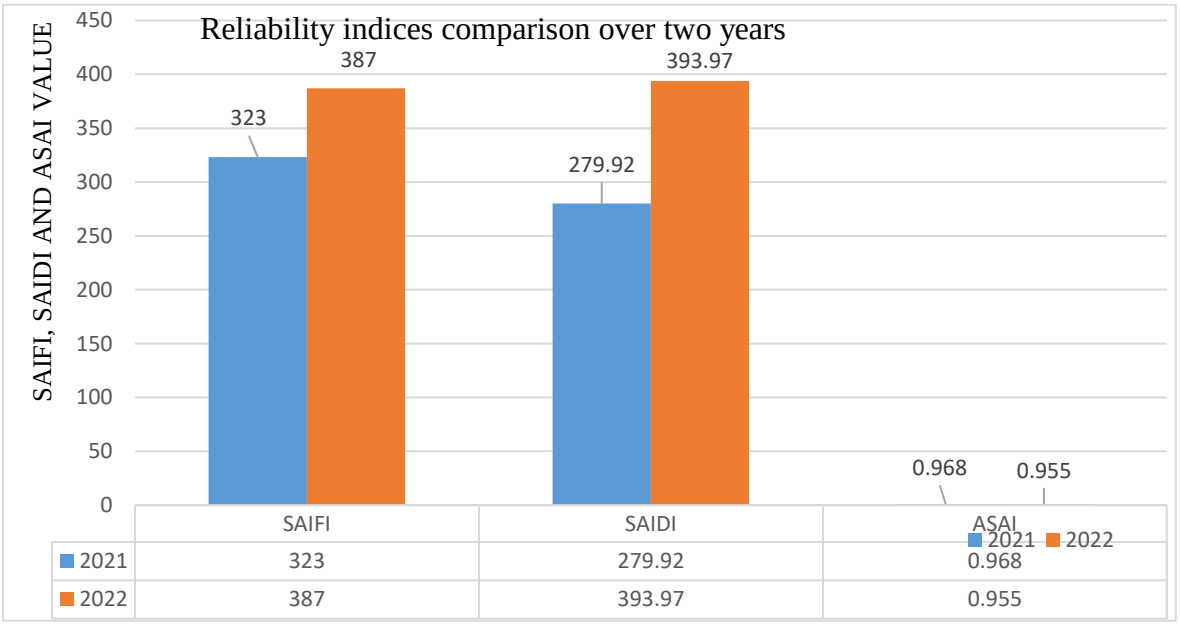

Figure 3.4 comparisons of SAIFI, SAIDI and ASAI in the two years' period.

The SAIFI and SAIDI indices increased from 2021 to 2022, as shown in Figure 3.4 above.

Table 3.20 Average reliability Indices of 2021 and 2022

	Indices				
Year	SAIFI	SAIDI	CAIDI	ASAI	ASUI
Av. 2021 and 2022	355	336.945	0.95	0.962	0.038

According to Table 3.20, the system is generally 0.962(96.2 %) available. However, consumers expected uninterrupted access to electricity for the full 8760 hours (24 hours) per year. The APPA distribution system reliability and operations survey reported on November 2013 by Alex Hofmann, which states that between 99.9%, and 99.999% of the time, the utility will be able to provide power((APPA), 2014). As compared by the international reliability indices of the nations with the most experience, the chosen feeder's reliability is insufficient.

3.5. Reliability Indices Comparison with Benchmark Standards

In Table 3.21 shown below, the fundamental reliability indices of SAIDI, SAIFI, and ASAI for nine developed countries are considered as a benchmark. The average values for SAIFI, SAIDI, and ASAI in the reliability evaluation of the Ambo distribution substation are 355, 336.945 and 96.2 percent, respectively. Better reliability performance has fewer outages or outages for a shorter amount of time which is indicated by a lower number of the SAIDI, SAIFI, and ASAI indices. Poorer performance is indicated by higher SAIDI and SAIFI index numbers. When benchmarks are compared to the average SAIDI and SAIFI value of the Ambo distribution substation, poorer performance is observed.

Table 3.21: Standard bench marking reliability indices (Bewketu Getie, 2020)

Developed Country	SAIFI (int./cust./yr.)	SAIDI (hr./cus./yr.)	ASAI (%)
USA	1.5	4	99.91
France	1	1.03	99.97
Germany	0.5	0.383	99.99
Austria	0.9	1.2	99.97
Denmark	0.5	0.4	99.98
UK	0.8	1.5	99.96
Italy	2.2	0.967	99.99
Spain	2.2	1.733	99.96
Netherland	0.3	0.55	99.97
Ethiopia	20	25	99.425

As per standard bench mark, Ambo distribution substation has the highest reliability index value. Even so, it performs worse than Ethiopia's typical benchmark value.

3.6. Load Flow Analysis of Radial Distribution System

The operation, control, and planning of power systems now extensive use of efficient and reliable load flow solution techniques as Gauss-Seidel (G S), Newton Rapson (N-R), and fast decoupled load flow. However, it has been repeatedly demonstrated that these techniques may become ineffective when used to analyze distribution systems because of the unique characteristics of such networks, including radial structure, high resistance-reactance(R/X) ratio, un-transposed lines, unbalanced loads, and single-phase and two-phase laterals.

In addition to these issues, distribution network matrices are typically unreliable, which could lead to numerical issues with the traditional power flow algorithm. Methods created to fix radial distribution networks with poor conditions can be categorized into two groups. The first category of methods includes N-R and G-S. The second set of approaches, on the other hand, are based on forward and/or backward sweep processes that employ Kirchhoff's principles or the well-known bi-quadratic equation(Abu-Mouti & El-Hawary, 2011). The forward and/or backward sweep load flow approach is used in this work.

3.6.1. Forward and Backward Sweep Load Flow

The majority of backward/forward sweep-based power flow algorithms use the radial network topology and are made up of either forward or backward sweep operations. The backward sweep is essentially the branch current and/or power summing from the far end to the sending end of the feeder and laterals, whereas the forward sweep is mostly the node voltage calculation from the sending end to the far end of the feeder and laterals. Some algorithms also compute the node voltages in backward sweeps in addition to the branch current and/or power summing.

3.6.2. Forward Backward Sweep Load Flow Algorithm

Both the branch current to bus voltage matrix (BCBV) and the bus injection to branch current matrix (BIBC) are two derived matrices that are used to build the forward and backward sweep algorithms. The corresponding current-injection-based model is more useful for distribution networks(Techno, 2015).

Step One: Backward sweep

Branch currents from loads to system are collected for each iteration k. The bus-injection to branch-current (BIBC), which connects the bus-injected current to the branch current, must first be determined in order to determine the branch current. The ith bus's current injection's kth iteration is,

$$\mathrm{Ii}^{k} = \mathrm{Ii}^{r}(\mathrm{vi}^{k}) + j\mathrm{Ii}^{i}(\mathrm{vi}^{k}) = \left(\frac{Pi+jQi}{vi^{k}}\right) + \cdots \quad (3.19)$$

Where vi^{k} and Ii^{k} are the bus voltage and current injection of the i^{th} bus at the k^{th} iteration respectively.

Ii^{r} and Ii^{i} are real and imaginary parts of the current injection of bus i at the k^{th} iteration, respectively.

Development of Relationship Matrix

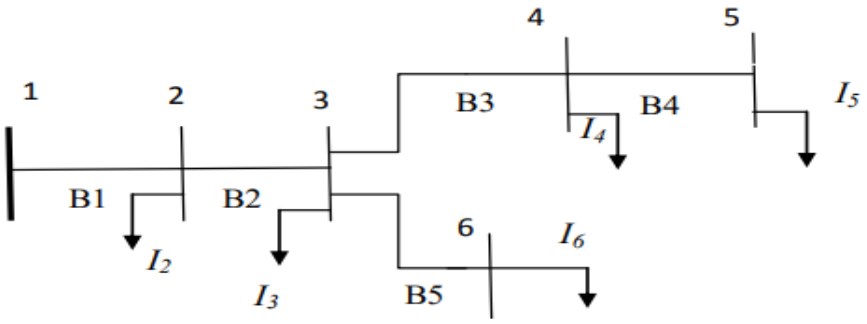

Figure 3.5: Sample distribution system(Abu-Mouti & El-Hawary, 2011)

Branch currents are calculated by applying Kirchhoff's current law (KCL) to the given network(Abu-Mouti & El-Hawary, 2011). Here simple radial distribution system network was considered as an example. From a given example here, the branch currents of B1, B2, B3, B4, and B5 can be expressed as defined in the below equations.

$$B_1 = I_2 + I_3 + I_4 + I_5 + I_6 \quad (3.20)$$

$$B_2 = I_3 + I_4 + I_5 + I_6 \quad (3.21)$$

$$B_3 = I_4 + I_5 \quad (3.22)$$

$$B_4 = I_5 \quad (3.23)$$

$$B_5 = I_6 \quad (3.24)$$

Consequently, the following is an expression of the relationship between bus current injections and branch currents:

$$\begin{bmatrix} B_1 \\ B_2 \\ B_3 \\ B_4 \\ B_5 \end{bmatrix} = \begin{bmatrix} 1 & 1 & 1 & 1 & 1 \\ 0 & 1 & 1 & 1 & 1 \\ 0 & 0 & 1 & 1 & 0 \\ 0 & 0 & 0 & 1 & 0 \\ 0 & 0 & 0 & 0 & 1 \end{bmatrix} \begin{bmatrix} I_2 \\ I_3 \\ I_4 \\ I_5 \\ I_6 \end{bmatrix} \quad (3.25)$$

The above equation (3.25) can be expressed as,

$$[B] = [BIBC]\,[I] \quad (3.26)$$

Where: BIBC is a bus injection to branch the current matrix

Step two: Forward sweep

From Figure 3.5 illustrated above, the link between branch currents and bus voltages is expressed as follows.

$$V_2 = V_1 - (Z_{12}B_1) \tag{3.27}$$

$$V_3 = V_1 - (Z_{12}B_1 - Z_{23}B_2) \tag{3.28}$$

$$V_4 = V_1 - (Z_{12}B_1 - Z_{23}B_2 - Z_{34}B_3) \tag{3.29}$$

$$V_5 = V_1 - (Z_{12}B_1 - Z_{23}B_2 - Z_{34}B_3 - Z_{45}B_5) \tag{3.30}$$

$$V_6 = V_1 - (Z_{12}B_1 - Z_{23}B_2 - Z_{56}B_5) \tag{3.31}$$

Where, Zij- the line impedance between bus i and j and Vi- is the voltage at bus i. Other buses can be operated in a similar manner, therefore the relationship between branch currents and bus voltages can be defined as follows:

$$\begin{bmatrix} V_2 \\ V_3 \\ V_4 \\ V_5 \\ V_6 \end{bmatrix} = \begin{bmatrix} V_1 \\ V_1 \\ V_1 \\ V_1 \\ V_1 \end{bmatrix} - \begin{bmatrix} Z_{12} & 0 & 0 & 0 & 0 \\ Z_{12} & Z_{23} & 0 & 0 & 0 \\ Z_{12} & Z_{23} & Z_{34} & 0 & 0 \\ Z_{12} & Z_{23} & Z_{34} & Z_{45} & 0 \\ Z_{12} & Z_{23} & 0 & 0 & Z_{56} \end{bmatrix} \begin{bmatrix} B_1 \\ B_2 \\ B_3 \\ B_4 \\ B_5 \end{bmatrix} \tag{3.32}$$

In general, equation (3.32) above can be expressed as follows:

$$V^{k+1} = [V_1] - [BCBV][B] \tag{3.33}$$

3.6.3. Formulation of the BIBC and BCBV Matrix

Branch currents and bus current injections are related, as shown by the BIBC matrix. The BIBC matrix can immediately calculate the corresponding variations at branch currents that are produced by variations at bus current injections. Branch currents and bus voltages are represented by a matrix called the BCBV matrix. The BCBV matrix can directly compute the corresponding fluctuations at bus voltages, which are caused by variations at branch currents. The following steps are what must be taken in order to form the BIBC and BCBV.

Procedure 1: BIBC Formation:

The equation formulated below can be used to convert the power injections at each node into comparable current injections, and by applying Kirchhoff's Current Law (KCL) at each node, a series of comparisons can be created. Now, the network's branch currents may all be sculpted as a function of the corresponding current injections (Meychw, 2021).

$$\mathrm{Iii}^{iter} = \mathrm{Iii}^{r}\left(\mathrm{vii}^{iter}\right) + j\mathrm{Iii}^{ii}\left(\mathrm{vi}^{iter}\right) = \left(\frac{PS(ii) - jQS(ii)}{vii^{iter}}\right)^{*} \quad (3.34)$$

Equivalent current injection for the load flow solution is as shown in the equation above for the iter-th iteration at the ii-th node.

$$[\mathrm{I_B}] = [BIBC][I] \quad (3.35)$$

For a general network, the following steps could be used to shape the BIBC matrix.

Step 1: The BIBC matrix's dimension is m x (n-1) for a distribution system having n-bus and m-branch section.

Step 2: : If a line section (Bk) is located between bus i and bus j, copy the column of the ith bus of the BIBC matrix to the column of the jth bus and fill a 1 to the position of the k-th row and the j-th bus column.

Step 3: Repeat steps 2 until the BIBC matrix contains all of the network's branches.

Procedure 2: BCBV formulation:

The relationship between branch current and node voltages is defined by the Branch-Current to Node Voltage (BCBV) matrix. Kirchhoff's Voltage Law (KVL) can be used to quickly determine the relationships between the branch currents and node voltages. The general form can be represented as:

$$[\Delta V] = [BCBV]\ [IB] \quad (3.36)$$

Where BCBV=ZB*BIBC*IB^{-}, ZB=diagonal impedance

For a universal network, the following steps can be used to create the BCBV matrix:

Step 1: The BCBV matrix's dimension for a distribution system with m branch sections and n buses is (n-1) x m.

Step 2: If a line section is located between bus i and bus j, copy the row of the ith bus of the BCBV matrix to the column of the jth bus and fill the line impedance (Zij) to the position of the kth column and the jth bus row.

Step 3: Steps 2 should be repeated until all network branches are represented in the BCBV matrix.

3.7. Incorporation of DG into Load Flow

Assume that a single source radial distribution network with NL branches, a DG source connecting to node i will be installed at node i. Although it is well known that the DG provides active power (PGi^{DG})to the systems, and reactive power(QGi^{DG}) is dependent on the DG's source and can either be provided to or consumed by the systems. This active and reactive power causes an active current ($IDGi^{r}$) and a reactive current ($IDGi^{i}$) to flow through the system, changing the active and reactive components of the branch current set α. At the i^{th} node, the total apparent power is:

$$S = SD_i = \sum pD_i + jQD_i \qquad i=1, 2, 3,..... NB \tag{3.37}$$

Current at $i\ th$ node:

$$ID = I^{wth\ out\_DG}\ D\_i = \left(\frac{SD\_i}{Vi}\right)^* \tag{3.38}$$

The active and reactive power demand at the i^{th} node, where a DG unit is installed must be modified in order to take the DG model into account.

$$P^{with\ \_DG}\ D_i \ = \ P^{with\ out_{DG}}\ D_i \ - \ PGi^{DG} \tag{3.39}$$

$$Q^{with\ \_DG}\ D_i \ = \ Q^{with\ out_{DG}}\ D_i \mp \ QGi^{DG} \tag{3.40}$$

DG power at i^{th} node:

$$SD\_i = \sum \ PG\_i^{DG} \pm QG\_i^{DG} \qquad i= 1, 2, 3.....NB \tag{3.41}$$

i^{th} node total new apparent power:

$$S = \ SD_i - SDG\_i \tag{3.42}$$

New current at the i^{th} node:

$$ID = I^{with\_DG}\ D\_i = \left(\frac{SD\_i\ \ SDG\_i}{Vi}\right)^* \tag{3.43}$$

The updated network power can be stated in matrix form as follow:

$$[S] = [SD\_i] - [SDG\_i] \quad (3.44)$$

3.8. Distribution Networks Load Flow with DG Algorithm

A list of algorithmic steps for distribution networks power flow is discussed below:

Step one: Read line and bus data of distribution networks.

Step two: Determine each node's DG power and update the system bus information.

Step three: Determine the overall power demand with DG.

The relationships can be described as: $[S] = [SD\_i] - [SDG\_i]$

Step four: compute power flow solution of distribution networks.

A. Reducing power loss by using DG

The following explanation illustrates how DG decrease power loss in the radial distribution system using the optimal size and location.

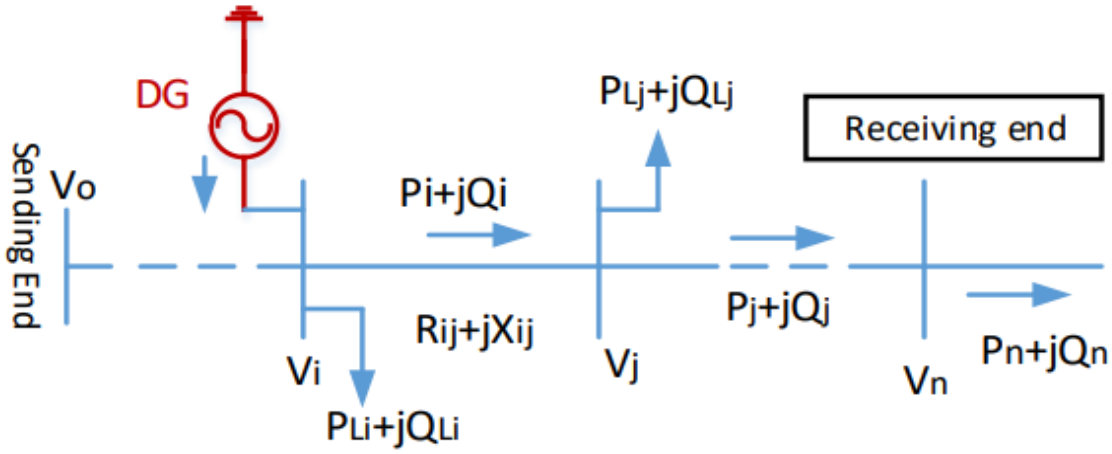

Figure 3.6: Radial distribution system with DG integration at bus i (Keerio et al., 2019)

Given that DG inject real power P_{DG} at bus i is assumed that the load on this bus will deviated from P_{Li} to $(P_{Li} - P_{DG})$

With DG added on branch ij, mathematically active power loss is given by

$$P_{Loss\ i,j}^{DG} = \frac{Ri,j}{vi^2}[(Pi - PDG)^2 + Qi^2] \quad (3.45)$$

After inserting the DG, each branch of power loss is provided by;

$$P_{T\,loss}^{DG} = \sum_{i,j=1}^{n} P_{Loss\,i,j}^{DG} \quad (3.46)$$

Power loss change (ΔP_{loss}^{DG})with the integration of DG is calculated as expressed in equation below:

$$\Delta P_{loss}^{DG} = \sum_{i,j=1}^{n} P_{Loss\,i,j} - \sum_{i,j=1}^{n} P_{Loss\,i,j}^{DG} \quad (3.47)$$

3.9. Proposed Methods for DG placement and Sizing

The first condition has aimed to find the best optimal sizing and placement of DG by using MOPSO algorithm. The system is expected to fulfill a number of constraints that are part of the multi-objective function derives from a number of different objective functions in the power distribution system.

3.9.1. Multi-objective particle swarm Optimization (MOPSO)

The Particle Swarm Optimization (PSO) algorithm has a variation called Multi-Objective Particle Swarm Optimization (MOPSO) that is specially made to address multi-objective optimization issues. The Pareto front is a collection of solutions that represents the trade-offs between various objectives, and it extends the conventional MOPSO method by taking into account numerous competing purposes at once.

In MOSPO, to locate the Pareto-optimal solutions, a population of particles (possible solutions) flows around the search space. The program investigates the search space and moves closer to the Pareto front by repeatedly updating the positions and velocities of the particles.

3.9.1.1.Basic Multi-Objective Particle Swarm Optimization

Each individual member of the MOPSO algorithm is referred to as "particle," and each particle moves around the multi-dimensional search space with a velocity that is continuously updated by the particle's experience as well as the experience of its neighbors or the swarm.

A basic MOPSO technique is straightforward because it just uses two model equations. In this case, each particle's coordinates stand for a potential resolution connected to vectors of position (Xi) and velocity (Vi). Every iteration's step will see a change in each particle's velocity in the direction of its pbest and gbest values. The last position will then be added to the new velocity to determine each particle's new position. The next two equations are the two main ones.

$$Vi(I+1) = w * vi(I) + c1 * r1 * (pbi - xi) + c2 * r2 * (gbi - xi) \quad (3.48)$$

$$Xi(I+1) = xi(I) + vi(I+1) \quad (3.49)$$

Where:

Vi- velocity for the particle i,

W- is weight of inertia

I – iteration

c1& c2- acceleration coefficients with the range of [0, 4]

Pbi- the previous best particles' optimal position

Xi- is i th present position of particles

r1& r2- random variables with a range of [0, 1]

Gbi- optimum position within the particles' population

The following are the fundamental MOPSO techniques:

1. Particle X (I): - is a potential solution represented by a real-valued vector with D dimensions, where D is the total number of optimized parameters.

2. Population: - is the collection of x particles at time t.

3. Fitness Function: - is used to identify the ideal response. It is typically an objective function.

4. Swarm: - A population of moving particles that appears to be randomly moving has a tendency to group together.

5. Particle's velocity V (I): - is the vector which measures the velocity and direction of moving particles. It is represented by a real valued D-dimensional vector.

6. Velocity Update: The equation updates the velocity (I).

7. Update on Position: To locate the global optimum, each particle in MOPSO changes their positions.

8. Inertia weight w (I): This control parameter regulates how much the previously speed affects the speed of the moment.

9. Personal best (pbi): - As it progresses across the area of search, the particle compares its current position's fitness value to the best fitness value, and it has ever achieved at any point in the past. Every particle in the swarm has an individual best position, which can be identified and updated throughout the search process and is related to the best fitness achieved. In general, it is the particle's most advantageous place out of all those it has already visited.

10. Global best (gbi): - is the best position out of all the individual best spots that have been visited so far where the best fitness is obtained.

11. Stopping criteria: - are the conditions that will cause the search to come to an end.

3.9.1.2.Parameters of Multi-Objective Particle Swarm Optimization

There are a few parameters in the basic MOPSO that need to be fixed. The basic MOPSO parameters are:

Population (swarm) size Particle Velocity

Random Numbers Iteration numbers

Velocity Components Acceleration coefficients

The population's size is the first factor. This is frequently established empirically based on the complexity and perceived difficulty of a problem. Values between 20 and 50 are very common. The second parameters in Equation (3.48), c1 and c2, are also known as acceleration coefficients because they govern the magnitude of random forces acting in the direction of gbi for both the personal best and the neighborhood best.

The values of c1 and c2 have a significant impact on how a MOPSO behaves. Every particle keeps going to move at their present speed until they collide with the search space boundary when c1=c2=0. On the other hand, all particles are independent when c1>0 and c2=0. When c1=0 and c2>0, all of the particles in the swarm are drawn to a single point, when c1=c2, all of the particles are drawn to the average of pbest and gbest, and when c1>c2. When c2>c1 then all particles are much more influenced by the global best position, which causes all particles to run prematurely to the optimal in all cases, the velocity update equation is changed, and each particle is more strongly influenced by its personal best position, leading to excessive wandering. However, the c1=c2=2.0 value was virtually always used in early MOPSO studies.

The MOPSO algorithm's iteration number is another crucial component for obtaining better results. A search that is iterated to few times may end prematurely, whereas one that iterates too many times adds unnecessary computing complexity and demands more time.

3.9.1.3. MOPSO Implementation Steps

1. Problem formulation: Specify the optimization problem's constraints and objective functions. The goal of this situation is to reduce line losses in system while keeping in mind limitations like DG capacity limits, voltage limits, and network constraints.

2. Initialization: Set the parameters of the MOPSO algorithm, such as the population size, the variety of DG sizes, iterations, inertia weight, acceleration coefficients, and locations, to their initial values.

3. Particle Initializing: Each particle in this population represents a potential solution. Give the particles within the boundaries random placements and velocities.

4. Assess Fitness: Assess the fitness of each particle by computing the distribution system's power losses for the relevant DG sizes and locations.

5. Update Personal Best: Based on every particle's current dominance and fitness, update the personal (Pbest) best position for that particle.

6. Update Global Best: Update the Gbest by locating the non-dominated solutions among all particles.

7. Update Velocities and Positions: Update the particle's velocities and positions in accordance with their present velocities, positions, PBest, and GBest. To update the particle locations and speeds, use the MOPSO equations.

8. Boundary Constraint Handling: Use boundary constraint handling strategies to make sure that the particle positions stay within the acceptable range of DG sizes and locations.

9. Evaluate Convergence: Look for criteria for convergence, such as the maximum number of iterations or a suitable level of convergence.

10. Continue step 4 to 9 until the convergence requirements are satisfied.

11. Output Analysis: After the algorithm converges, examine the Pareto-optimal results to determine how both power losses are traded off. These solutions show several DG location and sizing possibilities in the distribution system.

12. Choose the Best Solution: Depending on your tastes and requirements, choose the best option from the Pareto-Optimal Front that achieves the desired balance between active and reactive power losses.

3.9.1.4. Problem formulation

For the operator to decide on the capacity of the chosen distribution network, there are several performance-related parameters that must be taken into account. The objective function and constraints are included in the algorithm's problem formulation.

A. Objective Function:

The MOPSO algorithm's objective function seeks to reduce both power loss and voltage variation. The following is a definition of it:

I. Reduction of power loss

The goal of power loss reduction is to eliminate overall losses in the distribution system to a minimum. The total amount of power lost throughout all system branches and lines might be used to describe it. It can be modeled mathematically as:

$f1 = \sum (Pl)$ (for all lines), and $\sum (Ql)$ (for all lines) (3.50)

By adding each network branch losses, the overall power loss in a distribution network may be computed. The following is the power loss formula:

Total real power loss (PTL) = $\Sigma (I_{ij}^2 * R_{ij})$ (3.51)

Total reactive power loss (QTL) = $\Sigma (I_{ij}^2 * X_{ij})$ (3.52)

Where;

I_ij - is the current flowing through branch (line) ij.

R_ij- is branch resistance

X_ij - is branch reactance

B. Constraints

The MOPSO algorithm includes a number of constraints to guarantee that the solutions are feasible. These limitations frequently include DG power, voltage range, and size.

I. DG Size Constraint

The DG size constraint makes sure that the DG units' size or capacity are within a predetermined range. It can be stated as follows:

$DG_{min.} \leq DG_{size} \leq DG_{max.}$

Where, D_min. and D_max shows the minimum and maximum DG sizes, respectively.

II. Voltage Range Constraint

Bus voltages are kept within allowable bounds by the voltage range limitation. It can be stated as follows:

$V_{min.} \leq V \leq V_{max.}$

Where, V_min. and V_max indicates the minimum and maximum voltage limits, respectively.

3.9.1.5.Optimal DG size and location using MOPSO algorithm

Let's assume that DG unit is connected to bus k in a radial distribution network. The power flow equations can be expressed as:

$P_k = Pload_k - Ploss_k + Pdg_k$ (3.53)

$Q_k = Qload_k - Qloss_k + Qdg_k$ (3.54)

Where;

P_k and Q_k are the injected active and reactive powers at bus k, respectively.

Pload_k and Qload_k are the active and reactive loads at bus k, respectively.

Ploss_k and Qloss_k are the active and reactive power losses at bus k, respectively.

P_dg_k and Qdg_k are the active and reactive power injected by the DG unit at bus k, respectively.

The voltage drop equation can also be used to express voltage at the DG connection point.

$V_k = V_{src} - I_k * Z_k$ (3.55)

Where;

V_k -is the voltage at bus k

V_src- is the source voltage

I_k -is the current flowing through the lines

Z_k -is the impedance of the line

The following steps can be accomplished objectively by using MOPSO technique to address the DG placement and size issue:

Step1: Load case information: The system data, including the generator data, bus data, and branch data, are saved in a MATLAP m-file.

Step 2: Determine the voltages at each node and the overall power loss in the distribution network at the initial condition.

Step3: Initialize the Swarm parameters:

- Establish the limits of the DG size PDGrmax and PDGrmin as well as the velocity Vmax and Vmin.
- Indicate the values of the acceleration coefficients c1 and c2 as well as the inertial weight w.
- Assign the initial velocity and position ($X_i = [X_{i1}, X_{i2},..., X_{in}]$, and $Vi = [V_{i1}, V_{i2},..., V_{in}]$).
- Generate a random initial population of N particles with a D-dimensional search space.

Step 4: Obtain the fitness function's value and store the Pbest and Gbest values.

Step 5: By using equations, (18) and (19) respectively update the position and speed of a particle

Step 6: Using the most recent particle position and velocity, determine the new fitness value of the fitness function for the entire particle.

- For each particle's new position, new fitness values are computed. If a particle's new fitness value is higher than its previous Pbest value, the particle's Pbest value is changed to reflect the improved fitness value.

Step7: Update the Gbest and new Pbest. Each particle provides the ideal DG sizes and positions, as well as the related fitness value, which represents the least amount of power loss.

Step 8: Carry out the previously described process, beginning with step 5, as many times as is physically possible before printing the target problems best solution.

3.9.1.6.Procedure for applying MOSPO algorithm

1. Set the initial values for the population size, iterations, inertia weight, acceleration coefficients, and range of DG sizes and locations in the MOPSO algorithm (determining the initial values for the population size, iterations, inertia weight, acceleration coefficients, and range of DG sizes and locations in the MOPSO algorithm requires careful consideration and may vary based on the specific problem and domain. For instance, a common practice to set the population size is between 20 and 100, depending on the complexity of the problem).

2. Create a population of particles with each particle standing in for a potential solution. Within the boundaries, give the particles random placements and speeds.

3. Determine the voltage drop and power loss in the distribution system for the respective DG sizes and positions in order to assess each particle's fitness. Power loss reduction and voltage deviation control are both taken into account by the fitness function.

4. Based on the fitness and dominance of each particle, update the $P_{best}$for that particle. In the search space, every particle keeps its optimal position.

5. Update G_{best}position by figuring out which particles have non-dominated solutions. Power loss reduction and voltage deviation management are balanced by the Pareto-optimal front, which is represented by the GBest.

6. Adjust the particle's velocities and positions in accordance with their present positions, velocities, PBest, and GBest. Update the particle locations and velocities using the MOPSO equations while taking the DG size, voltage range, and power limitations into account.

7. Use boundary constraint management strategies to make sure the particle positions stay within the range of DG sizes and locations that are practical.

8. Look for convergence requirements, such as the maximum number of iterations or an acceptable degree of convergence. Repeat steps 3 to7 if the convergence conditions are not satisfied.
9. After the algorithm converges, examine the generated Pareto-optimal solutions to determine how voltage deviation control and power loss reduction are traded off. These solutions show several DG location and sizing possibilities in the distribution system.
10. Based on your unique tastes and requirements, choose the best option from the Pareto-optimal front while keeping in mind the ideal balance between power loss reduction and voltage deviation management.

3.9.1.7. Flow Chart of Multi-Objective Particle Swarm Optimization

A flowchart of the OPSDG using the MOPSO algorithm is shown in Figure 3.7.

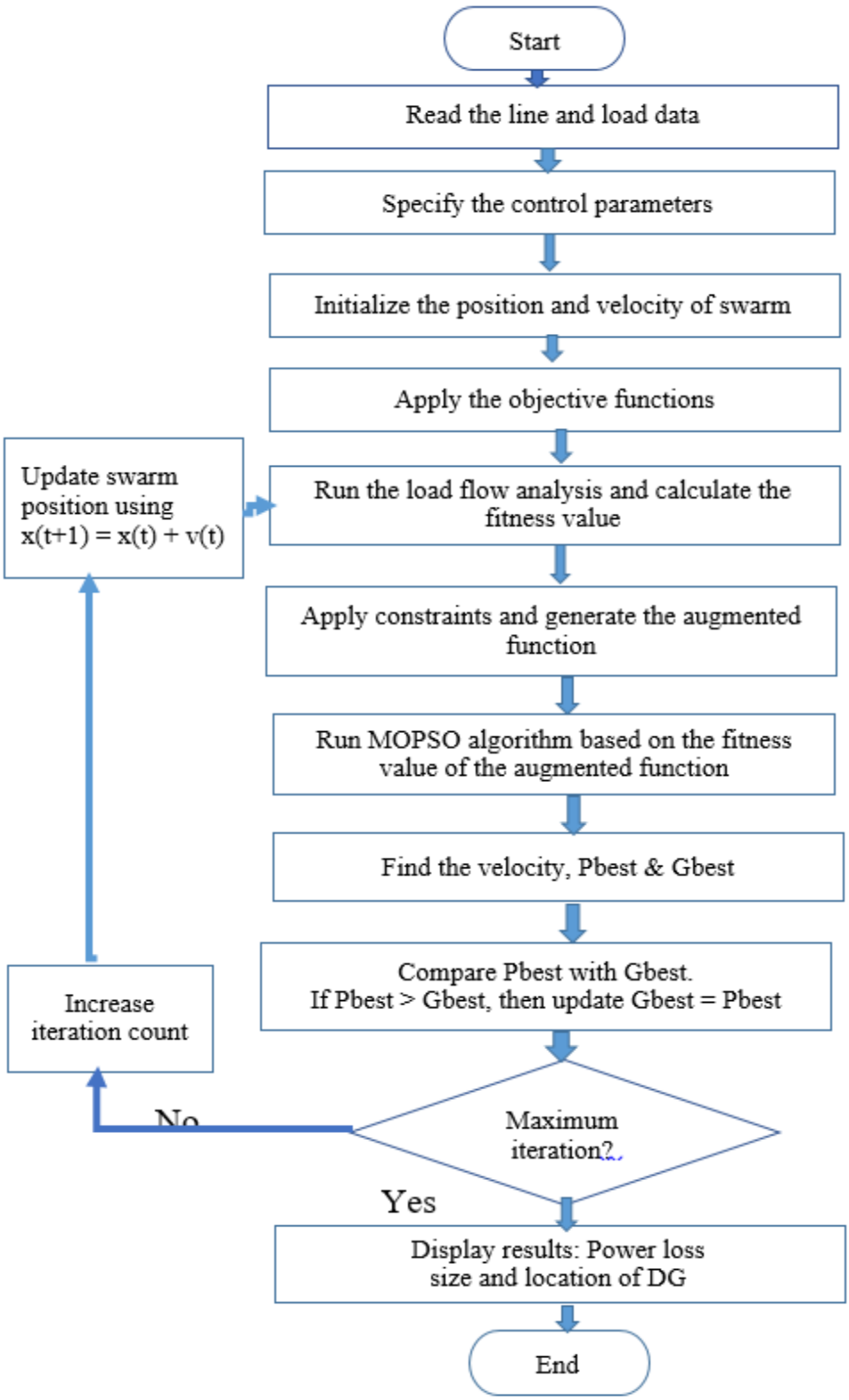

Figure 3.7 Flowchart of the proposed approach

3.10. DG Installation

Solar PV modules, inverters, batteries, and charge controllers are collectively the components of solar PV power plants.

PV modules must be selected based on a variety of criteria, such as their efficiency, price, and lifetime. In order to offer the best performance and fair rates, these variables must be taken into account during the selection process.

A well-known and reliable type of solar cell is a monocrystalline panel of the ART245-60-1 module, which can be used in grid-tied solar power plants. Polycrystalline panels are more expensive than monocrystalline(Design of large scale solar Pv system, 2016). As a result, the monocrystalline-type PV module was utilized in this work. In table under appendix c, the basic characteristics of the selected modules are discussed in detail.

A. Size of PV modules required

The equation below determines how many PV modules are needed in both parallel and series configurations. Loss factors due to temperature and the like has been considered during finding number of PV modules needed. From PV module detail specifications discussed in table under appendix c the selected PV power is 245W per individual module. But, the power used per each module for the calculation is 240W (5W is considered as loss factor due to temperature and other factors).

$$\text{Number of modules required}(N_m) = \frac{\text{Rated power}(P_{rated})}{\text{Panel maximum power}(P_{max})} \tag{3.56}$$

In this work, four DGs having 1MW each was used. Therefore, based on DGs capacity, it is possible to determine parallel and series PV module configurations for each DGs as follow;

Hence, $N_m = \frac{P_{rated}}{P_{max}} = \quad = \frac{1{,}000{,}000\ \text{W}}{240\ \text{W}} = 4{,}166.66 \approx 4{,}167$ modules for 1MW PV (power required per field).

As discussed in PV specification table under appendix c, 240W required 1.62cm^2, then by having this value from PV specification, it possible to obtain area required for install 1MW PV as follows: then by simple calculation, 1MW(1,000,000W) required 6,750 cm^2.

From the total number of modules required, the number of necessary PV modules in series (NS_{PV}) and parallel (NP_{PV})is obtained as given in equations (3.57) and (3.58) respectively:

$$\text{Number of modules in series } \left(N_{S_{PV}}\right) = \frac{\text{Dc nominal voltage}(V_{DC})}{\text{Maximum power point voltage}(V_{mpp})} \quad (3.57)$$

$$= \frac{1000}{30.65} = 32.62 \approx 33\ modules$$

$$\text{Modules in parallel}\left(N_{P_{PV}}\right) = \frac{\text{Total Number of modules}}{\text{Modules in series}} \quad (3.58)$$

$$= \frac{4{,}167}{33} = 126.26 \approx 127\ modules$$

As a result, to generate 1,000,000W of power, 4167 modules with a maximum capacity of 240W each was distributed as 33 series modules and 127 parallel strings. By the same step, it is possible calculate for each DGs. Actually, each DG has 1MW power, hence total number of modules required to generate 4MW (4,000,000W) is 4x4,167 = 16,668 modules.

B. Size of an Inverter

For grid-connected systems, the input rating of the inverter should be comparable to the rating of the PV array to enable safe and efficient operation(Ndagijimana & Kunjithapathan, 2019).

For this study, since it is suitable with design and has high power starting capacity, the inverter PVS800-57-1000KW-C made by ABB was selected.

Based on the design the overall power was grouped into four fields. Each field has 1MW power capacity. Given that the maximum power of each module is 240 W, it is simple to determine how many modules will be needed in per field as follow:

$$\text{Number of modules per field}(N_{Tm}) = \frac{\text{Rated power}(P_{rated})\ per\ field}{\text{Maximum module power}(P_{max})} \quad (3.59)$$

$$= \frac{1{,}000{,}000\text{W}}{240\text{W}} = 4{,}166.66 \approx 4{,}167 modules$$

According to calculation obtained in part ‘a’ above the maximum number of series-connected modules per string is 33. Therefore, 33 modules are the most number of modules allowable for series connections. It is important to consider the short circuit and maximum power point currents

into account when determining the maximum number of parallel strings. The quantity of parallel strings is determined as follows:

$$String_{\max number/inverter} = \frac{I_{max\ Inverter}}{I_{Sc}\ \text{module}} = \frac{1710\text{A}}{8.33\text{A}} = 205.3\ strings$$

This indicates that the input of the inverter can support up to 205 parallel strings. The total number of modules per field to be 4,167 modules.

The string will include 33 series modules for improved performance and security, the number of parallel strings is then calculated as follows:

$$\text{Number of String /inverter} = \frac{\text{Total module String per inverter}}{\text{Maximum modules per string}} = \frac{4{,}167}{33} = 126.27 < 205.3 \text{ strings}$$

According to the calculation obtained, the design uses $126.27 \approx 127$ strings of 33 modules while respecting to the inverter and module standards. As a result, four inverters with a 1000 Kw total output are needed.

C. Battery Sizing

The basic goal of battery bank sizing is to obtain an energy source that can handle the load generated by the PV panel array and supply enough stored power for needs when there is no sunlight.

$$\text{Size of the battery} = \frac{E_{Tot(Wh)} * G_{ft}}{V_{dc} * DOD_{max} * \eta\text{inv}} \quad (3.60)$$

Where,

$E_{Tot(Wh)}$= Total energy (Wh)

DOD_{max}= Maximum depth of discharge

V_{dc}= Maximum DC System Voltage

G_{ft} = Grid failure time

ηinv = Inverter efficiency

Let's consider the battery supplies the grid during failure/loaded for 3 hours per day. So that, for DG1 E_{Tot}= 1,000,000 W*3= 3,000,000 Wh, DOD =0.7, because DOD of the lead acid storage battery is 70%, and G_{ft} = 3/24 hr.

$$\text{Then, battery size} = \frac{E_{Tot(Wh)} * G_{ft}}{V_{dc} * DOD_{max}} = \frac{3{,}000{,}000 \text{ Wh} * \frac{3}{24\text{hr}}}{48 * 0.7 * 0.99} = 11{,}273.45 \text{ Ah}$$

For this study, Lead acid batteries with product number of S1900 and 2900Ah /12V battery was chosen. The design-rated power of the battery is,

$$\text{Total batteries required} = \frac{\text{Total battery bank capacity}}{\text{capacity of chosen battery}} = \frac{11{,}273.45\text{Ah}}{2900\text{Ah}} = 3.88 \approx 4$$

Depending on the voltage that the solar system generates, the battery bank system voltage may be 12 volts, 24 volts, 48 volts, or 96 volts (Ndagijimana & Kunjithapathan, 2019). In this study, a system voltage of 48 V was selected.

$$\text{Total number of batteries in series}(N_{bs}) = \frac{\text{System voltage}(V_s)}{\text{battery voltage}(V_{battry})} = \frac{48}{12} = 4$$

$$\text{Total batteries in parallel}(N_{bp}) = \frac{\text{Total number of batteries}(N_{bt})}{\text{Number of batteries in serie}(N_{bs})} = \frac{4}{4} = 1$$

Therefore, four batteries having 2900Ah/12V is required per field.

D. Charge Controller Sizing

The most popular charge controllers are maximum power point tracking (MPPT) or pulse width modulation (PWM). A MPPT solar charge controller will automatically and effectively convert the lower voltage panels, battery bank, and PV charge to be equal in voltage when it detects a difference in voltage. The size of a series charge controller is determined by the total PV input current given to the controller as well as by the PV panel layout.

In this PV module type, the short circuit current is 8.33A.

$$\text{Charge controller rating} = \text{Parallel modules} * \text{Module short circuit current} * \text{Safety factor}$$

Here, 48v, 60amp charge controller is chosen for this study, and total number of charge controller per field is calculated as follows,

$I_{rated} = N_{P\,PV} * I_{sc} * 1.3 = 127 * 8.33 * 1.3 = 1{,}375.28\text{A}$

Total number of charge controller $= \frac{\text{charge controller rating}}{Amperes\ of\ individual\ controller} = \frac{1{,}375.28\text{A}}{60A} = 22.92 \approx 23$

CHAPTER FOUR

4. RESULT ANALYSIS AND DISCUSSION

4.1. Introduction

This chapter explains how to model and simulate the existing system by using various DG sizes to raise the Ambo town feeder's system reliability. The ETAP Software simulation has examined a variety of cases. The goal of the simulation is to assess how Distributed Generation (DG) affects the system's reliability and power loss.

The duration and frequency of outages, which are the two general categories of any distribution system reliability analysis. In this study, the frequency of interruption is significantly higher than the benchmark values, which should need mitigation techniques.

4.2. Introduction to ETAP Software

A completely graphical enterprise called Electrical Transient Analysis Program (ETAP) works with several Microsoft Windows operating systems (window 7, 8 and 10). For the purpose of constructing one-line diagrams, ETAP offers an intuitive, fully graphical user interface (GUI) that can be used to graphically add, delete, relocate, zoom in or out, turn on or off the grid, connect elements, change element size, change symbols, change the color of equipment and devices, make custom viewing themes, hide or show protective devices, set operating status, etc. ETAP is one of the well-integrated software for electrical systems, which gives engineers access to a variety of system presentations for various analysis and design needs. The program is used to examine various electrical analyses, including short circuit, reliability, load flow, arc flash, protection coordination, and others.

4.3. Reliability and Power Loss Evaluation with ETAP

ETAP software is one of the power system reliability analysis programs, as it was stated in the introduction part. Lines, transformers, loads, DG, external grid, bus bars, and other devices are among the ETAP equipment analyzed in this investigation. Failure rates and mean time to repair values for each component are needed in order to predict the reliability indices of the Ambo town distribution system. The performance of the distribution system as a whole and the availability of individual lines are using reliability assessments including failure rate and mean time to repair.

Equations 4.1 and 4.2 can be used to compute the reliability indices of the existing substation(Asfaw, 2007).

$$\text{Failure rate}(\lambda) = \frac{\text{Number of outage of a system at agiven period}}{\text{Number of failures}} \quad (4.1)$$

$$\lambda = \frac{279.92}{323} + \frac{393.97}{387} = 0.8667 + 1.018 = 1.88 \text{ failure/ yr.}$$

$$\text{Mean time to repair(MTTR)} = \frac{\text{Total Duration of outages}}{\text{Frequency of outage}s} \quad (4.2)$$

$$\text{MTTR} = \frac{(279.92+393.97)/2}{(323+387)/2} = \frac{336.945}{355} = 0.95 \text{ hrs/int.}$$

The basic reliability parameters for reliability analysis are predicted by the ETAP software using the μA and MTTR equation. The failure rates of active and passive components are combined in ETAP to estimate a component's failure rate. The active failure rate is linked to the component failure mode that activates the primary protection zone around the failed component. It should be noted that only after repair or replacement could the failed component be put back in service. Electrical and failure inputs are present in all equipment. In a distribution system, for instance, a bus bar is provided inputs for its ratings, such as repair time, and failure inputs. Because EEU lacks such data, the failure rate and mean time to repair data are obtained from some reference papers and IEEE standards. Table 4.1 below shows the failure rates and repair times for various components including distribution transformers, and bus bars (IEEE Std C37.20.2-2015: IEEE Standard for Metal-Clad Switchgear, EPRI Technical Report(Bimrew Sendekie Belay, 2022)).

Table 4. 1 Electrical equipment and failure inputs

Equipment Name	Failure rate (λ) (Failure/yr.)	Mean time to repair (MTTR) (Hr.)	Voltage level (KV)
Distribution transformer	0.015	200	15
Bus bar	0.001	2.00	15

4.3.1. Single Line Diagram of Ambo Town Feeder

In this case single line diagram of the selected feeder is designed and named as single line diagram of figure E-1 in Appendix E.

In this study, five cases were considered for the reliability and power loss analysis. These are base case, and four cases at optimal DG size and placement with the help of MOPSO algorithms for different placements and sizes.

Case1: Base case reliability and power loss analysis

The reliability indices of the existing system were shown in Table 4.2 below, and the single line diagram of the system for this scenario is discussed in figure E-2 of appendix E.

Table 4.2: Base case reliability indices result before DG penetration

Project: MSc Thesis	ETAP	Page:1
Location: ASTU	12.6.0H	Date: 05-30-2023
Contract:		SN:
Engineer: Getahun Shanko	Study Case: Hormat Substation II	Revision: Base case
Filename: Reliability Improvement and power loss reduction		Config.: Normal

SUMMARY

System Indexes

SAIFI	355.0820 f / customer. yr
SAIDI	335.9636 hr/customer. yr
CAIDI	0.946 hr/customer interruption
ASAI	0.9616 pu
ASUI	0.03835 pu
EENS	2851.479 MW hr / yr
AENS	32.4032 MW hr/customer. yr

SAIFI	System Average Interruption Frequency Index
SAIDI	System Average Interruption Duration Index
CAIDI	Customer Average Interruption Duration Index
ASAI	Average Service Availability Index
ASUI	Average Service Unavailability Index
EENS	Expected Energy Not Supplied
AENS	Average Energy Not Supplied

Table 4.2 above shows the system reliability indices of the existing system. The existing reliability indices SAIFI, SAIDI, and EENS have values of 355.0820 fr/cust.yr, 335.9636 hr/cust.yr, and 2851.479 MWhr/yr, respectively. Since the indices provided here are greater than standard reliability indices, the existing system has a reliability problem. The feeder's real and reactive power losses for the existing system is 759.7 KW and 403.5 KVar, respectively. This result shows that the real and reactive power loss of the existing system is more, and it needs improvement.

Case 2: Reliability and power loss analysis when 2DGs penetrated at bus 114, and 131with a capacity of 1MW, and 0.9968MW respectively.

This scenario shows the results obtained by penetrating 2DGs to the network as indicated in single line diagram in figure E-3 of appendix E. The summary results are also shown in Table 4.3 as follows.

Table 4.3: Reliability result for case-2

Project: MSc Thesis	ETAP	Page: 1
Location: ASTU	12.6.0H	Date: 06-12-2023
Contract:		SN:
Engineer: Getahun Shanko	Study Case: Hormat Substation II	Revision: Case-2
Filename: Reliability Improvement and Power loss reduction		Config.: Normal

SUMMARY

System Indexes

SAIFI	73.4321 f / customer.yr
SAIDI	115.0485 hr / customer.yr
CAIDI	1.567 hr / customer interruption
ASAI	0.9869 pu
ASUI	0.01313 pu
EENS	1146.248 MW hr / yr
AENS	13.0255 MW hr / customer.yr

SAIFI	System Average Interruption Frequency Index
SAIDI	System Average Interruption Duration Index
CAIDI	Customer Average Interruption Duration Index
ASAI	Average service Availability Index
ASUI	Average Service Unavailability Index
EENS	Expected Energy Not Supplied
AENS	Average Energy Not Supplied

Table 4. 4 shows the overall reliability indices and power loss simulation results for case 2

Parameters	Base case	With 2DGs	Percentage improvement (%)
Active power loss (KW)	759.7	481.805	36.58
Reactive power loss (KVar)	403.5	237.081	41.24
SAIFI (f/cust.yr)	355.0820	73.4321	79.32
SAIDI (hr/cust.yr)	335.9636	115.0485	65.76
EENS (MWh/yr.)	2851.479	1146.248	59.8
DGs locations (bus)	- - - -	114, and 131	- - - -
DGs size (MW)	- - - -	1, and 0.9968	- - - -

As observed, the values of the SAIFI, SAIDI, and EENS indices, which were previously 355.0820 fr/cust.yr, 335.9636 hr/cust.yr, and 2,851.479 MWhr/yr were decreased to 73.4321fry/cust.yr, 115.0485 hr/cust.yr, and 1146.248 MWhr/yr respectively. For SAIFI, SAIDI, and EENS observed, the improvement percentages would have been 79.32%, 65.76%, and 59.8%, respectively. And also, the real and reactive power loss has been decreased from 759.7 KW and 403.5 KVar to 481.805 KW and 237.081 KVar, which shows a reduction of 36.58%, and 41.24% in real and reactive power loss respectively.

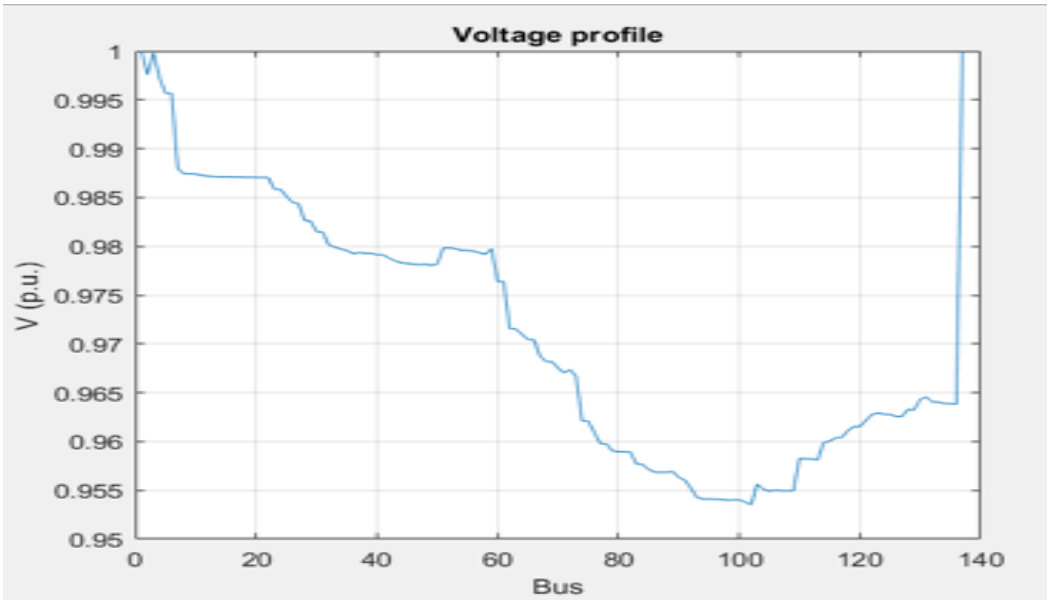

Figure 4.1: Voltage profile of the system after 2DGs penetrated at 114, and 131 buses

Case 3: Analysis of reliability and power loss when 3DGs connected at bus 97,106, and 114 with a capacity of 0.9062MW, 0.9727MW, 0.9785 MW respectively.

This scenario shows the results obtained by penetrating 3DGs to the network as indicated in single line diagram in Figure E-4 of appendix E. The summary results are also shown in Table 4.5 as follows.

Table 4.5: Reliability simulation result after 3DGs penetration

Project: MSc Thesis	ETAP	Page: 1
Location: ASTU	12.6.0H	Date: 06-01-2023
Contract:		SN:
Engineer: Getahun Shanko	Study Case: Hormat Substation II	Revision: Case-3
Filename: Reliability Improvement and Power loss reduction		Config.: Normal

SUMMARY

System Indexes

SAIFI	65.6085 f / customer. yr
SAIDI	93.7154 hr / customer. yr
CAIDI	1.428 hr / customer interruption
ASAI	0.9893 pu
ASUI	0.01070 pu
EENS	944.905 MW hr / yr
AENS	10.7376 MW hr / customer. yr

SAIFI	System Average Interruption Frequency Index
SAIDI	System Average Interruption Duration Index
CAIDI	Customer Average Interruption Duration Index
ASAI	Average service Availability Index
ASUI	Average Service Unavailability Index
EENS	Expected Energy Not Supplied
AENS	Average Energy Not Supplied

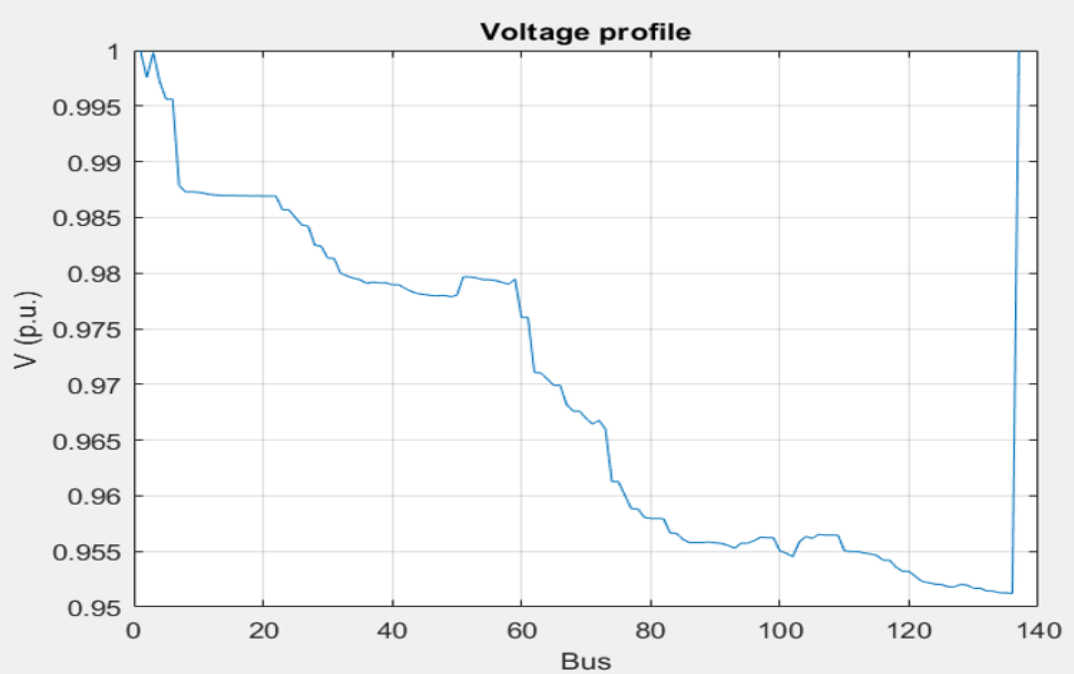

Figure 4.2: Voltage profile of the system after 3DGs connected at bus 97, 106, and 114

From the simulation result, reliability improvement and system power loss were observed. In this case, after three DGs with capacities of 0.9062 MW, 0.9727MW, and 0.9785 MW penetrated at 97, 106, and 114 buses, system reliability indices of SAIFI and SAIDI decreased from 355.0820 f/customer.yr to 75.1824 f/customer.yr and 335.9636 hr./customer.yr to 94.7812 hr/cust.yr respectively.

Additionally, the EENS before DG placement was 2,851.479 MWhr/yr, and after optimization, it was further reduced to 944.405 MWhr/yr. This shows that DG placed and sized properly has been saved 1,907.074 MWhr/yr.

Additionally, the system's active and reactive power losses decreased from 759.7 KW to 475.074KW and from 403.5KVar to 232.103KVar, respectively. Therefore, integrating DG lowers the system's real and reactive power loss by 37.5% and 57.52 %, respectively.

Table 4.6 shows summary of simulation results for case -3

Parameters	Base case	With DG	Percentage improvement (%)
Active power loss (KW)	759.7	475.074	37.5
Reactive power loss (KVar)	403.5	232.103	57.52
SAIFI (f/cust.yr)	355.0820	65.6085	81.52
SAIDI (hr/cust.yr)	335.9636	93.7154	72.1
EENS (MWh/yr.)	2851.479	944.905	66.86
DGs locations (bus)	- - - -	97, 106, 114	- - - -
DGs size (MW)	- - - -	0.9062, 0.9727, 0.9785	- - - - -

Case -4: Reliability and power loss result when 3DGs connected with a capacity of 1.9496, 1.9593, and 2 MW at bus 92, 66, and 122 respectively.

In this scenario, the impact of penetrating 3DGs to the existing system is observed and this implementation is indicated in one line diagram in Figure E-5 of appendix E and summary of the results obtained in this scenario is discussed as shown in Table 4.7 below.

Table 4.7: Reliability results after 3DGs integrated at bus 92, 66, and 122

Project: MSc Thesis	ETAP	Page: 1
Location: ASTU	12.6.0H	Date: 06-05-2023
Contract:		SN:
Engineer: Getahun Shanko	Study Case: Hormat Substation II	Revision: Case-4
Filename: Reliability Improvement, and power loss reduction		Config.: Normal

SUMMARY

System Indexes

SAIFI	64.8109 f / customer.yr
SAIDI	95.6292 hr / customer.yr
CAIDI	1.476 hr / customer interruption
ASAI	0.9891 pu
ASUI	0.01092 pu
EENS	974.049 MW hr / yr
AENS	11.0687 MW hr / customer.yr

SAIFI	System Average Interruption Frequency Index
SAIDI	System Average Interruption Duration Index
CAIDI	Customer Average Interruption Duration Index
ASAI	Average service Availability Index
ASUI	Average Service Unavailability Index
EENS	Expected Energy Not Supplied
AENS	Average Energy Not Supplied

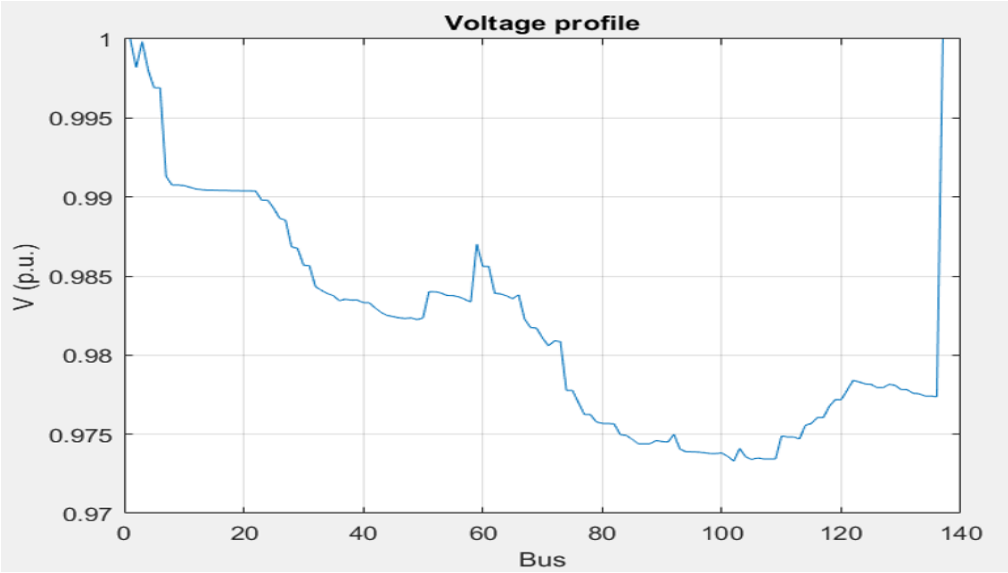

Figure 4.3 Voltage profile of the system for case-4

Table 4.8: Over all simulation result for case-4

Parameters	Base case	With 3DGs	Percentage improvement (%)
Active power loss (KW)	759.7	336.657	55.7
Reactive power loss (KVar)	403.5	167.403	58.51
SAIFI (f/cust.yr)	355.0820	64.8109	81.75
SAIDI (hr/cust.yr)	335.9636	95.6292	71.54
EENS (MWh/yr.)	2851.479	974.049	65.84
DGs locations (bus)	- - - -	92, 66, and 122	- - - -
DGs size (MW)	- - - -	1.9496, 1.9593, 2	- - - - -

As seen from simulation result tabulated above, the active, and reactive power loss decreased by 55.7%, and 58.51% respectively, whereas system reliability indices of SAIFI, SAIDI, and EENS is improved by 81.75%, 71.54%, and 65.84% respectively.

Case -5: Reliability and power loss result when 4DGs connected with a capacity of 1 MW each at bus 53, 102, 111, and 132 respectively.

In this scenario, the impact of penetrating 4DGs to the existing system on reliability and power loss is observed and the implementation is shown in one line diagram in Figure E-5 of appendix E and summary of the results obtained and discussed as shown in Table 4.9 below.

Table 4.9: Reliability results after 4DGs integrated to the system

Project: MSc Thesis	ETAP	Page: 1
Location: ASTU	12.6.0H	Date: 06-11-2023
Contract:		SN:
Engineer: Getahun Shanko	Study Case: Hormat Substation II	Revision: Case5
Filename: Reliability Improvement and Power loss reduction		Config.: Normal

SUMMARY

System Indexes

SAIFI	44.0533 f / customer.yr
SAIDI	55.6486 hr / customer.yr
CAIDI	1.263 hr / customer interruption
ASAI	0.9936 pu
ASUI	0.00635 pu
EENS	460.955 MW hr / yr
AENS	5.2381 MW hr / customer.yr

SAIFI	System Average Interruption Frequency Index
SAIDI	System Average Interruption Duration Index
CAIDI	Customer Average Interruption Duration Index
ASAI	Average service Availability Index
ASUI	Average Service Unavailability Index
EENS	Expected Energy Not Supplied
AENS	Average Energy Not Supplied

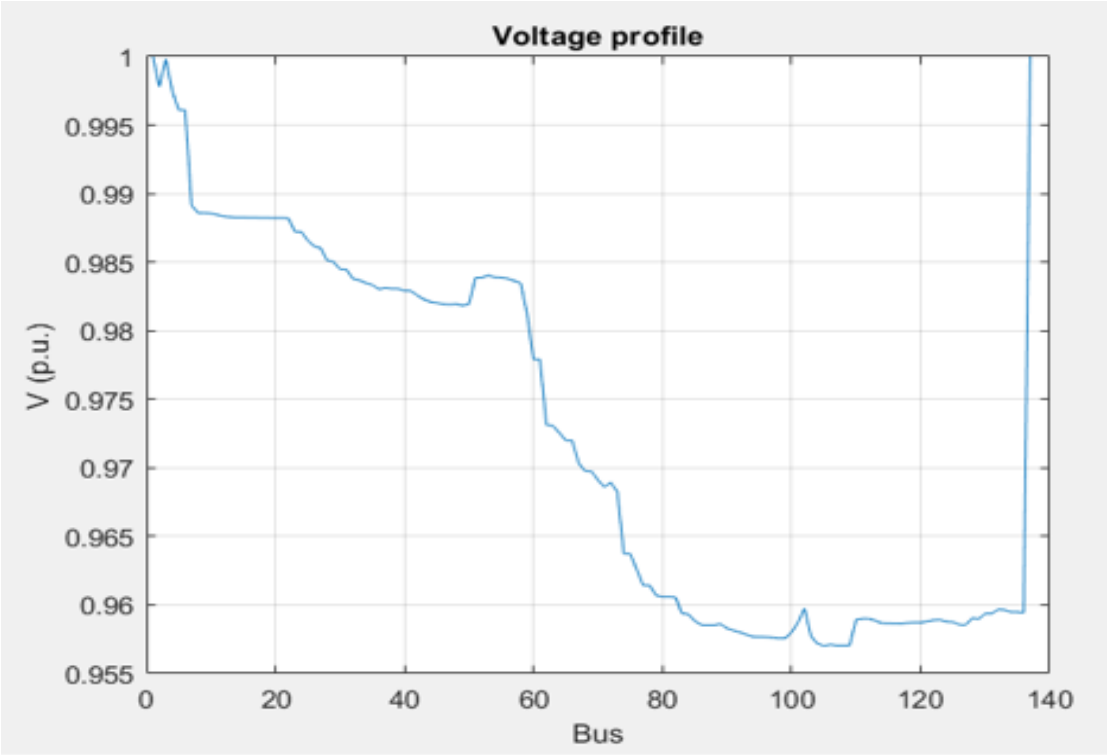

Figure 4.4 Voltage profile of the system for case-5

Table 4.10: Over all simulation result for case-5

Parameters	Base case	With 4DGs	Percentage improvement (%)
Active power loss (KW)	759.7	412.995	45.64
Reactive power loss (KVar)	403.5	203.117	50.34
SAIFI (f/cust.yr)	355.0820	44.0533	87.6
SAIDI (hr/cust.yr)	335.9636	55.6486	83.44
EENS (MWh/yr.)	2851.479	460.955	83.83
DGs locations (bus)	- - - -	53, 102, 111and 132	- - - -
DGs size (MW)	- - - -	1, 1, 1 and 1	- - - - -

As seen from simulation result tabulated above, the active, and reactive power loss decreased by 45.64%, and 50.34% respectively, whereas system reliability indices of SAIFI, SAIDI, and EENS is improved by 87.6%, 83.44%, and 83.83% respectively.

Table 4.11: Over all comparison of results before and after DGs Penetration

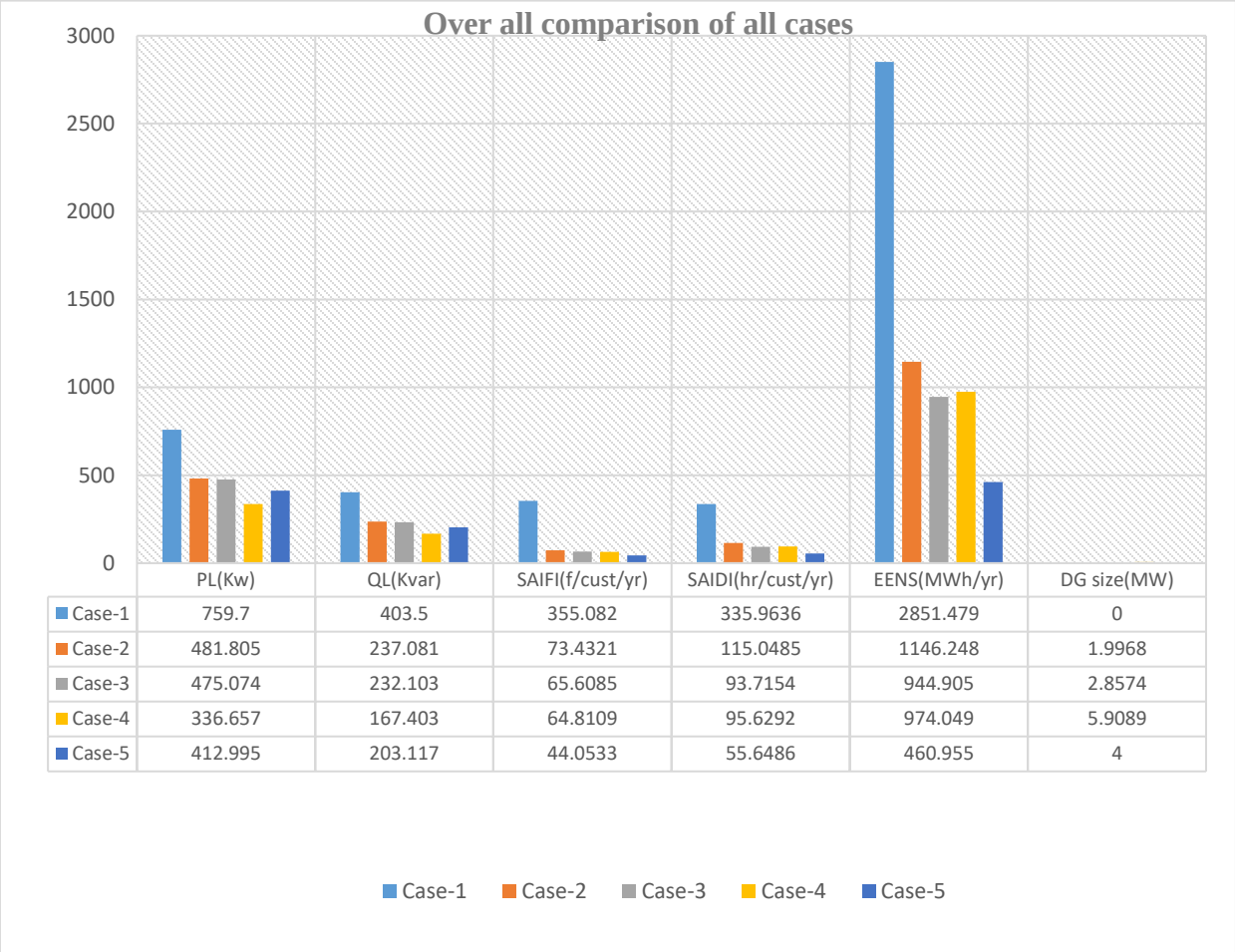

	PL(Kw)	QL(Kvar)	SAIFI(f/cust/yr)	SAIDI(hr/cust/yr)	EENS(MWh/yr)	DG size(MW)
Case-1	759.7	403.5	355.082	335.9636	2851.479	0
Case-2	481.805	237.081	73.4321	115.0485	1146.248	1.9968
Case-3	475.074	232.103	65.6085	93.7154	944.905	2.8574
Case-4	336.657	167.403	64.8109	95.6292	974.049	5.9089
Case-5	412.995	203.117	44.0533	55.6486	460.955	4

4.4. DG Installation Cost

Both utilities and customers gain from the integration of DGs into the existing system. For Ambo town feeders, solar-based DG is preferable due to the abundance of natural resources, environmental advantages, and low maintenance and operating costs.

The installation price of solar based DG significantly changes from time to time. Based on the data obtained from (Mekonnen et al., 2021), the average price of PV will be 589USD/KW, and 320 USD/KW for 2030, and 2050 respectively. For this work with the consideration of PV price changes from year to year, it is possible to estimate the current PV price based on this reference. Therefore, an average PV price for 2023 is estimated 683.15USD/KW. Finally, with the consideration of case-5, cost of DG installation is calculated and tabulated in Table 4.12 below.

Table 4.12: Cost Summary of DGs

DGs size (MW)	Price per KW ($)	Total price ($)
DG1 = 1	683.15	683,150
DG2 = 1	683.15	683,150
DG3 = 1	683.15	683,150
DG4 = 1	683.15	683,150
Total		2,732,600

4.5. Cost of Energy Not Supplied Due to Power Loss and Interruptions

Installation of DG lowers lost costs and improves the performance of the distribution system.

Cost of Energy not supplied = Power not supplied * Electric tariff*Time (4.3)

Cost of Energy lost due to power loss = Power loss (Kw)*time (hr/year) *Electric tariff

= 759.7 Kw*8760hr/yr*2birr/Kwh = 13,309,944birr (average price of electricity is 2birr/kwh).

Cost of Energy not supplied due to interruption = EENS (Mwhr/yr) *year*tariff (birr/Kwh)

= 2851.479 MWh/yr*1yr*2birr/Kwh = 5,702,958birr.

Total Cost of energy lost = Cost of energy lost due to interruption+ cost of energy lost due to power loss = (13,309,944 + 5,702,958) = 19,012,902 birr.

4.6. Cost of Energy Saved due to DG installation

Cost of energy saved due to power loss reduction = Power saved (Kw)*Time (hr/yr) *Electric tariff

= 346.705Kw*8760hr/yr*2birr/Kwh = 6,074,271.6 birr.

Cost of energy saved due to interruption improvement = Power saved (Mwhr/yr) *yr* Elec.tariff

= 2,390.524Mwh/yr*1yr*2birr/Kwh = 4,781,048 birr.

Total Cost saved per year = cost of energy saved due to power loss + cost of energy saved due to interruption.

Total cost saved per year = (6,074,271.6+4,781,048) = 10,855,319.6 birr.

CHAPTER FIVE

5. CONCLUSIONS, RECOMMENDATIONS AND FUTURE WORKS

5.1 CONCLUSIONS

In this study, renewable Distributed Generation (DG) is used to increase distribution system reliability and reduce power loss in Ambo town distribution network. System model and simulation result was carried out by ETAP and MATLAB software. As a result, the system reliability indices of SAIFI, SAIDI, and EENS have been obtained, and analyzed. Therefore, from the recorded result, the system average interruption frequency index (SAIFI) is 355.0820 f/customer/yr, the system average interruption duration index (SAIDI) is 335.9636 hr/cust.yr, and the feeder's total real and reactive power losses of the network is 759.7 KW and 403.5 KVar respectively. Additionally, 2,851.479 MWh/yr of energy is unsold energy due to power outages. This shows that, as a result of planned and unplanned outages, there is significant unavailability of electric power in the distribution network, as well as significant energy loss. According to this study, the existing system reliability does not satisfy the standards established by the Ethiopian Electric Agency. Therefore, in order to increase the system reliability and power loss reduction of the network, four DGs were integrated at optimal placement, and sizing by MOPSO algorithm.

After four DGs located at optimal placement by MOPSO algorithm, the system reliability indices values of SAIFI, SAIDI, and EENS were decreased to 44.053 f/customer/yr, 55.65 hr/cust.yr, and 460.95 MWh/yr respectively. According to this result, the system reliability indices of SAIFI, SAIDI, and EENS is improved by 87.6%, 83.44%, and 83.83% respectively.

Additionally, the overall real and reactive power loss was also decreased to 412.9KW, and 203.12KVar respectively. This result indicates that, both active and reactive power loss is decreased by 45.64%, and 50.34% respectively. At the end, cost estimation of DGs and revenue obtained from the study was calculated.

Finally, in this work the impact of DGs in distribution network has been carried out, and also the result obtained before and after DGs penetration is compared and analyzed. Over all, the result obtained met the objectives mentioned in the study.

5.2 RECOMMENDATIONS

Based on the findings of this study, the following are recommended for whom it may concern.

The electric utility company should encourage distributed generation technology not only for stand-alone power generation but also for grid-connected power generation, and even as a backup. Therefore, here it is recommended that the stakeholders should make encouragements to the government or concerned body to implement distributed generation in the distribution network.

Because DG integration has various negative impacts on distribution systems protection, updating the distribution systems protection must come before installing the DG. Therefore, it is strongly recommended here, as the implementation of automatic protection is necessary while integrating DG into the distribution network.

5.3 FUTURE WORKS

In order to further improve the reliability, and line loss reduction of the radial distribution system, simultaneous DG, and FACT device allocation is suggested here as future work.

In this study, only PV type DG was considered. It would be preferable to investigate alternative distributed generation for improving feeder reliability. And also further detail analysis of individual cost of PV components is recommended as future work.

Research Fund Acknowledgment

This research thesis was funded by Adama Science and Technology University under the grant number of ASTU/SM-R/729/23, Adama, Ethiopia.

REFERENCES

(APPA), A. P. P. A. (2014). Evaluation of Data Submitted in APPA ' s 2013 Distribution System Reliability & Operations Survey.

Abu-Mouti, F. S., & El-Hawary, M. E. (2011). Optimal distributed generation allocation and sizing in distribution systems via artificial bee colony algorithm. IEEE Transactions on Power Delivery, 26(4), 2090–2101. https://doi.org/10.1109/TPWRD.2011.2158246

Adefarati, T., & Bansal, R. C. (2016). Integration of renewable distributed generators into the distribution system: A review. IET Renewable Power Generation, 10(7), 873–884. https://doi.org/10.1049/iet-rpg.2015.0378

Adefarati, T., & Bansal, R. C. (2017). The Impacts of PV-Wind-Diesel-Electric Storage Hybrid System on the Reliability of a Power System. Energy Procedia, 105, 616–621. https://doi.org/10.1016/j.egypro.2017.03.364

Aditya Prasad Padhy. (2020). Optimal Allocation and Size Selection of Dispersed Generation in Radial Distribution System. International Journal of Engineering Research And, V9(07), 145–150. https://doi.org/10.17577/ijertv9is070036

Arram, A. A., Farrag, M. A., & El-Sayed, M. A. (2015). A Generalized Multistage Economic Planning Model for Distribution System Containing DG Units. International Journal of Engineering Research and Development, 11(07), 2278–67.

Asfaw, B. (2007). Anomaly Detection Modeling In The school of Graduate Studies of Addis Ababa University in partial fulfillment of the requirements for the Degree of Masters of Science in Computer Science.

B. S., M. R., V K, M. V., & Veeramanju, D. K. T. (2020). Evaluation of Distributed Generation Impact on Reliability of a Distribution System using DIgSILENT PowerFactory. International Journal of Innovative Technology and Exploring Engineering, 9(10), 381–389. https://doi.org/10.35940/ijitee.j7586.0891020

Behailu Abebe, 2015. (2015). Federal Democratic Republic of Ethiopia Ministry of Defense Defense University , College of Engineering Office of Postgraduate Programs and Research Minimization of Harmonics using shunt active filter Minimization of Harmonics using shunt active filter.

Bewketu Getie, 2017. (2020). Improvement Of Distribution System Reliability Using Distributed Generation And Circuit Reclosers (Case Study : Motta Substation).

Bimrew Sendekie Belay. (2022). Distribution System Reliability Assessment And Enhancement By Using Tie Switches And Sectionalizer's, 8.5.2017, 2003–2005.

Borges, C. L. T., & Falcão, D. M. (2003). Impact of distributed generation allocation and sizing on

reliability, losses and voltage profile. 2003 IEEE Bologna PowerTech - Conference Proceedings, 2, 5–9. https://doi.org/10.1109/PTC.2003.1304342

Braide, S. L. (2018). Improved Reliability Analysis of Electricity Power Supply to Port Harcourt Distribution Network. International Journal of Engineering Science Invention, 7(7), 23–36.

Debrul, A. (2016). By: abeba debru teshome advisor: getachew biru worku (dr.-ing).

Design Of A Large Scale Solar Pv System. (2016).

Essallah, S., Bouallegue, A., & Khedher, A. (2018). Optimal sizing and placement of DG units in radial distribution system. International Journal of Renewable Energy Research, 8(1), 166–177. https://doi.org/10.20508/ijrer.v8i1.6666.g7291

Fernnandez Sarabia, A. (2011). Impact of distributed generation on distribution system By. Aalborg University Denmark, June, 106.

Gana, N. N., & Akpootu, D. O. (2013). Estimation of global solar radiation using four sunshine based models in Kebbi, North-Western, Nigeria. Pelagia Research Library Advances in Applied Science Research, 4(5), 409–421.

Hailemariam, A. (2018). Addis Ababa Institute of Technology School of Electrical and Computer Engineering Study on Planning of Distribution System (Case Study At Cotobie Substation)

Hegvik, A. (2012). Case Study Analysis of Running Distributed Generators in Island Mode Effects on Reliability of Supply. June.

Hiluf, A. (2020). Reliability Assessment of Electrical Distribution Network u sing Analytical Method : A C ase S tudy of Maychew C ity Distribution System. 9(08), 977–985.

Hussain, I., Khan, F., Ahmad, I., Khan, S., & Saeed, M. (2021). Power Loss Reduction via Distributed Generation System Injected in a Radial Feeder. Mehran University Research Journal of Engineering and Technology, 40(1), 160–168.

Idowu, K., Uhunmwangho, R., Okafor, E. C. N., & Big-Alabo, A. (2021). Reliability Improvement Study of a Distribution Network with Distributed Generation. Applications of Modelling and Simulation, 5, 53–65.

Jaleel, A. M., & Abd, M. K. (2021). Reliability Evaluation of Electric Distribution Network with Distributed Generation Integrated. International Journal of Intelligent Engineering and Systems, 14(5), 306–319. https://doi.org/10.22266/ijies2021.1031.28

Keerio, M. U., Ali, A., Laghari, J. A., & Shiana, B. (2019). Minimization of Power Loss in Radial Distribution Network Using Optimal Feeder Reconfiguration and Distributed Generation Allocation. Pakistan Journal of Science, 71(4), 179.

Maduforo, P. C., Emechebe, J. N., Eronu, E. M., & Benson, S. A. (2020). Sensitivity Based

Approach for the Optimal Sizing and Allocation of Distributed Generation in a Radial Network. European Journal of Engineering Research and Science, 5(6), 751–756. https://doi.org/10.24018/ejers.2020.5.6.1978

Manadhar, S. (2013). Reliability Assessment of Smart Distribution System and Analysis of Automatic Line Switches.

Maradin, D., Cerović, L., & Mjeda, T. (2017). Economic Effects of Renewable Energy Technologies. Naše Gospodarstvo/Our Economy, 63(2), 49–59. https://doi.org/10.1515/ngoe-2017-0012

Mehammed, A. (2020). … Improvement By Intelligent Placement of Distributed Generation (Dg) on Case Study of Gonder City Power Distribution ….

Mekonnen, T., Bhandari, R., & Ramayya, V. (2021). Modeling, analysis and optimization of grid-integrated and islanded solar pv systems for the Ethiopian residential sector: Considering an emerging utility tariff plan for 2021 and beyond. Energies, 14(11).

Meteku, C. (2020). Reliability Analysis of 15kv Distribution System Network (Case Study: Addis Alem Substation Network). January.

Meychw, A. (2021). Hawassa University Insititute Of Technology School Of Electrical And Computer Engineering Second Year Post Graduate In Power System And Energy Engineering.

Mindaye, H. (2020). Investigation And Reliability Improvement Of Radial Distribution System Using Flisr Technology / Case Study On Asella Distribution System /.

Ndagijimana, & Kunjithapathan, B. (2019). Design and implementation pv energy system for electrification rural areas. International Journal of Engineering and Advanced Technology

Nikolova-Poceva, S. (2021). Optimization of Hybrid Renewable Energy System. Journal of Electrical Engineering and Information Technologies, 6(1), 5–13.

Ogunsina, A. A., Petinrin, M. O., Petinrin, O. O., Offornedo, E. N., Petinrin, J. O., & Asaolu, G. O. (2021). Optimal distributed generation location and sizing for loss minimization and voltage profile optimization using ant colony algorithm. SN Applied Sciences, 3(2).

Okereafor, F. C.1, Idoniboyeobu, D.C.2, and Bala, T. K. . (2017). Open Access Analysis of 33 / 11KV RSU Injection Substation for Improved Performance with Distributed Generation (DG) Units American Journal of Engineering Research (AJER). 9, 301–316.

Rind ++, M. H., Rathi, M. K., Hashmani, A. A., & Lashari ++, A. A. (2019). Sindh Universityresearch Journal(Science Series) Optimal placement and sizing of DG in Radial Distribution System using PSO Technique. 51(04), 653–660.

Sasi Kumar, G., Sarat Kumar, S., & Kumar, S. V. J. (2018). DG Placement Using Loss Sensitivity Factor Method for Loss Reduction and Reliability Improvement in Distribution System. International Journal of Engineering & Technology, 7(23), 236–240.

Talukdar, B. K. (2019). Electrical Distribution System (an Overview). Internation Journal Of Advance Research And Innovative Ideas In Education, 5(4), 22–33.

Techno, I. (2015). Load Flow Analysis & Loss Allocation for Unbalanced Radial Power Distribution Systems. November.

Yadav, D. L., & Choube, S. C. (2021). DG placement in distribution systems using analytical techniques. International Journal of Engineering Trends and Technology, 69(9), 236–241.

APPENDIX A: Reason of fault and interruption data for 2021/22

Month	**January, 2021**											
Feeder Name	Causes of Interruptions										Total Frequency	Total Duration
	DEF		DPSC		DTE		DTSC		OP			
	F	D	F	D	F	D	F	D	F	D	F	D
Ambo water	0	0	4	3.01	0	0	1	0.06	3	3.98	8.00	7.05
Ambo town	0	2	6	10.11	0	2	10	3.29	10	18.46	26.00	27.86
Guder town	0	0	5	6.21	0	0	6	0.64	3	3.28	14.00	10.13
Month	**February, 2021**											
Feeder Name	Causes of Interruptions										Total Frequency	Total Duration
	DEF		DPSC		DTE		DTSC		OP			
	F	D	F	D	F	D	F	D	F	D	F	D
Ambo water	1	2.57	4	3.32	0	0	6	0.49	10	19.54	21.00	25.92
Ambo town	3	3.45	11	15.38	6	2.57	7	2.6	6	2.14	33.00	34.14
Guder town	3	2.48	6	5.67	0	0	12	1.64	9	11.65	30.00	21.44
Month	**March 2021**											
Feeder Name	Causes of Interruptions										Total Frequency	Total Duration
	DEF		DPSC		DTE		DTSC		OP			
	F	D	F	D	F	D	F	D	F	D	F	D
Ambo water	0	0	1	0.58	1	0.06	0	0	4	4.26	6.00	4.90
Ambo town	2	2.61	7	11.93	1	2.05	10	2.89	11	2.51	31.00	29.99
Guder town	0	0	12	10.11	2	0.22	8	0.84	7	3.11	29.00	14.28

Month	April 2021											
Feeder Name	Causes of Interruptions										Total Frequency	Total Duration
	DEF		DPSC		DTE		DTSC		OP			
	F	D	F	D	F	D	F	D	F	D	F	D
Ambo water			4	4.27	2	0.14	4	2.68	5	4.73	15.00	11.82
Ambo town		3	8	6.8		4	7	2.41	11	7.37	26.00	23.58
Guder town	1	1.6	9	12.7	1	0.08	8	0.66	9	11.42	28.00	26.46
Month	May 2021											
Feeder Name	Causes of Interruptions										Total Frequency	Total Duration
	DEF		DPSC		DTE		DTSC		OP			
	F	D	F	D	F	D	F	D	F	D	F	D
Ambo water	1	14.98	8	9.82	1	0.06	1	0.37	5	10.8	16.00	36.03
Ambo town	2	7.77	10	14.61	1	2.08	10	3.7	2	2.48	25.00	30.64
Guder town	5	6.21	11	28.66	2	0.23	5	0.6	4	1.8	27.00	37.50
Month	June 2021											
Feeder Name	Causes of Interruptions										Total Frequency	Total Duration
	DEF		DPSC		DTE		DTSC		OP			
	F	D	F	D	F	D	F	D	F	D	F	D
Ambo water			6	22.76			4	8.48	1	0.08	11.00	31.32
Ambo town		2.05	8	8.05		4	1	2.05	6	3.85	15.00	20.00
Guder town	3	2.13	27	20.74			6	0.6	2	2.69	38.00	26.16

Month	**July 2021**											
Feeder Name	Causes of Interruptions										Total Frequency	Total Duration
	DEF		DPSC		DTE		DTSC		OP			
	F	D	F	D	F	D	F	D	F	D	F	D
Ambo water	0	0	2	0.78	0	0	4	2.61	4	5.88	10.00	9.27
Ambo town		0.49	9	4.51	0	0	4	1.92	12	7.84	25.00	14.76
Guder town	2	0.9	14	16.81	1	0.08	5	0.44	3	1.47	25.00	19.70
Month	**August 2021**											
Feeder Name	Causes of Interruptions										Total Frequency	Total Duration
	DEF		DPSC		DTE		DTSC		OP			
	F	D	F	D	F	D	F	D	F	D	F	D
Ambo water	0		2.0	2.15			2.0	0.16	4	4.97	8.00	7.28
Ambo town	2	2.00	3.00	3.81	2	2	12	4.30	10	11.83	29.00	23.94
Guder town	2	14.69	4.0	9.04	3	0.74	5.0	0.36	11	8.69	25.00	33.52
Month	**September 2021**											
Feeder Name	Causes of Interruptions										Total Frequency	Total Duration
	DEF		DPSC		DTE		DTSC		OP			
	F	D	F	D	F	D	F	D	F	D	F	D
Ambo water		2	6	15.3	3	2	8	2.16	9	3.1	36.00	32.91
Ambo town			4	13.3	1	0.35	6	0.16	7	1.1	18.00	14.91
Guder town	3	13.03	6	19.58	2	0.76	12	2.03	7	4.7	30.00	40.10

Month	October 2021											
Feeder Name	Causes of Interruptions										Total Frequency	Total Duration
	DEF		DPSC		DTE		DTSC		OP			
	F	D	F	D	F	D	F	D	F	D	F	D
Ambo water			1.0	1.76	1	0.78	4.0	0.87	4.0	15.21	10.00	18.62
Ambo town	2	2.00	4.00	4.79	2	2	12	4.04	12	11.00	32.00	31.83
Guder town			4.0	6.75	2	0.84	7	2.87	12	14.18	25.00	24.64
Month	November 2021											
Feeder Name	Causes of Interruptions										Total Frequency	Total Duration
	DEF		DPSC		DTE		DTSC		OP			
	F	D	F	D	F	D	F	D	F	D	F	D
Ambo water					1	0.85			1	0.53	2.00	1.38
Ambo town	2	2	3	3.08	2	2	10	4.87	5	4.52	19.00	16.47
Guder town			5	7.89	2	0.34	7	3.21	9	2.38	23.00	13.82
Month	December 2021											
Feeder Name	Causes of Interruptions										Total Frequency	Total Duration
	DEF		DPSC		DTE		DTSC		OP			
	F	D	F	D	F	D	F	D	F	D	F	D
Ambo water	0	0	3	7.01	0	0	1	0.06	2	0.41	6.00	7.48
Ambo town	0	2	12	15.9	0	2	11	3.05	11	8.12	34.00	31.07
Guder town	1	0.28	6	3.13	1	0.08	3	0.24	5	10.68	16.00	14.41

Month	**January 2022**											
Feeder Name	Causes of Interruptions										Total Frequency	Total Duration
	DEF		DPSC		DTE		DTSC		OP			
	F	D	F	D	F	D	F	D	F	D	F	D
Ambo water	1	0.7	1	1.88	1	0.07	3	0.17	9	11.41	15.00	14.23
Ambo town	2	3	8	6.53	2	3	10	3.72	7	8.35	29.00	24.60
Guder town	2	3.75	7	19.63	2	0.2	2	0.14	1	0.5	14.00	24.22
Month	**February 2022**											
Feeder Name	Causes of Interruptions										Total Frequency	Total Duration
	DEF		DPSC		DTE		DTSC		OP			
	F	D	F	D	F	D	F	D	F	D	F	D
Ambo water	3	14.45	2	4.02			1	0.12	5	6.41	11.00	25.00
Ambo town	2	3	12	17.08	2	3	6	3.37	8	12.04	30.00	38.49
Guder town	1	0.13	11	28.24					4	0.54	16.00	28.91
Month	**March 2022**											
Feeder Name	Causes of Interruptions										Total Frequency	Total Duration
	DEF		DPSC		DTE		DTSC		OP			
	F	D	F	D	F	D	F	D	F	D	F	D
Ambo water	2	5.33	4	4.85			1	0.08	14	33.59	21.00	43.85
Ambo town		3	6	5.25		3	2	3.18	9	21.38	17.00	35.81
Guder town	5	3.73	17	21.16			1	0.07	6	1.76	29.00	26.72

Month	**April 2022**											
Feeder Name	Causes of Interruptions										Total Frequency	Total Duration
	DEF		DPSC		DTE		DTSC		OP			
	F	D	F	D	F	D	F	D	F	D	F	D
Ambo water	1	3.95	5	6.76			2	0.06	14	24.31	22.00	35.08
Ambo town	3	3.87	13	20.43	2	3.11	4	3.17	13	18.99	35.00	49.57
Guder town	4	11.46	10	13.27	3	0.12	5	0.32	6	10.37	28.00	35.54
Month	**May 2022**											
Feeder Name	Causes of Interruptions										Total Frequency	Total Duration
	DEF		DPSC		DTE		DTSC		OP			
	F	D	F	D	F	D	F	D	F	D	F	D
Ambo water	4	2.31	2	5.95					6	15.68	12.00	23.94
Ambo town	9	26.33	13	20.57	6	3.63	1	3.2	16	8.93	45.00	62.66
Guder town	5	6.58	19	44.53	1	0.02	2	0.15	11	4.34	38.00	55.62
Month	**June 2022**											
Feeder Name	Causes of Interruptions										Total Frequency	Total Duration
	DEF		DPSC		DTE		DTSC		OP			
	F	D	F	D	F	D	F	D	F	D	F	D
Ambo water	3	1.89	2	2					10	4.85	15.00	8.74
Ambo town	10	10.11	13	12.83	2		4	0.2	19	7.3	48.00	30.44
Guder town	12	14.56	16	10.59	1	0.12	4	0.41	17	15.83	50.00	41.51

Month	July 2022											
Feeder Name	Causes of Interruptions										Total Frequency	Total Duration
	DEF		DPSC		DTE		DTSC		OP			
	F	D	F	D	F	D	F	D	F	D	F	D
Ambo water	2	2.75	2	2.12					3	5.99	7.00	10.86
Ambo town	5	3.16	8	7.18	7	3.73	3	3.44	14	5.42	37.00	22.93
Guder town	18	18.94	15	25.47	2	0.21	3	0.37	8	7.14	46.00	52.13
Month	August 2022											
Feeder Name	Causes of Interruptions										Total Frequency	Total Duration
	DEF		DPSC		DTE		DTSC		OP			
	F	D	F	D	F	D	F	D	F	D	F	D
Ambo water			2	6.53					6	13.72	8.00	20.25
Ambo town	1	0.46	3	5.39			4	1.18	9	3.46	17.00	10.49
Guder town	1	11	10	16.6			4	0.29	6	1.94	21.00	29.83
Month	September 2022											
Feeder Name	Causes of Interruptions										Total Frequency	Total Duration
	DEF		DPSC		DTE		DTSC		OP			
	F	D	F	D	F	D	F	D	F	D	F	D
Ambo water	0	0	1	2.16	1	0.06	0	0	2	0.68	4.00	2.90
Ambo town	2	3	15	18.94	4	3.18	10	3.9	10	10.55	41.00	39.57
Guder town	3	8.41	21	11.4	3	0.32	1	0.08	7	3.75	35.00	23.96

Month	October 2022											
Feeder Name	Causes of Interruptions										Total Frequency	Total Duration
	DEF		DPSC		DTE		DTSC		OP			
	F	D	F	D	F	D	F	D	F	D	F	D
Ambo water			2	10.92			2	0.15	3	0.71	7.00	11.78
Ambo town	3	8.1	8	5.26	2	3	14	3.97	5	3.91	32.00	24.24
Guder town	6	3.24	9	6.76	1	0.06	2	0.16	5	1.22	23.00	11.44
Month	November 2022											
Feeder Name	Causes of Interruptions										Total Frequency	Total Duration
	DEF		DPSC		DTE		DTSC		OP			
	F	D	F	D	F	D	F	D	F	D	F	D
Ambo water			2	1.42			5	3.72	5	12.97	12.00	18.11
Ambo town	2	3	10	15.72	2	3	9	6.54	9	5.72	32.00	33.98
Guder town	5	3.63	20	10.59	1	0.28	5	0.3	5	8.41	36.00	23.21
Month	December 2022											
Feeder Name	Causes of Interruptions										Total Frequency	Total Duration
	DEF		DPSC		DTE		DTSC		OP			
	F	D	F	D	F	D	F	D	F	D	F	D
Ambo water	1	1.03	3	2.5	2	0.12	3	0.35	9	5.99	18.00	9.99
Ambo town	2	3	8	8.66	4	3.2	7	3.3	3	3.03	24.00	21.19
Guder town	2	9.73	7	12.88	3	0.2	5	0.34	2	1.04	19.00	24.19

APPENDIX B: Ethiopian Electric Utility of electric tariffs since 2022

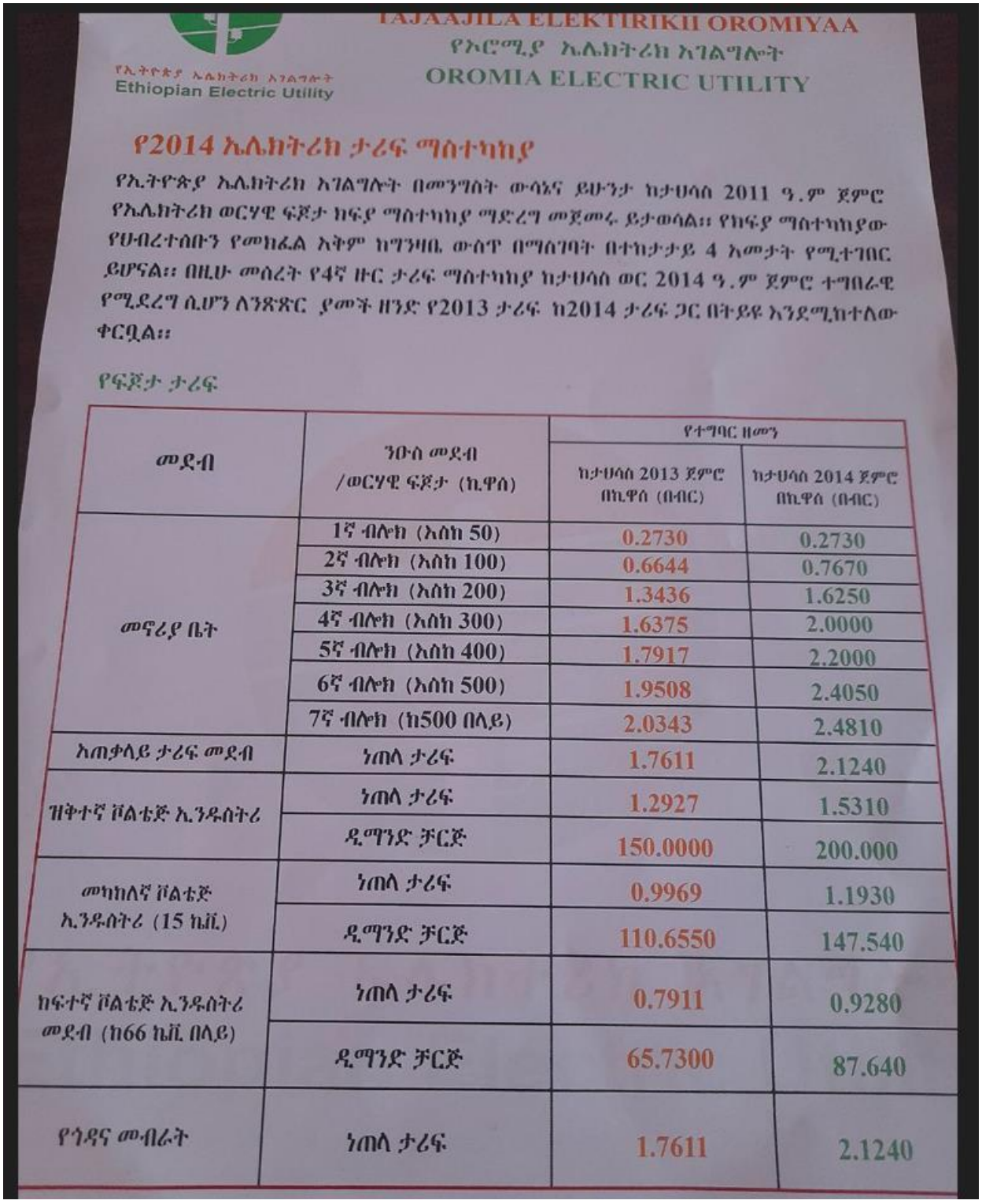

TAJAAJILA ELEKTIRIKII OROMIYAA
የኦሮሚያ ኤሌክትሪክ አገልግሎት
OROMIA ELECTRIC UTILITY

የኢትዮጵያ ኤሌክትሪክ አገልግሎት
Ethiopian Electric Utility

የ2014 ኤሌክትሪክ ታሪፍ ማስተካከያ

የኢትዮጵያ ኤሌክትሪክ አገልግሎት በመንግስት ውሳኔና ይሁንታ ከታህሳስ 2011 ዓ.ም ጀምሮ የኤሌክትሪክ ወርሃዊ ፍጆታ ክፍያ ማስተካከያ ማድረግ መጀመሩ ይታወሳል። የክፍያ ማስተካከያው የህብረተሰቡን የመክፈል አቅም ከግንዛቤ ውስጥ በማስገባት በተከታታይ 4 አመታት የሚተገበር ይሆናል። በዚሁ መሰረት የ4ኛ ዙር ታሪፍ ማስተካከያ ከታህሳስ ወር 2014 ዓ.ም ጀምሮ ተግበራዊ የሚደረግ ሲሆን ለንጽጽር ያመች ዘንድ የ2013 ታሪፍ ከ2014 ታሪፍ ጋር በትይዩ እንደሚከተለው ቀርቧል።

የፍጆታ ታሪፍ

መደብ	ንዑስ መደብ /ወርሃዊ ፍጆታ (ኪዋሰ)	የተግባር ዘመን	
		ከታህሳስ 2013 ጀምሮ በኪዋሰ (በብር)	ከታህሳስ 2014 ጀምሮ በኪዋሰ (በብር)
መኖሪያ ቤት	1ኛ ብሎክ (እስከ 50)	0.2730	0.2730
	2ኛ ብሎክ (እስከ 100)	0.6644	0.7670
	3ኛ ብሎክ (እስከ 200)	1.3436	1.6250
	4ኛ ብሎክ (እስከ 300)	1.6375	2.0000
	5ኛ ብሎክ (እስከ 400)	1.7917	2.2000
	6ኛ ብሎክ (እስከ 500)	1.9508	2.4050
	7ኛ ብሎክ (ከ500 በላይ)	2.0343	2.4810
አጠቃላይ ታሪፍ መደብ	ነጠላ ታሪፍ	1.7611	2.1240
ዝቅተኛ ቮልቴጅ ኢንዱስትሪ	ነጠላ ታሪፍ	1.2927	1.5310
	ዲማንድ ቻርጅ	150.0000	200.000
መካከለኛ ቮልቴጅ ኢንዱስትሪ (15 ኪቩ)	ነጠላ ታሪፍ	0.9969	1.1930
	ዲማንድ ቻርጅ	110.6550	147.540
ከፍተኛ ቮልቴጅ ኢንዱስትሪ መደብ (ከ66 ኪቩ በላይ)	ነጠላ ታሪፍ	0.7911	0.9280
	ዲማንድ ቻርጅ	65.7300	87.640
የጎዳና መብራት	ነጠላ ታሪፍ	1.7611	2.1240

APPENDIX C: Basic characteristics of Suniva ART245-60-3-1PV (Nikolova-Poceva, 2021)

The Suniva ART245-60-3-1 PV module data	**Values**	**Unit**
Maximum power(P_{max})	240	W
Maximum power point voltage(V_{mpp})	30.65	V
Maximum power point current(I_{mpp})	7.82	A
Open circuit voltage(V_{oc})	37.08	V
Short circuit current(I_{sc})	8.33	A
Voltage temperature coefficient(β)	-0.332	%/C
Current temperature coefficient(α)	0.036	%/C
Efficiency	14.9	%
Module Temperature	-40 to +90	°C
Irradiance	1000	W/m^2
Length	165.3	Cm
Width	98.2	Cm
Area	1.62	Cm^2
Max system DC voltage	1000	V
Warranty	25	Years

APPENDIX D: Technical specifications of the chosen inverter(Nikolova-Poceva, 2021)

Inverter model:- PVS800-57-1000KW-C	
DC Inputs	
Maximum input power (P_{PVmax})	1000KW
DC voltage range ($V_{mpp\ DC}$)	600 to 850V
Maximum DC voltage ($V_{max\ DC}$)	1100V
Maximum DC current ($I_{max\ DC}$)	1710A
Number of protected DC inputs	8 to 20(+/-)
AC Output	
Nominal power($P_{nom\ AC}$)	1000 KW
Maximum output power	1200 KW
Power at 0.9 pf	950 KW
Nominal AC current($I_{nom\ AC}$)	1445 A
Nominal output voltage($V_{nom\ AC}$)	400 V
Frequency	50/60 HZ
Maximum efficiency	98.8%
External auxiliary voltage	230 V, 50 HZ

APPENDIX E: Single line diagram of the system for each scenarios

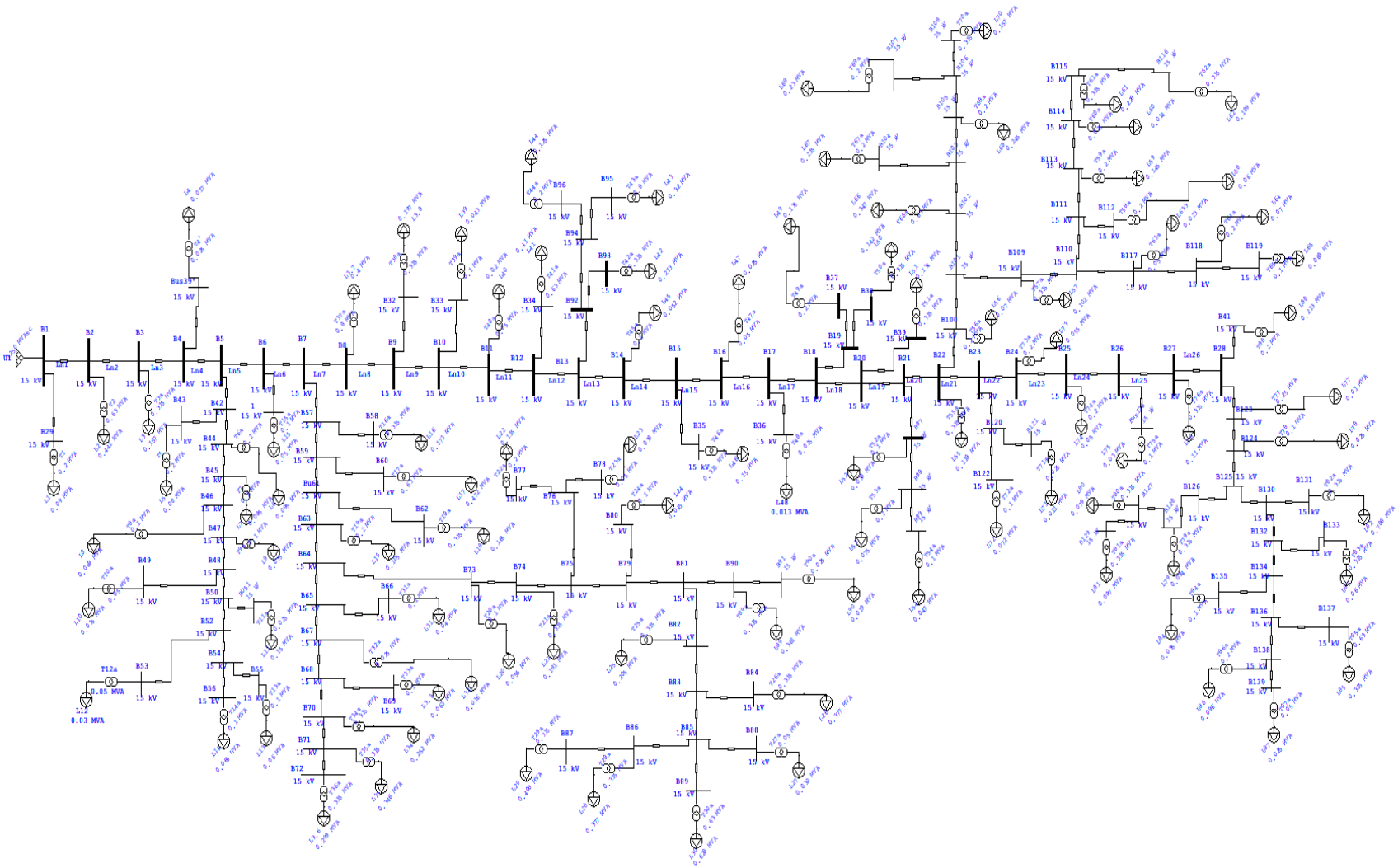

Figure E-1: Existing system single-line diagram

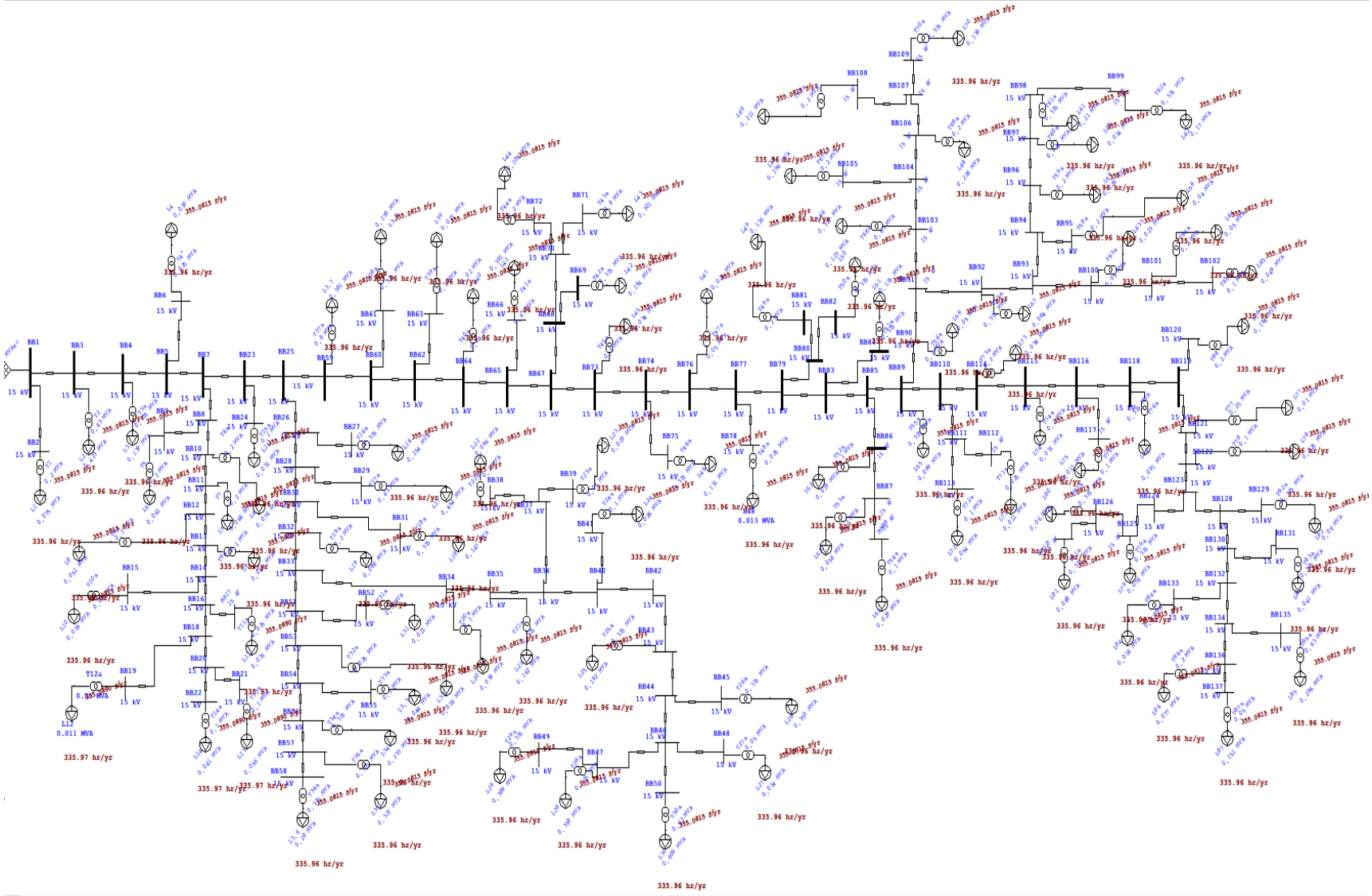

Figure E-2: Single line diagram of Ambo town feeder before DG penetration

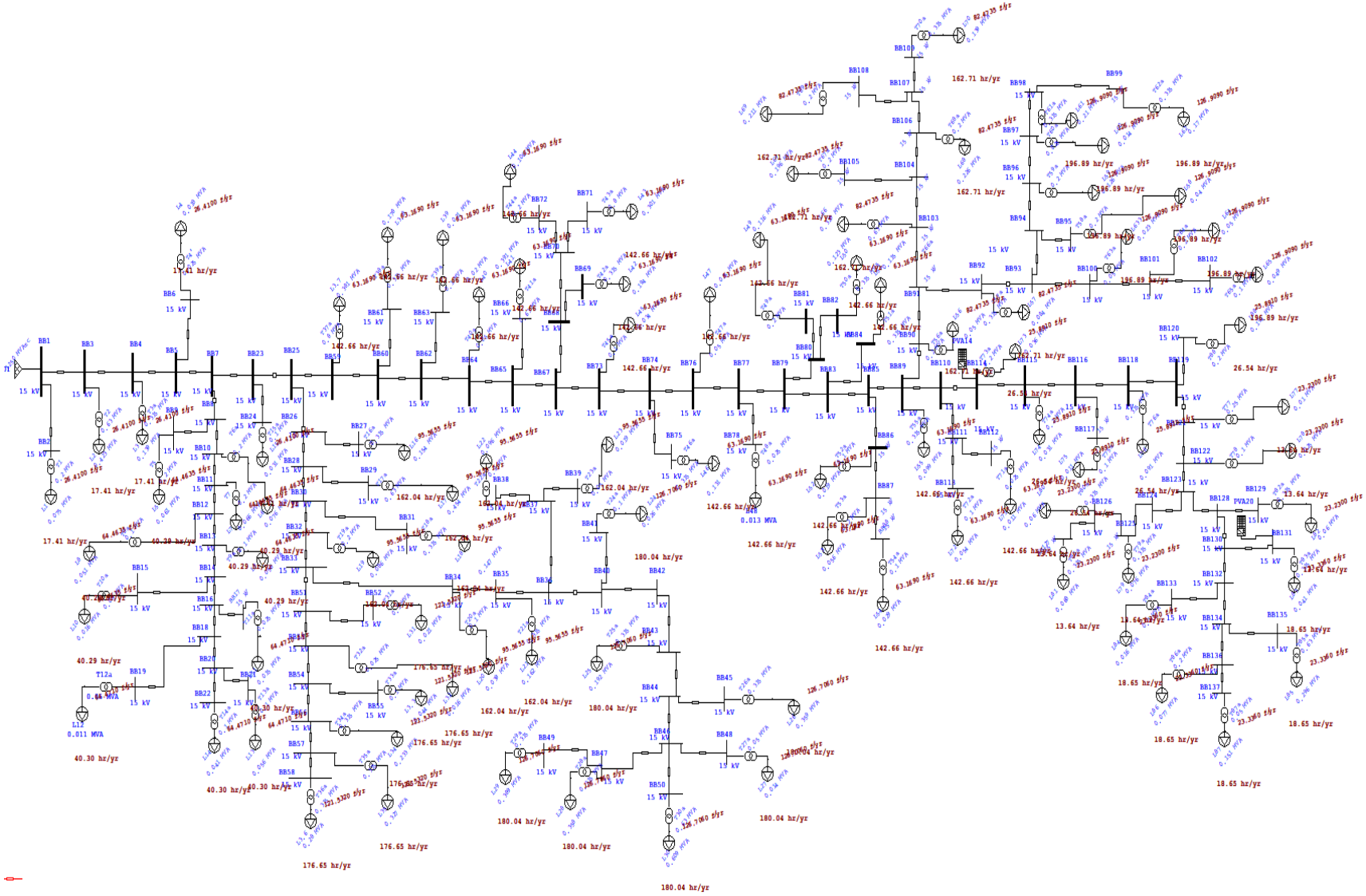

Figure E-3: Single line diagram of the system with 2DGs penetration at bus 114, and 131

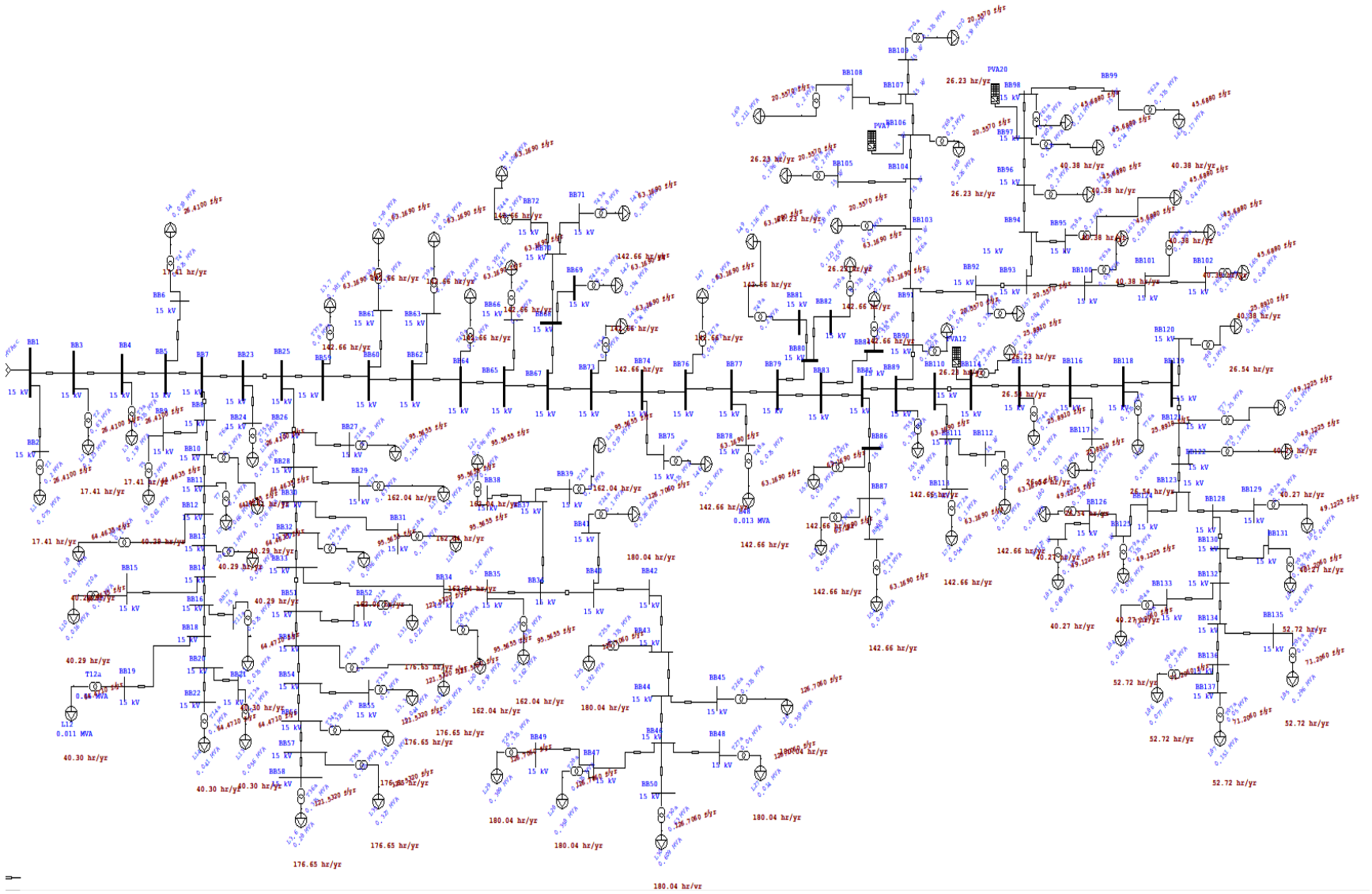

Figure E-4: Single diagram of the network after 3DGs connected at bus 97, 106, and 114

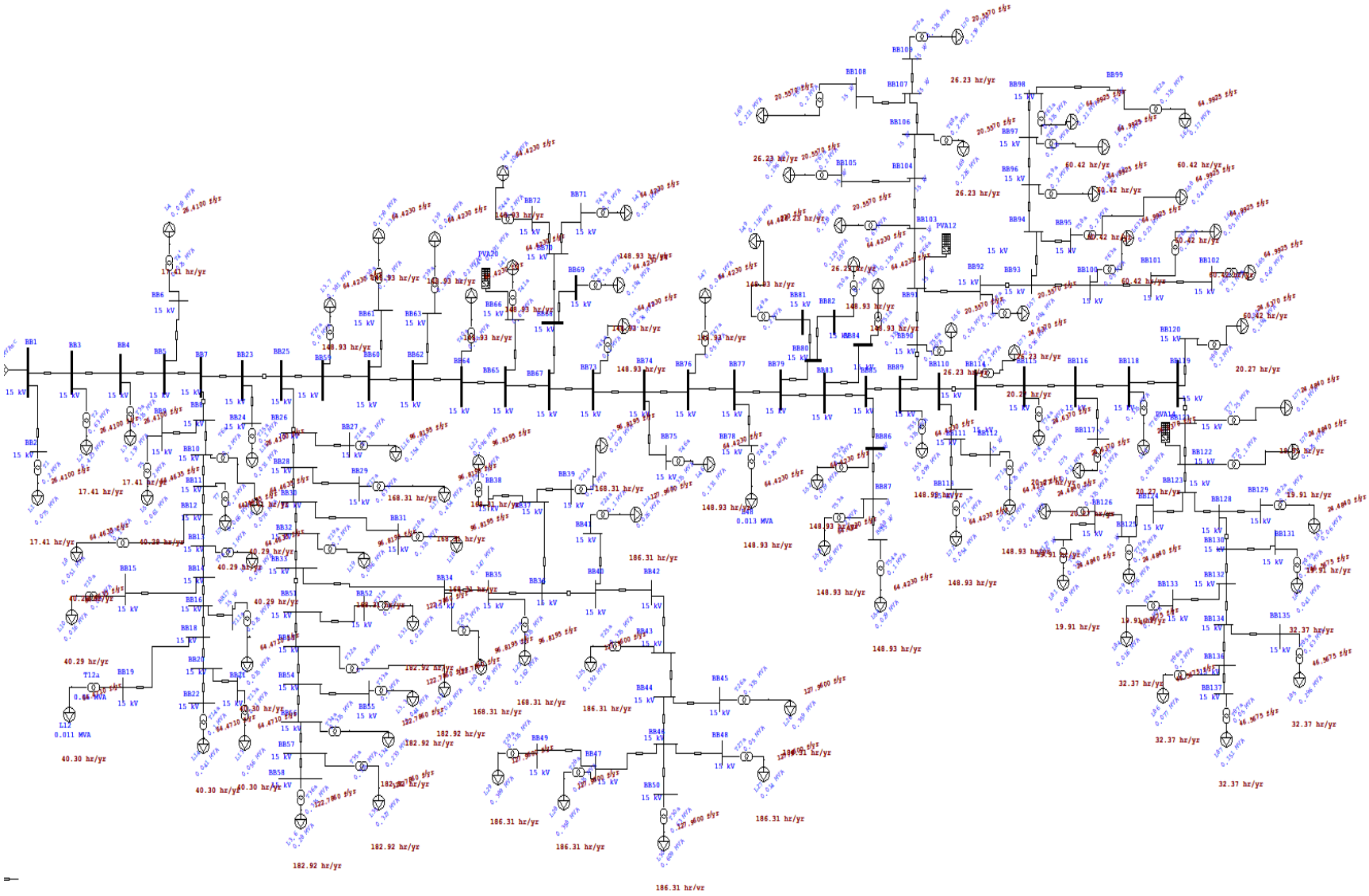

Figure E-5: System network with integration of 3DGs at bus 92, 66, and 122

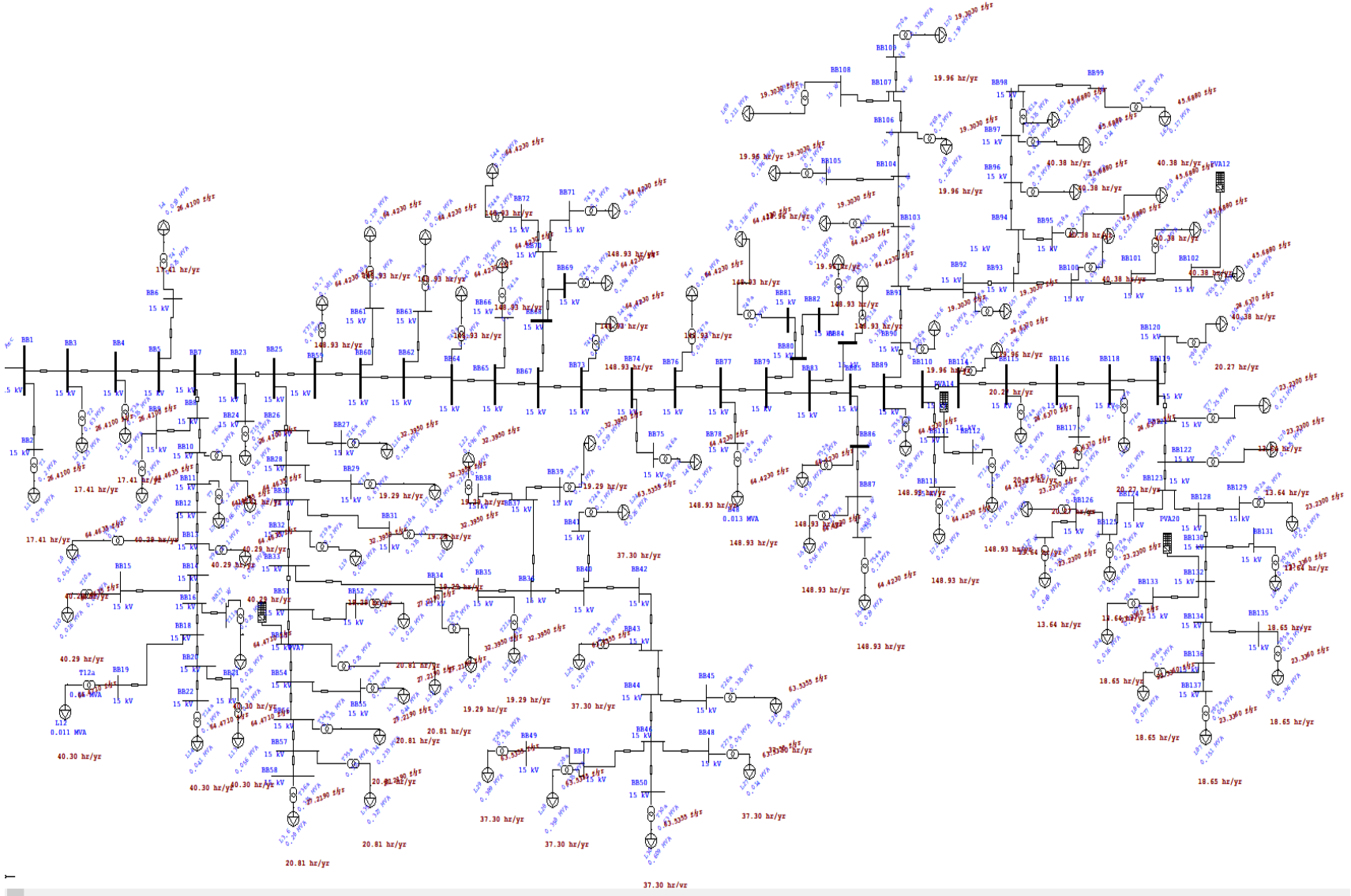

Figure E-6: System network with integration of 4DGs at bus 53, 102, 111, and 132